THE EFFECT OF A SPLITTER PLATE ON THE FLOW AROUND A SURFACE-MOUNTED FINITE CIRCULAR CYLINDER

A Thesis Submitted to the College of Graduate Studies and Research

in Partial Fulfillment of the Requirements for the Degree of Master of Science

in the Department of Mechanical Engineering,

University of Saskatchewan,

Saskatoon,

Saskatchewan,

Canada

By

Adeola Igbalajobi

PERMISSION TO USE

The author grants permission to the Libraries of the University of Saskatchewan to make this thesis available for inspection. Permission for copying of this thesis in any manner, in whole or in part, for scholarly purposes should be granted by my supervisors, Prof. D. Sumner and Prof. D.J. Bergstrom, the Head of the Department of Mechanical Engineering, or the Dean of the College of Graduate Studies and Research. It is understood that any copying or publication or use of this thesis or parts thereof for financial gain shall not be allowed without my written permission. It is also understood that due recognition shall be given to me and to the University of Saskatchewan in any scholarly use which may be made of any material in my thesis. Requests for permission to copy or to make other use of material in this thesis, in whole or part, should be addressed to:

Head of the Department Mechanical Engineering,

University of Saskatchewan,

57 Campus Drive,

Saskatoon, Saskatchewan, S7N 5A9

Canada

ACKNOWLEDGMENTS

I would like to express my sincere gratitude to my supervisors, Prof. D. Sumner and Prof. D.J. Bergstrom, for giving me this research opportunity. I am also grateful for their guidance and patience during my coursework and research. The technical expertise of Mr. Dave Deustcher is highly appreciated; it would have been hard to accomplish this research without it. I would also like to thank my advisory committee members, Prof. J.D. Bugg and Prof. K.A. Mazurek, for the positive criticisms that helped improve my research. My gratitude also goes to the staff of Engineering Shops for the assistance in the manufacture of models and facilities used. Finally, I would like to appreciate the support and encouragement from my family, friends and Mr. S.M. Adaramola throughout my Master's program.

DEDICATION

To GOD ALMIGHTY.

Thanks for seeing me through my program.

ABSTRACT

Splitter plates are passive flow control devices for reducing drag and suppressing vortex shedding from bluff bodies. Most studies of splitter plates involve the flow around an "infinite" circular cylinder, however, in the present study the flow around a *surface-mounted finite-height* circular cylinder, with a wake-mounted splitter plate, was studied experimentally in a low-speed wind tunnel using a force balance and single-component hot-wire anemometry. Four circular cylinders of aspect ratios AR = 9, 7, 5 and 3 were tested for a Reynolds number range of Re = 1.9×10^4 to 8.2×10^4. The splitter plates had lengths, relative to the cylinder diameter, of L/D = 1, 1.5, 2, 3, 5 and 7, thicknesses ranging from T/D = 0.10 and 0.15, and were the same height as the cylinder being tested. The cylinders were partially immersed in a flat-plate turbulent boundary layer, where the range of boundary layer thickness relative to the cylinder diameter was δ/D = 1.4 to 1.5.

Measurements were made of the mean drag force coefficient, the Strouhal number at the mid-height position, and the Strouhal number and power spectra along the cylinder height. For all four finite circular cylinders, the splitter plates were effective at reducing the magnitude of the Strouhal number, and weakening or even suppressing vortex shedding, depending on the specific combination of AR and L/D. Compared to the case of an infinite circular cylinder, the splitter plate is less effective at reducing the mean drag force coefficient of a finite circular cylinder. The largest drag reduction was obtained for the cylinder of AR = 9 and splitter plates of L/D = 1 to 3, while negligible drag reduction occurred for the shorter cylinders.

TABLE OF CONTENTS

NOMENCLATURE

English Symbols

AR	Aspect ratio of the finite circular cylinder
C_D	Mean drag force coefficient
C_{PB}	Mean base pressure coefficient
D	Diameter of the circular cylinder [mm]
f	Vortex shedding frequency [Hz]
F_D	Mean drag force [N]
G	Gap between the base of the cylinder and the leading edge of the splitter plate [mm]
H	Height of the finite circular cylinder [mm] or boundary layer shape factor
H_{SP}	Height of the splitter plate [mm]
L	Length of the splitter plate [mm]
Re	Cylinder Reynolds number
Re_θ	Reynolds number based on boundary layer momentum thickness
S	Power spectral density
St	Strouhal number
T	Thickness of the splitter plate [mm]
U	Freestream velocity [m/s]
u	Streamwise velocity component [m/s]
x	Streamwise coordinate [mm]
y	Cross-stream coordinate [mm]

z Wall-normal coordinate [mm]

Greek Symbols

δ Boundary layer thickness [mm]

δ^* Boundary layer displacement thickness [mm]

θ Boundary layer momentum thickness [mm]

μ Dynamic viscosity of fluid [Ns/m^2]

ρ Fluid density [kg/m^3], autocorrelation coefficient

τ Time difference [s]

ω Frequency [rad/s]

Abbreviations

2D two-dimensional

3D three-dimensional

CC circular cylinder

FP flat plate

FV flow visualization

PIV particle image velocimetry

SCC semi-circular cylinder

CHAPTER ONE

INTRODUCTION

1.1 Flow around Bluff Bodies

Generally, bodies immersed in fluid flow may be categorized under two main headings, streamlined and non-streamlined bodies. Examples of streamlined bodies include aerofoils and wings, while examples of non-streamlined bodies include cylinders, prisms, and spheres. Non-streamlined bodies are often referred to as "bluff bodies" and many engineering structures fall into this category such as buildings, towers, chimneys, overhead power transmission lines, bridge pylons, undersea cables and pipelines, etc. (Irwin, 2008). Some features associated with the flow around bluff bodies include flow separation, high drag forces, a large wake downstream of the body, and vortex shedding.

The classic example of a two-dimensional or "infinite" (where the body length far exceeds the body width) bluff body is the circular cylinder. The flow around a circular cylinder has been well-studied both experimentally and numerically, and is the subject of several books (Sumer and Fredsøe, 1997; Zdravkovich, 1997; Zdravkovich, 2003) and review papers (Morkovin, 1964; Gerrard, 1978; Coutanceau and Defaye, 1991; Williamson, 1996).

The total drag force experienced by a body immersed in a moving fluid comes from two sources: the *pressure drag*, which is related to the body's overall shape and cross-sectional area, and the *skin-friction drag*, which is related to the body's surface area in contact with the moving

fluid (Smits, 2000). In general, the skin-friction drag is more sensitive to Reynolds number compared to the pressure drag. The viscous shear stresses developed within the boundary layers on the surfaces of the body are the source of the skin-friction drag, while the magnitude of the pressure drag depends on where flow separation occurs on the body, and the size and extent of the wake formed downstream of the body. For the flow around a bluff body at sufficiently high Reynolds number, which is dominated by a large region of separated flow, the pressure drag is the dominant factor contributing to the total drag force. The high drag forces experienced by bluff bodies are often detrimental, leading to large wind loads and the need for stronger structures. For non-streamlined vehicles, high aerodynamic drag leads to increased wind resistance and increased fuel consumption. Consequently, much research has been devoted to drag reduction strategies. For bluff bodies, which are dominated by pressure drag, some of these strategies include streamlining the body (both the upstream and downstream edges), and incorporating specific drag reduction devices (such as a splitter plate) to prevent or delay flow separation on the body surfaces, and hence reduce the size and width of the wake.

The flow around bluff bodies is often characterized by the periodic formation and shedding of vortices, in an alternating fashion, from either side of the body. Kármán vortex shedding leads to the formation of a Kármán vortex street in the wake of the body and an alternating pressure force experienced by the body. For engineering structures, vortex shedding may lead to unwanted structural motion known as flow-induced vibration. Consequently, much research has been devoted to either weakening or suppressing vortex shedding from bluff bodies, using various flow control strategies or add-on devices.

1.2 Splitter Plates

The undesirable vortex shedding and high aerodynamic drag forces experienced by bluff bodies have led researchers to consider strategies to control this phenomenon. Active (requiring external energy input) and passive (no external energy input required) flow control strategies are used for weakening or suppressing vortex shedding and/or reducing the aerodynamic drag force. An overview of these strategies is given in the monograph by Gad-el-Hak (2000). A review of passive flow control devices applied to bluff bodies for vortex shedding suppression was compiled by Zdravkovich (1981).

Extensive research has been done since the early experiments of Roshko (1954) on the addition of passive flow control devices, such as small control cylinders and splitter plates, in the near wakes of bluff bodies, especially the infinite circular cylinder. The devices are used to suppress vortex shedding and reduce the drag force. One of the simplest such devices is the two-dimensional "splitter plate", a thin, flat plate typically mounted behind the bluff body parallel to the flow on the wake centreline. Most splitter plate studies have involved the flow around an infinite circular cylinder and its effect on suppressing vortex shedding and reducing drag e.g., Roshko (1954, 1955), Apelt et al. (1973), Apelt and West (1975), Anderson and Szewczyk (1997). A summary of splitter plate studies from the literature is given in Table 1.1[*]. Splitter plates have also been used with other bluff body shapes, including infinite square prisms (e.g., Hasan and Budair (1994), Rathakrishnan (1999), Ali et al. (2011)) and semi-circular cylinders (SCC) (e.g., Nakamura (1996), Boisaubert and Texier (1998), Farhadi et al. (2009)). In a few studies, the splitter plate has been located off the centreline (e.g., Dehkordi and Jafari (2010),

[*] All tables are found at the end of the thesis.

Yucel et al. (2010)), upstream and/or downstream of the cylinder (e.g., Hwang and Yang (2007)) or in pairs (e.g., Dehkordi and Jafari (2010)). The performance of a permeable splitter plate was investigated by Cardell (1993).

The main drawback of a rigidly mounted splitter plate is that it is a "unidirectional" device (Zdravkovich, 1981), and is only effective if the plate is aligned with the mean flow. In a few studies, however, either the plate was hinged to the cylinder and allowed to freely rotate, or the cylinder-plate combination together was free to rotate, in response to the flow conditions (e.g., Cimbala and Garg (1991), Xu et al. (1993), Hu and Koterayama (1994), Shukla et al. (2009)); this modification allows the splitter plate to be used as an "omnidirectional" flow control device (Zdravkovich, 1981).

However, very few studies, if any, have considered the effect of a splitter plate on the flow around *surface-mounted finite-height* bluff bodies, which is the subject of the thesis research. The bluff body of interest here is a surface-mounted finite-height circular cylinder (of diameter, D, height, H, and aspect (or slenderness) ratio, AR = H/D) partially immersed in a flat-plate boundary layer (with mean streamwise velocity profile, $U(z)$, thickness, δ, and freestream velocity, U). A schematic is shown in Figure 1.1[†], where a rectangular splitter plate (of length, L, thickness, T, and height, H_{SP}) is mounted on the wake centreline behind the finite circular cylinder (with a gap, G, between the base (trailing edge or downstream side) of the cylinder and the leading edge of the plate). Note that the vortex shedding frequency is expressed as the dimensionless Strouhal number, St (= fD/U, where f is the vortex shedding frequency), and the mean drag force is expressed as the dimensionless mean drag coefficient, C_D (= $2F_D/(\rho U^2 DH)$, where F_D is the mean drag force).

[†] All figures are found at the end of the thesis.

The effect of the splitter plate on the flow field, and therefore on St and C_D, is a function of several parameters, including the splitter plate's relative length, L/D, the relative gap between the base of the cylinder and the leading edge of the plate, G/D, and the plate's relative thickness, T/D. Other influencing parameters are the cylinder Reynolds number, Re (= $\rho UD/\mu$, where ρ is the fluid density, and μ is the dynamic viscosity), the cylinder's aspect ratio, AR, the relative boundary layer thickness, δ/D or δ/H, and the relative splitter plate height, H_{SP}/H.

Although the effects of any of the parameters listed above cannot be considered in isolation, the L/D ratio is perhaps the most important geometrical parameter since this determines (based on studies of an infinite circular cylinder, see Chapter 2) if both vortex shedding suppression (or weakening) and drag reduction are to occur simultaneously.

1.3 Objective

The main objective of this research is to experimentally investigate the effect of a splitter plate on the drag force and vortex shedding frequency of a surface-mounted finite-height circular cylinder. Parameters to be measured are the mean drag coefficient, C_D, and the Strouhal number, St. Parameters to be varied are the length of the splitter plate, L/D, and the cylinder aspect ratio, AR. The results are compared to published data, for the case of an infinite circular cylinder with a wake-mounted splitter plate, and to a finite circular cylinder with no splitter plate.

1.4 Scope

The finite circular cylinders had aspect ratios of AR = 9, 7, 5, and 3. The experiments were conducted at Reynolds numbers in the range of Re = 1.9×10^4 – 8.2×10^4 which is within the

subcritical Reynolds number regime as defined for an infinite circular cylinder. These are the same aspect ratios and Reynolds numbers used in earlier finite-cylinder studies by Sumner et al. (2004) and Adaramola et al. (2006) at the University of Saskatchewan.

The cylinders were mounted normal to a ground plane and partially immersed in the turbulent flat plate boundary layer developed on the ground plane. A constant relative boundary layer thickness ratio of approximately $\delta/D \approx 1.5$ was used; this boundary layer thickness is relatively thick (compared to many of the finite-cylinder studies in the literature) but similar to the earlier studies by Sumner et al. (2004) and Adaramola et al. (2006). It is noted that varying the boundary layer thickness, while keeping the cylinder size and Reynolds number constant, is more difficult to achieve experimentally; most studies in the literature have therefore opted for a constant boundary layer thickness.

The thickness-to-diameter ratios of the splitter plates was $T/D = 0.10$ or 0.15, chosen mainly for structural rigidity since the plates were cantilevered from the ground plane. It is noted that in this study the splitter plate cannot be fastened to the cylinder itself, since this would affect the C_D measurements. For finite-cylinder experiments, only one mounting point exists for the splitter plate that being the ground plane, in contrast to infinite-cylinder experiments where the splitter plate can be fastened to both the roof and floor of the wind tunnel test section. Similar thickness ratios (T/D) have been used in some splitter plate studies in the literature (see the summary of splitter plate studies in Table 1.1).

Seven splitter plate length-to-diameter ratios were chosen, of $L/D = 0$, 1, 1.5, 2, 3, 5, and 7. These ratios cover the range of splitter plate lengths considered in other studies in the literature (see Table 1.1). It is noted that the $L/D = 0$ case corresponds to a cylinder with no splitter plate. With seven splitter plate length ratios and four cylinder aspect ratios, this created

28 different cylinder-plate configurations. These aspect ratios were tested earlier without a splitter plate, by Sumner et al. (2004) and Adaramola et al. (2006). The selected L/D values correspond to other splitter plate studies in the literature (see Chapter 2).

The gap (G/D) considered was zero. The heights of the plates were chosen to be identical to the heights of the cylinders, i.e. $H_{SP}/H = 1$ for all cylinder-plate configurations.

1.5 Outline of Thesis

Chapter 2 gives a review of the background information and previous studies on the flow around an infinite circular cylinder, flow around a finite circular cylinder, and use of splitter plates. The experimental apparatus and the instrumentation used during the course of the research are described in Chapter 3. Chapter 4 contains the results and discussion of the research work. Chapter 5 presents the conclusions and recommendations. It should be noted that all of the figures and tables are placed at the end of the thesis.

CHAPTER TWO

LITERATURE REVIEW

2.1 Introduction

In this chapter, brief reviews of the literature are presented pertaining to the flow around an infinite circular cylinder (Section 2.2), the use of splitter plates (Section 2.3), and the flow around a finite circular cylinder (Section 2.4).

2.2 Flow around an Infinite Circular Cylinder

The flow around an infinite circular cylinder has a strong dependence on the Reynolds number. A number of flow regimes have been identified for the flow around an infinite circular cylinder, as summarized by various authors (e.g., Coutanceau and Defaye (1991), Williamson (1996), Sumer and Fredsøe (1997), Zdravkovich (1997)). Although there is general agreement on the flow behaviour, the Reynolds number boundaries of the different regimes, and the number of regimes, vary slightly from author to author.

Coutanceau and Defaye (1991) specified ten flow regimes: (i) $Re \leq 0.1$ (fore-aft symmetrical flow), otherwise known as the regime of creeping flow, no separation occurs, the vorticity is dominant, and the flow follows exactly the cylinder surface; (ii) $0.1 \leq Re \leq 4.5$ (fore-aft asymmetrical flow), still no flow separation but the streamline pattern has lost the fore and aft symmetry; (iii) $4.5 \leq Re \leq 35$ (presence of an attached closed recirculating bubble and a stable

far wake), the flow has clearly separated from the cylinder to form a pair of recirculating eddies; (iv) $35 \leq Re \leq 60$, here flow instability begins to appear, there is a slight asymmetry of the attached bubble and slight irregularities of its boundary as the centre of the two standing eddies begins to shift; (v) $60 \leq Re \leq 100$ (Kármán vortex shedding), shedding of vortices occurs in this regime as the separated free shear layers alternately roll up into vortices; (vi) $100 \leq Re \leq 2000$ (Kármán vortex shedding), alternate shedding of vortices directly from the cylinder continues and a growing formation zone emerges; (vii) $2000 \leq Re \leq 1.5–2.0\times10^5$ (lower subcritical regime) small-scale Kelvin-Helmholtz instabilities form within the separated shear layers at the boundary of the formation zone; (viii) $1.5–2.0\times10^5 \leq Re \leq 4.0–5.0\times10^5$ (upper subcritical and critical regimes), the flow field is characterized by an unstable boundary layer which separates and consequently transitions to turbulence, hence a decrease in the wake width is observed, a sharp decrease of the drag coefficient also occurs in addition to an increase in the Strouhal number; (ix) $4.0–5.0\times10^5 \leq Re \leq 3.5\times10^6$ (supercritical regime), turbulent boundary layer separation occurs from both sides of the cylinder, but the transition to turbulence is not yet completed, the boundary layer becomes fully turbulent on one side of the cylinder whilst the other side is partly laminar and partly turbulent; (x) $Re \geq 3.5\times10^6$, here the boundary layers are completely turbulent, and it is referred to as the "transcritical regime".

Within the subcritical Reynolds number regime, which corresponds to the range of Reynolds numbers in the present research, laminar boundary layers on the surfaces of the cylinder separate to form a pair of shear layers enclosing the near-wake region. The shear layers roll-up periodically and alternately from either side of the cylinder to form Kármán vortices, which are periodically and alternately shed into the turbulent wake downstream of the cylinder. The wake contains a regular pattern of vortices known as the Kármán vortex street. Within this

flow regime, the cylinder's mean drag coefficient and Strouhal number remain relatively constant with Reynolds number. A pictorial view of the flow field is shown in Figure 2.1.

2.3 Splitter Plates

The issue of controlling the effects of fluid flow on bluff bodies (specifically the drag force, and vortex shedding) led Roshko (1954, 1955) to study the effects of placing an impediment in the wake of a two-dimensional or infinite bluff body, specifically a "splitter plate". Since then, the application and study of the splitter plate as a flow control device for two-dimensional bluff bodies has been widespread.

As mentioned in Section 1.2, the splitter plate is an example of a passive flow control technique; such techniques may be used to suppress or weaken vortex shedding, typically by attaching additional devices in the flow field (like Roshko's splitter plate), or by trying to modify the shape of the bluff body altogether. Other examples of passive control techniques include control cylinders and small rods (e.g., Strykowski and Sreenivasan (1990), Igarashi (1997), Lee et al. (2004)), base bleed (e.g., Bearman (1967), Schumm et al. (1994), Hangan and Kim (2003), Koutmos et al. (2004)), helical wires (e.g., Naudascher and Rockwell (1994), Lee and Kim (1997)), and roughness elements (e.g., Sakamoto et al. (1991)). The reader is also referred to the review of vortex shedding suppression devices compiled by Zdravkovich (1981).

The use of splitter plates to manipulate flow fields around two-dimensional bluff bodies, with special consideration given to the circular cylinder, has been extensively studied both experimentally and numerically (e.g., Bearman (1965), Apelt et al. (1973), Apelt and West (1975), Unal and Rockwell (1987), Sakamoto and Haniu (1994), Kwon and Choi (1996), Nakamura (1996), Anderson and Szewczyk (1997), Prasad and Williamson (1997), Ozono

(1999, 2003), Nakayama and Noda (2000), Hwang et al. (2003), Tiwari et al. (2005), Dehkordi and Jafari (2010)). Table 1.1 gives a more complete list of these and other studies.

Feedback control and acoustic excitation systems, suction and blowing, and rotary oscillation of cylinders, are some examples of active control techniques. Roussopoulos (1993) and Park et al. (1994), amongst others, worked on the feedback control and acoustic excitation type, while researchers such as Delaunay and Kaiktsis (2001) and Li et al. (2003) favoured the suction and blowing aspect. Guilmineau and Queutey (2002) carried out their study on rotary oscillation of cylinders. Wu and Shu (2011) used their recently developed boundary condition-enforced immersed boundary-lattice Boltzmann method for this same purpose.

Returning to the subject of the splitter plate, and the summary of experimental and numerical studies of splitter plates in Table 1.1, the flow parameters of greatest interest have been the Strouhal number (St), mean drag force coefficient (C_D), and the mean base pressure coefficient (C_{PB}, measured at the rear of the cylinder), and how the splitter plate affects these parameters. Taken together, the studies in the literature have shown that a splitter plate of appropriate geometry and location (L/D, G/D, and T/D, for instance) can simultaneously reduce the drag coefficient, increase the mean base pressure coefficient, and weaken or suppress vortex shedding.

The introduction of the splitter plate has several effects on the flow field around the infinite circular cylinder, which lead to the observed weakening or suppression of vortex shedding and the reduction in drag. Anderson and Szewczyk (1997), who experimented on infinite circular cylinders with short splitter plates (L/D = 0 to 2.0), noticed that the width of the wake was significantly narrowed following the introduction of a splitter plate. Boisaubert and Texier (1998), who studied the flow around a semi-circular cylinder (SCC) with a wake-mounted

splitter plate, noticed that the presence of a splitter plate helps to generate secondary vortices in the near-wake recirculation zone. By dividing the near-wake region into two separate parts, the formation of strong vortices at the base (the rear surface) of the cylinder is prevented, leading to an increase in the base pressure, and consequently a reduction in drag (Rathakrishnan, 1999). For vortices to be shed, there must be close interaction between the shear layers from either side of the cylinder, as they roll-up periodically and alternately; this interaction is prevented by the introduction of a splitter plate, which makes it impossible for the shear layers to "see" each other.

2.4 Flow around a Finite Circular Cylinder

The flow around a surface-mounted finite-height circular cylinder has received less attention (due to the complexity of the flow) than the more familiar case of the infinite circular cylinder. The flow around the finite cylinder is more complex than the flow around the infinite cylinder and is strongly three-dimensional. The main features of the flow field include the Kármán vortex shedding from the sides of the cylinder, a pair of counter-rotating tip vortices that originates from the top of the cylinder and extend in the streamwise direction into the wake, a pair of counter-rotating base vortices near the ground plane also extending in the streamwise direction, the horseshoe vortex that forms at the cylinder-wall junction upstream of the cylinder, a downward-directed velocity, known as "downwash", induced by the streamwise tip vortex pair and an upward-directed velocity, known as "upwash", which is as a result of the base vortex pair. A sketch of the flow field is shown in Figure 2.1.

The flow field around the finite circular cylinder is strongly influenced by the cylinder aspect ratio (AR) as well as the thickness of the boundary layer (δ/D or δ/H) on the ground plane (Kawamura et al., 1984; Okamoto and Sunabashiri, 1992; Tanaka and Murata, 1999; Park and

Lee, 2004; Sumner et al., 2004; Adaramola et al., 2006). For very small AR (where the aspect ratio is less than the critical aspect ratio), the wake structure of finite cylinders are different from those of finite cylinders of larger AR. The small-aspect-ratio behavior is marked by symmetric "arch" vortex shedding (the familiar antisymmetric Kármán vortex shedding is absent) and an absence of base vortices. The critical aspect ratio below which the distinct behavior is observed is a function of δ/D or δ/H and other parameters. In the studies by Sumner et al. (2004) and Adaramola et al. (2006), which looked at the wake velocity and turbulence fields, vortex shedding, and streamwise vortex structures, the critical aspect ratio was found to lie between AR = 3 and AR = 5. The critical aspect ratio is sensitive to the boundary layer thickness, and increases as the boundary layer thickens relative to the size of the cylinder (Kawamura et al., 1984).

Okamoto and Sunabashiri (1992) experimentally investigated six aspect ratios (AR = 0.5, 1, 2, 4, 7, and 23.75) for Re = 2.5×10^4 to 4.7×10^4 and recorded the accompanying changes in the surface pressure and the turbulent wake as a function of aspect ratio. They noticed that C_D varied rapidly around AR = 4 as a result of the increase of the local drag due to the decrease in pressure in the vicinity of the free end of the cylinder. In the range of AR $\leq$ 4, C_D was observed to decrease below the value for AR $\geq$ 4. They stated that the decrease in drag was as a result of pressure recovery on the rear face of the cylinder due to the strong downwash from its free end.

The size of the horseshoe vortices noticed in Okamoto and Sunabashiri (1992) experiments decreased as the height of the cylinder increased, and the effect of the downwash from the cylinder free end weakened with an increase in AR. The recirculation region behind the circular cylinder was noted to enlarge with an increase in AR (Okamoto and Sunabashiri, 1992). Further explanation points to the fact that the free-end region for low aspect ratios extends to the

ground plane until AR = 4, after which further increases in AR lead to a decrease in the size and length of the recirculation region.

Tanaka and Murata (1999) investigated the wake structure of a finite circular cylinder of AR = 1.25 to AR = 10 at Re = 3.7×10^4 and the effects of different shapes of cylinder free-end geometry on the wake flow. It was seen that for a cylinder of AR = 10, significant influence of the free-end geometry on the wake appeared up to $5D - 6D$ below the tip, with less downwash near the ground plate. They also observed that the recirculatory region gradually shrinks, and strong downwash reaches the ground, with a decrease in AR, which is in agreement with the observation of Okamoto and Sunabashiri (1992).

Park and Lee (2004) employed particle image velocimetry (PIV) to experimentally study the effects of free-end corner shape (flat-tip, square tip, and beveled or rounded shape tip, etc.) on the flow structure around a finite cylinder of AR = 6 at Re $\approx 7.5\times10^3$ embedded in an atmospheric boundary layer over an open terrain. They confirmed that the size of the recirculation bubble formed as well as the turbulence intensity is dependent on these shapes. It was seen that the turbulence intensity around the tip decreases as the tip is modified to become more streamlined which is in agreement with the study carried out by Tanaka and Murata (1999).

Sumner et al. (2004) experimentally considered the wake structure of finite circular cylinders of AR = 3, 5, 7 and 9 mounted normal to a ground plane in the subcritical Reynolds number regime (Re = 6×10^4) with a boundary layer thickness of $\delta/D = 2.6$. They observed that the wake structure for the cylinder of AR = 3 was different (since, it was below the critical aspect ratio) from those of cylinders of AR = 5, 7 and 9. In particular, base vortices were absent. Sumner et al. (2004) also observed that for small-AR cylinders, the flow around the free end of

the cylinder affects the flow along the entire cylinder height by suppressing the antisymmetric Kármán vortex shedding from the cylinder.

In a study similar to Sumner et al. (2004), Adaramola et al. (2006) studied the turbulent wake of finite circular cylinders of small aspect ratio at Re = 6×10^4 and δ/D = 3.0. Their study revealed a distinct turbulent wake structure for the AR = 3 cylinder.

CHAPTER THREE

EXPERIMENTAL APPARATUS AND INSTRUMENTATION

3.1 Introduction

In this chapter, an overview is provided of the equipment used to perform the research, including the wind tunnel (Section 3.2), cylinders and splitter plates (Section 3.3), and the instrumentation (Section 3.4). Details of the boundary layer created on the wind tunnel ground plane are discussed in Section 3.5.

3.2 Wind Tunnel

The University of Saskatchewan's low-speed, closed-return wind tunnel shown in Figure 3.1 was used for the thesis research experiments. The test section has dimensions of 1.96 m (length) × 0.91 m (height) × 1.13 m (width). The streamwise freestream turbulence intensity in the test section is less than 0.6% and the mean velocity non-uniformity outside the test section wall boundary layers is less than 0.5%.

The wind tunnel's test section contains an aluminium ground plane on which a turbulent flat-plate boundary layer develops. The cylinders and splitter plates were mounted normal to this

ground plane and were partially immersed in this boundary layer. Figure 3.2 shows some details of the wind tunnel test section.

Imbedded within the ground plane was a turntable (the turntable was not rotated in the present experiments), which was modified to include a series of holes used to firmly hold the splitter plates in place during the course of the experiments (Figure 3.3a). Each cylinder was mounted to a force balance as described below.

3.3 Apparatus

Four flat-tipped, smooth aluminium circular cylinders, all of the same diameter, D = 31.5 mm, were used for the experiments. Each cylinder had a different height, giving aspect ratios of AR = 9, 7, 5, and 3, similar to the experiments of Sumner et al. (2004) and Adaramola et al. (2006). Each cylinder was positioned normal to the ground plane and was partially immersed in the turbulent boundary layer on the ground plane. The cylinders were inserted through a hole in the ground plane's turntable and attached to the six-component force balance located outside and below the test section (Figure 3.2). The cylinders were located 900 mm from the leading edge of the ground plane. To prevent contact between the cylinder and the ground plane (which would affect the drag force measurements), a circumferential gap of about 1 mm existed between the cylinder and the hole in the turntable.

For each cylinder, six different splitter plates were tested, with length ratios of L/D = 1, 1.5, 2, 3, 5 or 7, in addition to the case of no splitter plate (L/D = 0). In all cases, the height of the plate matched the height of the cylinder being tested, i.e., H_{SP}/H = 1. The plates were constructed from aluminium and had sharp edges on all sides. The plates were fastened in a cantilevered fashion to the ground plane (turntable) immediately behind the cylinder on the wake

centreline with the help of holes drilled unto the turntable for this purpose (see Figure 3.3a). A gap of about 0.5 mm was left between the leading edge of the plate and the base of the cylinder to ensure the plate did not contact the cylinder and affect the drag force measurements. This gap corresponds to a ratio of $G/D = 0.016$; according to the results of Cardell (1993), who considered the influence of very small gap ratios for splitter plates, gaps of $G/D < 0.13$ should have no appreciable effect on the mean base pressure and vortex shedding frequency. The thickness ratio of the splitter plates was $T/D = 0.10$ for the cylinders of AR = 7, 5 and 3. However, for AR = 9, a thickness ratio of $T/D = 0.15$ was chosen to prevent vibration. It is noted that these T/D ratios are consistent with other splitter plates used in the literature (see Table 1), but had to be on the thicker side since they were cantilevered to the ground plane and not attached to the cylinder or mounted between two wind tunnel side walls, as in the case of the infinite-cylinder experiments in the literature. A photograph of a cylinder with a splitter plate is shown in Figure 3.3b.

To attain cylinder Reynolds numbers from $\mathrm{Re} = 1.9\times10^4 - 8.2\times10^4$, the wind tunnel was operated at freestream velocities of $U = 10 - 45$ m/s. The solid blockage ratio (the ratio of the frontal area of the cylinder to the cross-sectional area of the test section) did not exceed 0.9%.

3.4 Instrumentation

The wind tunnel data were acquired using a computer with a 1.8-GHz Intel Pentium 4 processor, a National Instruments PCIe-6259 16-bit data acquisition board, and LabVIEW software. Some details of the data acquisition and wind tunnel control systems are shown in Figure 3.4. The freestream conditions were obtained with a Pitot-static probe (United Sensor, 3.2-mm diameter) mounted on the side wall of the test section (shown in Figure 3.2),

Datametrics Barocell absolute and differential pressure transducers, and an Analog Devices AD590 integrated circuit temperature transducer.

Measurements of the vortex shedding frequency were made with a six-channel Dantec Streamline constant-temperature anemometer, using a single-component normal-wire hot-wire probe (Dantec 55P11), utilizing the same data acquisition described above. The probe was positioned at $y/D = 1.5$ in the cross-stream direction and $x/D = 3$ downstream from the cylinder axis for each cylinder-splitter plate combination, similar to the experiments of Sumner et al. (2004). In addition to the $x/D = 3$ streamwise measurement position, for the cases of an attached splitter plate a second position of $x/D = 3 + L/D$ was also used in order to measure the vortex shedding frequency, three cylinder diameters downstream of the trailing edge of the splitter plate. By taking measurements downstream of the splitter plate, this ensured that measurements would be made of the shed vortices (beyond the vortex formation region). The wall-normal (z/D) position of the hot-wire probe was allowed to vary along the cylinder height, from $z/D = 0.5$ (close to the ground plane) to $z/H = 1$ (corresponding to the top of the cylinder), to obtain information on how the Strouhal number varies with height. The wind tunnel's computer-controlled traversing system (seen in Figure 3.2) was used to position the hot-wire probe. A more detailed description of how the vortex shedding frequencies were obtained is found in Appendix A.

3.5 Boundary Layer Measurements

The mean streamwise velocity profile of the boundary layer on the ground plane, at the location of the cylinder, was measured with a boundary layer Pitot tube and a Validyne differential pressure transducer. Velocity profiles (see Figure 3.5) were obtained at several

freestream velocities. These were used to determine the boundary layer thickness, δ, and other boundary layer parameters at the location of the cylinder (see Table 3.1).

CHAPTER FOUR

RESULTS AND DISCUSSION

4.1 Introduction

In this chapter, the results obtained during the course of the research are presented and discussed. For the mean drag coefficient experiments (presented in Section 4.2), measurements were made for a Reynolds number range of Re = 1.9×10^4 – 8.2×10^4 (corresponding to freestream velocities of approximately U = 10 – 45 m/s, respectively). For the Strouhal number experiments at the *mid-height* ($z = H/2$) position (presented in Section 4.3), measurements were made over the complete Reynolds number range given above. Measurements of the Strouhal number *along the height* of the cylinders, varying the z-position, (presented in Section 4.4) were made at a single Reynolds number (corresponding to U = 40 m/s or Re ≈ 7.5×10^4).

4.2 Mean Drag Coefficient

The mean drag coefficient data for the finite circular cylinders with the splitter plates are presented in Figure 4.1 for the complete range of Reynolds number. Data for the case of no splitter plate (L/D = 0) are included as a reference.

The experimental results in Figure 4.1 show that the mean drag coefficient data for all four aspect ratios (AR = 9, 7, 5, 3) and all seven splitter plate lengths (L/D = 0, 1, 1.5, 2, 3, 5, and 7) are insensitive to Reynolds number over the range of Re tested (Re = 1.9×10^4 – 8.2×10^4).

This result is consistent with the behaviour of the mean drag coefficient for an infinite circular cylinder, which remains relatively constant within the subcritical Reynolds number regime ($C_D \approx$ 1.2).

The results in Figure 4.1 also show how the addition of the splitter plate affects the mean drag coefficient. For all four aspect ratios, the highest measured drag coefficients were recorded for the case of no splitter plate ($L/D = 0$). The addition of a splitter plate, in most cases, resulted in a small reduction in the mean drag coefficient. The smallest measured drag coefficients, however, did not necessarily occur for the longest splitter plates, and this varies depending on the particular combination of AR and L/D. For the larger aspect ratios, the most effective splitter plate lengths for reducing the mean drag coefficient were L/D = 1, 1.5, 2, and 3. For AR = 9 (Figure 4.1a), the smallest measured C_D value was for L/D = 1; for AR = 7 (Figure 4.1b), the smallest measured C_D value was for L/D = 3; for AR = 5 (Figure 4.1c), the smallest measured C_D value was for L/D = 1.5; and for AR = 3 (Figure 4.1d), the smallest measured C_D value was for L/D = 5.

It is noted that at the lower Reynolds numbers, the cylinders experienced very small drag forces, which in some cases were on the order of the measurement uncertainty of the force balance (estimated at ± 0.08 N). The resulting measurement uncertainty in the mean drag coefficient for the lower Reynolds number experiments was therefore quite high. Note the large error bars for the mean drag coefficient data at the lower Reynolds numbers in Figure 4.1 which approached ± 77 % for the case of AR = 3 (Figure 4.1d). The high measurement uncertainty at the lower Reynolds numbers means that the small changes in the mean drag coefficient caused by the splitter plate cannot be reliably measured at the lower Reynolds numbers, particularly for the smallest cylinders of AR = 3 and 5. Based on the above considerations, the mean drag

coefficient data for U = 40 m/s (Re ≈ 7.5×10^4), where the measurement uncertainty was less, were selected as the main point of reference for evaluating the effectiveness of the splitter plate. These data are presented in Table 4.1.

The data in Table 4.1 show that for AR = 9 and AR = 7, the mean drag coefficient for the longest splitter plate (L/D = 7) is the same as the case for no splitter plate (L/D = 0). For these two cylinders, therefore, a longer splitter plate is not effective in drag reduction. This result might be due to the flow reattaching onto the splitter plate, or the wake flow becoming more two-dimensional in nature (noting that for a given cylinder shape, the three-dimensional body has a lower mean drag coefficient compared to the two-dimensional body).

For the cases of AR = 5 and AR = 3, however, the longer splitter plates (L/D = 5 and 7) have the most impact in reducing the mean drag coefficient with the most effective splitter plate being L/D = 5 (see Table 4.1). The effect of splitter plates L/D = 1 and 3 on these two cases (AR = 5 and AR = 3) are the same. Neglecting the cases of the longer splitter plates (L/D = 5 and 7) for the smaller aspect ratios (AR = 5 and AR = 3), it can be seen from Figure 4.1 that the mean drag coefficient decreases with increase in length of splitter plate apart from the case of L/D = 3 for AR = 5; and L/D = 1 for AR = 3.

Generally, the mean drag coefficient reduces as aspect ratio decreases from AR = 9 to AR = 3 for the case of no splitter plate (see Table 4.1). This trend is also repeated with the addition of splitter plates except for a few cases (AR = 7, L/D = 1 and AR = 5, L/D = 3). This means that the overall smallest mean drag coefficient was recorded for the AR = 3 circular cylinder.

The data in Table 4.1 are also plotted in Figure 4.2, normalized against the mean drag coefficient for the case of no splitter plate, i.e., C_D/C_{D0}. This figure more clearly illustrates the

effectiveness of the splitter plate (for certain combinations of AR and L/D) in reducing the mean drag coefficient of the finite circular cylinder.

Also plotted in Figure 4.2 are splitter plate data from the literature for the case of an infinite circular cylinder. From these results, it is clear that the splitter plate is more effective at drag reduction for the case of the infinite cylinder than for the finite cylinder. Mean drag coefficient values for finite circular cylinders are lower than that of an infinite circular cylinder due to the effect of downwash, which enters the wake and adds higher momentum fluid (Okamoto and Sunabashiri 1992; Lee 1997; Sumner et al. 2004).

4.3 Strouhal Number and Vortex Shedding at Mid-Height

Strouhal number measurements were made at the mid height position ($z/H = 0.5$) for the complete range of Re considered (Re = 1.9×10^4 to 8.2×10^4) and for all values of L/D. In the other two coordinate directions, the probe was first positioned at $y/D = 1.5$ in the cross-stream direction and at $x/D = 3$ in the streamwise direction, similar to the experiments of Sumner et al. (2004). For the cases when the splitter plates were used, a second streamwise measurement position for the hot-wire probe was adopted, at $x/D = 3 + L/D$, giving streamwise positions of $x/D = 4$, 4.5, 5, 6, 8, and 10 for the splitter plates of $L/D = 1$, 1.5, 2, 3, 5 and 7, respectively. For this measurement location, the hot-wire was positioned downstream of the splitter plate-cylinder combination, in the wake of the combined body.

To find the Strouhal number, a power spectrum was first computed from the velocity-time signal from the hot-wire probe using the FFT Power Spectrum VI (virtual instrument) from the LabVIEW programming language. The velocity-time signal was sampled at 5 kHz for a duration of 1 s, since similar sampling parameters have been used in other vortex shedding

experiments in the wind tunnel. Each power spectrum shown in the subsequent figures represents an average of 100 individual spectra. The vertical scale for the spectra in the subsequent figures is arbitrary, but the same scale is used for each spectrum. More information can be found in Appendix A.

The presence of a peak in the power spectrum indicates the presence of a periodic flow phenomenon, such as vortex shedding, with a dominant frequency (or Strouhal number). Of particular interest are the height and width of the peak. A tall peak corresponds to a strong vortex shedding signal, while a short peak means a weak vortex shedding signal. A narrow peak means the frequency of vortex shedding is fairly consistent over a narrow band, while a wide or broad-banded peak means the frequency wanders over a small range of frequencies and the vortex shedding may be more irregular. The absence of a peak is taken to mean the absence (or suppression) of periodic vortex shedding.

Figure 4.3 shows the power spectra at mid-height for the $x/D = 3$ measurement location, while Figure 4.4 shows the power spectra for the $x/D = 3 + L/D$ measurement location. The corresponding Strouhal numbers for these two measurement positions are given in Tables 4.2 and 4.3.

4.3.1 Mid-height Strouhal Number Measurements for AR = 9

For AR = 9 (Figures 4.3a and 4.4a), strong vortex shedding occurs when no splitter plate was used ($L/D = 0$); this can be observed from the strong, narrow vortex shedding peaks in the power spectra at St = 0.163. Similar strong vortex shedding peaks are seen for the case of the shortest splitter plate ($L/D = 1$) at both measurement positions, while the Strouhal number is reduced to St = 0.130 – 0.133. For the splitter plates of $L/D = 1.5$ and $L/D = 2$, two weak broad-

banded peaks occur in the power spectra at $x/D = 3$ (Figure 4.3a); however, only a single weak broad-banded peak is observed at $x/D = 4$ (Figure 4.4a). A weak vortex shedding peak is also seen at both measurement positions for $L/D = 3$. Vortex shedding peaks are absent in the power spectra for the longer splitter plates ($L/D = 5$ and 7), indicating that suppression of vortex shedding has occurred.

4.3.2 Mid-height Strouhal Number Measurements for AR = 7

Figures 4.3b and 4.4b show the power spectra at mid-height for AR = 7. The trends for AR = 7 are similar to those of AR = 9. The main difference for AR = 7 is that the shedding of vortices when no splitter plate is used ($L/D = 0$) occurs at a slightly lower Strouhal number compared to AR = 9, at St = 0.160 (Tables 4.2 and 4.3), and the vortex shedding peak is not as sharp (based on a visual comparison of Figures 4.3a and 4.3b). The absence of twin peaks in the power spectra is also noted for the AR = 7 cylinder, although two very weak broad-banded peaks might possibly be seen in the spectrum for $L/D = 5$ at $x/D = 3$ (Figure 4.3b). At the $x/D = 3$ measurement position (Figure 4.3b), the shorter splitter plates ($L/D = 1$, 1.5, 2, and 3) show vortex shedding peaks that are much weaker and more broad-banded in nature, but complete vortex shedding suppression seems to occur only for the longest splitter plates ($L/D = 5$ and 7). At the second measurement position (downstream of the splitter plate, Figure 4.4b), the absence of peaks in the power spectra for the splitter plates of $L/D = 2$, 3, 5 and 7 show that vortex shedding suppression has occurred. For $L/D = 1$ and 1.5, the splitter plate results in a reduction in vortex shedding frequency (to St = 0.127 and St = 0.140), as can be seen in Figure 4.4b and Table 4.3.

4.3.3 Mid-height Strouhal Number Measurements for AR = 5

The power spectra at mid-height for AR = 5 are shown in Figures 4.3c and 4.4c. For no splitter plate (L/D = 0), vortex shedding occurs from the cylinder and a strong vortex shedding peak is seen in the power spectrum, although the peak is somewhat weaker and a little bit more broad-banded compared to AR = 9 (Figures 4.3a and 4.4a) and AR = 7 (Figures 4.3b and 4.4b). A further reduction in Strouhal number, to St = 0.154, occurs for AR = 5 (Tables 4.2 and 4.3). The addition of a splitter plate causes a reduction in the Strouhal number, with the most effective splitter plate for Strouhal number reduction being that of L/D = 1. From the data in Table 4.2, it can be seen that the smaller splitter plates (L/D = 1, 1.5, 2 and 3) are more effective in Strouhal number reduction. At the x/D = 3 measurement position (Figure 4.3c), weak broad-banded peaks are seen in the power spectra for all splitter plates, suggesting that complete vortex shedding suppression does not occur. However, at the $x/D = 3 + L/D$ measurement position (Figure 4.4c), complete suppression of vortex shedding is obtained for the splitter plates of L/D = 1.5, 2 and 3. Weak broad-banded peaks can be still seen in the power spectra for the two longest splitter plates (L/D = 5 and 7).

4.3.4 Mid-height Strouhal Number Measurements for AR = 3

Figures 4.3d and 4.4d show the power spectra for AR = 3. For the case of no splitter plate (L/D = 0), vortex shedding occurs from the cylinder and a small vortex shedding peak at St = 0.161 is seen in the power spectrum. At x/D = 3 (Figure 4.3d), weak and very broad-banded peaks can be seen in the power spectra for all of the splitter plates. The most effective splitter plate for Strouhal number reduction is that of L/D = 1 (Table 4.2), similar to the case of AR = 5, with the Strouhal number being reduced to St = 0.141. For the measurement position further

downstream ($x/D = 3 + L/D$, Figure 4.4d), all of the splitter plate lengths lead to suppression of vortex shedding, and no discernible peaks are found in the power spectra.

4.3.5 Further Discussion

In general, for the cases with no splitter plate ($L/D = 0$), the Strouhal number decreases with a decrease in aspect ratio, with the exception of the AR = 3 circular cylinder. This result for AR = 3 is not surprising as Sumner et al. (2004) found that the wake structure and power spectra for AR = 3 were different from the more slender cylinders of AR = 5, 7 and 9.

For the cases where a splitter plate is used, the measurements close to the cylinder (at $x/D = 3$, Figure 4.3 and Table 4.2) showed that weak vortex shedding still persisted at mid-height for some combinations of AR and L/D. However, from the measurements made downstream of the splitter plate (at $x/D = 3 + L/D$, Figure 4.4 and Table 4.3), the effectiveness of the splitter plate at mid-height was more clearly shown; these results are therefore used below to summarize the performance of the splitter plate with respect to vortex shedding.

From Table 4.3, for AR = 9, a splitter plate of $L/D = 1$ reduced the magnitude of the Strouhal number but did not suppress vortex shedding, while the splitter plates of $L/D = 5$ and 7 completely suppressed vortex shedding. For AR = 7, the splitter plates of $L/D = 1$ and 1.5 reduced the magnitude of the Strouhal number but did not suppress vortex shedding, while the splitter plates of $L/D = 2$ to 7 completely suppressed vortex shedding. For AR = 5, vortex shedding suppression at mid-height occurred for the intermediate splitter plates of $L/D = 1.5$, 2 and 3 only; for the other splitter plates, of $L/D = 1$, 5 and 7, a reduction in Strouhal number occurred. For AR = 3, vortex shedding suppression occurred for all splitter plates.

The data in Table 4.2 (at $x/D = 3$) and Table 4.3 ($x/D = 3 + L/D$) are plotted in Figures 4.5a and 4.5b respectively, for the normalized Strouhal number (St/St_0) using the case of no splitter plate ($L/D = 0$) as the reference case. The smallest plate ($L/D = 1$) is the most effective in reducing drag for the AR = 3 cylinder (Figure 4.2). On attachment of splitter plates for AR = 7 and 9, a decrease in the Strouhal number is recorded for all the splitter plates except for $L/D = 2$ while for the AR = 5 cylinder, all the cases involving splitter plates recorded a decrease in the Strouhal number. For the position further downstream (see Figure 4.5b at $x/D = 3 + L/D$), vortices were completely suppressed for the AR = 3 cylinder for all splitter plates being used, and other cylinders also experienced either complete suppression of vortex shedding or its weakening with splitter plates used except for the case of $L/D = 2$ for the AR = 9 cylinder.

The result obtained here is similar to what Sumner et al. (2004) documented. The approximate value for St at mid-height for $L/D = 0$ from Table 4.2 is St = 0.16 which is in accordance with the values of Sumner et al. (2004). Also, other experimentalists like Okamoto and Yagita (1973), Sakamoto and Arie (1983), Sakamoto and Oiwake (1984), and Okamoto and Sunabashiri (1992), obtained similar values.

4.4 Strouhal Number and Vortex Shedding along the Height

Strouhal number measurements were also made along the heights of the cylinders (varying z position) at a single Reynolds number (corresponding to $U = 40$ m/s or $Re \approx 7.5\times10^4$) for all the splitter plates. For all of the measurements, the probe was positioned at $y/D = 1.5$ in the cross-stream direction. Similar to the mid-height measurements (discussed in Section 4.3), two streamwise measurement positions were used, at $x/D = 3$ (close to the cylinder) and then at $x/D = 3 + L/D$ (downstream of the splitter plate). The varying wall-normal (z) positions

considered were made in increments of 0.5D, with the first measurement at z/D = 0.5 (close to the ground plane) and the last measurement at z/H = 1 (at the height of the cylinder). This yielded 18, 14, 10, and 6 measurement positions at each streamwise position for the cylinders of AR = 9, 7, 5, and 3, respectively. Similar vertical measurement increments and positions were used by Sumner et al. (2004) for the finite circular cylinder.

The power spectra along the heights of the cylinders are found in Figures 4.6 to 4.13: Figures 4.6 and 4.7 contain the spectra for AR = 9, Figures 4.8 and 4.9 contain the spectra for AR = 7, Figures 4.10 and 4.11 contain the spectra for AR = 5, while Figures 4.12 and 4.13 contain the spectra for AR = 3.

It should be noted that the sharp, high-frequency peaks seen in some of the power spectra are the result of electronic noise; these peaks are present in the power spectra even when the wind tunnel flow is turned off. A pair of small, low-frequency peaks is also seen in some of the power spectra measured close to the free end. These peaks are attributed to other flow phenomena in the wind tunnel freestream, and are unrelated to the flow around the cylinder and splitter plate. These peaks are found in the power spectra when the air is flowing but no cylinder is present.

4.4.1 Power Spectra along the Height for AR = 9

The power spectra for the cylinder of AR = 9 are shown in Figures 4.6 and 4.7 for the x/D = 3 (behind the cylinder) and x/D = 3+ L/D (downstream of the splitter plate) measurement positions, respectively.

From the power spectra in Figures 4.6a and 4.7a, for the cylinder of AR = 9 with no splitter plate (L/D = 0), tall narrow peaks are present at the mid-height region of the cylinder,

weak peaks exist close to the free end, and vortex shedding is almost non-existent for the region next to the ground plane. This behaviour of the spectral peak along the cylinder height is consistent with the earlier results of Sumner et al. (2004).

Figures 4.6b and 4.7b show the spectra for L/D = 1, AR = 9. The general profiles for the mid-height region are similar to that for no splitter plate (Figures 4.6a and 4.7a) only that the peaks are somewhat shorter and more broad-banded in nature. Again, no shedding of vortices occurs close to the free end or the ground plane.

At the mid-height region for L/D = 1.5, it can be seen from Figure 4.6c that the peak at x/D = 3 is very short and broad-banded. In Figure 4.7c, the results are similar only the peaks around the mid-height region are not as broad. For both measurement positions, no peaks are observed close to the ground plane or free end of the cylinder.

For L/D = 2, vortex shedding peaks are found in the power spectra at x/D = 3 (Figure 4.6d) for positions from z/D = 1.5 – 8.0, but are absent for positions close to the ground plane or free end of the cylinder. Further downstream (Figure 4.7d), the main difference is that the peaks are smaller. Similar results are seen for L/D = 3 (Figures 4.6e and 4.7e).

For the two longest splitter plates, L/D = 5 (Figures 4.6f and 4.7f) and L/D = 7 (Figures 4.6g and 4.7g), the absence of vortex shedding is noted with the absence of peaks.

4.4.2 Power Spectra along the Height for AR = 7

The power spectra for the cylinder of AR = 7 are shown in Figures 4.8 and 4.9 for the x/D = 3 (behind the cylinder) and x/D = 3+ L/D (downstream of the splitter plate) measurement positions, respectively. For the case of no splitter plate (Figures 4.8a and 4.9a), tall narrow peaks are present in the mid-height region of the cylinder; the peaks here are not as tall as for AR = 9.

The behaviour at the free end and near the ground plane is similar to that observed for $L/D = 0$ for AR = 9 (Figures 4.6a and 4.7a). For the splitter plates of $L/D = 1$ (Figures 4.8b and 4.9b) and $L/D = 1.5$ (Figures 4.8c and 4.9c), the behaviour of the power spectra are similar to what was observed for the cylinder of AR = 9 (see Section 4.4.1).

For the splitter plate of $L/D = 2$ (Figures 4.8d and 4.9d), around the mid-height region, it can be seen that while there was strong vortex shedding for the upstream measurement position ($x/D = 3$, Figure 4.8d) indicated by the presence of the sharp peaks, there was suppression of vortex formation for the position further downstream ($x/D = 3 + L/D$, Figure 4.9d). No vortex shedding was recorded for both x positions close to the ground plane, and the upstream x position close to the free end, but there was vortex shedding recorded for the x position further downstream close to the free end.

Power spectra behavioral patterns for the three longest splitter plates, $L/D = 3$ (Figures 4.8e and 4.9e), $L/D = 5$ (Figures 4.8f and 4.9f), and $L/D = 7$ (Figures 4.8g and 4.9g), are somewhat similar to that of $L/D = 2$ shown in Figures 4.8d and 4.9d. At $x/D = 3$, vortex shedding peaks are seen in the power spectra near the mid-height region; however, downstream of the splitter plate, these peaks are almost completely suppressed. No vortex shedding is detected for regions close to the ground plane and free end at $x/D = 3$, as opposed to the peaks present for these regions for the x positions further downstream.

4.4.3 Power Spectra along the Height for AR = 5

The power spectra for the cylinder of AR = 5 are shown in Figures 4.10 and 4.11 for the $x/D = 3$ (behind the cylinder) and $x/D = 3 + L/D$ (downstream of the splitter plate) measurement positions, respectively.

For the case of no splitter plate (Figures 4.10a and 4.11a), tall, narrow peaks are detected along the entire height of the cylinder. With the addition of the smallest splitter plate (L/D = 1), however, these peaks become more broad-banded at x/D = 3 (Figure 4.10b) and even more so further downstream at x/D = 3 + L/D (Figure 4.11b). In both of the above cases, vortex shedding peaks are almost non-existent close to the ground plane.

For the splitter plates of L/D = 1.5, 2, and 3, close to the cylinder (at x/D = 3, Figures 4.10c, 4.10d, and 4.10e, respectively) vortex shedding peaks are seen from the mid-height region to the free end of the cylinder, while no vortex shedding occurs close to the ground plane. Downstream of the splitter plate, however, at x/D = 3 + L/D (Figures 4.11c, 4.11d, and 4.11e) vortex shedding peaks are absent both near the ground plane and in the mid-height region, yet vortex shedding peaks still appear close to the free end.

The spectra and peaks for the splitter plates of L/D = 5 and L/D = 7, at the x/D = 3 measurement position (shown in Figures 4.10f and 4.10g, respectively) are similar in profile to what was observed for the plates of L/D = 1.5, 2 and 3 at x/D = 3. The difference for these two sets of splitter plates occurs mainly at the downstream hot-wire measurement position (x/D = 3 + L/D). As can be seen from Figures 4.11f and 4.11g, vortex shedding peaks are present from the mid-height region to the free end while there is suppression of vortex shedding for regions close to the ground plane.

4.4.4 Power Spectra along the Height for AR = 3

The power spectra for the cylinder of AR = 3 are shown in Figures 4.12 and 4.13 for the x/D = 3 (behind the cylinder) and x/D = 3+ L/D (downstream of the splitter plate) measurement positions, respectively.

The spectra for the case of no splitter plate (L/D = 0, Figures 4.12a and 4.13a) show similarities to the cylinder of AR = 5 (Figures 4.10a and 4.11a). Strong vortex shedding peaks are seen along almost the entire height of the cylinder. This result contrasts with the results of Sumner et al. (2004) for a finite circular cylinder of AR = 3, where the vortex shedding peaks were much weaker. The stronger peaks in the present study might be attributed to the thinner boundary layer on the ground plane (δ/D = 1.5 here, compared to δ/D = 2.6 in Sumner et al. (2004)). The influence of δ/D or δ/H on the flow around a finite circular cylinder has not been extensively studied, however.

For the shortest splitter plate, of L/D = 1, peaks are found in the power spectra at the mid-height and free end regions of the cylinder at the x/D = 3 measurement position (Figure 4.12b), with some traces of vortex shedding close to the ground plane. These peaks are much more broad-banded compared to the case of no splitter plate (Figure 4.12a). This same behaviour is repeated for all the other splitter plates at the x/D = 3 measurement position (see Figures 4.12c, 4.12d, 4.12e, 4.12f, and 4.12g).

At the measurement position downstream of the splitter plate (x/D = 3 + L/D, Figures 4.13b, 4.13c, 4.13d, 4.13e, 4.13f, and 4.13g), no peaks exist in the spectra near the ground plane and mid-height regions, and the only peaks evident are found close to the free end. This "movement" of the vortex shedding peaks towards the free end (the upper part of the wake) is similar to what was found for the cylinder of AR = 5 (discussed in Section 4.4.3).

4.4.5 Further Discussion

For the reference case, which is the case of when no splitter plate was attached (L/D = 0), vortex shedding occurred for all four cylinders. The behaviour of the higher aspect ratio

cylinders is similar (AR = 9 and 7), while that of the smaller aspect ratio cylinders (AR = 5 and 3) is also similar but distinct from AR = 9 and 7. This distinct behaviour for the cylinders of AR = 5 and 3 may be related to the critical aspect ratio, which lies between AR = 5 and AR = 3 in the present experiments.

For the case of no splitter plate ($L/D = 0$), the behaviour of the power spectra were, for the most part, comparable to the earlier results of Sumner et al. (2004). In their study, they found a single Strouhal number of St ≈ 0.16 independent of the z-position or the aspect ratio of the cylinder. In the present study, there was only a very small variability in the Strouhal number with aspect ratio, with St = 0.17, 0.16, 0.16 and 0.16 for AR = 9, 7, 5 and 3, respectively. Considering the shape of the power spectra, they also noted a variation in the strength of the peak along the height of the cylinder, similar to what was recorded during the course of the present experiments, and broad-banded peaks were observed for the region close to the free end and ground plane as opposed to those around the mid-height region, where taller, narrower peaks were recorded, similar behaviour was also observed in other experiments by Okamoto and Yagita (1973), Okamoto (1991) and Okamoto and Sunabashiri (1992).

At the streamwise position of $x/D = 3$, no vortex shedding occurred near the free end and close to the ground plane for AR = 9 for the splitter plates of $L/D = 1$, 1.5, 2 and 3, but vortex shedding was recorded around the mid-height region. Suppression of vortex shedding occurred for the splitter plates of $L/D = 5$ and 7. Similar behaviour was observed for the other streamwise position as well ($x/D = 3 + L/D$), the only difference being that less vortex shedding was recorded for the position further downstream ($x/D = 3 + L/D$).

The AR = 7 cylinder exhibited similar characteristics to the AR = 9 cylinder. With splitter plates of $L/D = 1$, 1.5, 2, 3 and 5 mounted behind the cylinder, at the streamwise

measurement position of $x/D = 3$, no vortex shedding occurred close to the free end and near the ground plane, but there was vortex shedding detected at the mid-height region. The $L/D = 7$ splitter plate, however, led to complete suppression of vortex shedding. For the measurement position further downstream ($x/D = 3 + L/D$), suppression of vortex shedding was observed for all the splitter plates except for $L/D = 1$ and 1.5 (the two shortest plates tested).

For the cylinder of AR = 5, at the $x/D = 3$ measurement position, shedding of vortices took place all along the height of the cylinder except very close to the ground plane, for the splitter plates of $L/D = 1$, 5 and 7. However for the other measurement position ($x/D = 3 + L/D$), with splitter plates, shedding of vortices was observed at the free end of the cylinder, no shedding of vortices was found at the mid-height position for $L/D = 1.5$, 2 and 3, and no shedding of vortices was found near the ground plane except for the $L/D = 1$ splitter plate.

For the AR = 3 and 5 cylinders, the free end exhibited similar characteristics for both streamwise positions and also around the mid-height region with the use of splitter plates.

CHAPTER FIVE

CONCLUSIONS AND RECOMMENDATIONS

5.1 Conclusions

Locating a splitter plate in the near-wake region of a two-dimensional bluff body such as an "infinite" circular cylinder, is an effective means of passively controlling various aspects of vortex formation and shedding, and also the drag force. A lot of work has been done in regard to the use of splitter plates in trying to modify the wake flow characteristics of bluff bodies, and all the work points to the fact that the characteristics of the wake downstream of a bluff-body can be altered by placing a splitter plate as an impediment on the wake centerline downstream of the bluff-body, where the impact is the most felt. The size of the vortex formation region and near-wake region, and the way the shear layers interact with each other, are modified by varying the splitter plate length, L/D, thickness, T/D, gap between the base of the cylinder and the leading edge of the plate, G/D, and the lateral position of the plate relative to the wake centreline, y/D.

In the present study, the effect of a wake-mounted splitter plate was investigated for the flow around a surface-mounted finite-height circular cylinder. The flow was studied experimentally in a low-speed wind tunnel using a force balance and single-component hot-wire anemometry. Compared to the case of the infinite circular cylinder, the effectiveness of a splitter plate for a finite circular cylinder has not been extensively reported in the open literature. The flow around a finite circular cylinder is strongly influenced by the cylinder aspect ratio, AR, and

the flow field is more complex than that of the infinite circular cylinder. Four circular cylinders of aspect ratios AR = 9, 7, 5 and 3 were tested over a Reynolds number range of Re = 1.9×10^4 to 8.2×10^4. The cylinders were partially immersed in a flat-plate turbulent boundary layer, where the range of boundary layer thickness relative to the cylinder diameter was δ/D = 1.4 to 1.5. The splitter plates had lengths, relative to the cylinder diameter, of L/D = 1, 1.5, 2, 3, 5 and 7, thicknesses ranging from T/D = 0.10 to 0.15, and were the same height as the cylinder being tested, H_{SP}/H = 1. Measurements were made of the mean drag force coefficient, C_D, the Strouhal number, St, and power spectra at the mid-height position, and the Strouhal number and power spectra along the cylinder height.

Compared to the case of an infinite circular cylinder, the splitter plate is less effective at reducing the mean drag force coefficient of a finite circular cylinder. For the larger aspect ratios, AR = 9 and 7, the most effective splitter plate lengths for reducing the mean drag coefficient were L/D = 1, 1.5, 2, and 3 (the shorter plates). For the smaller aspect ratios, AR = 5 and 3, however, the most effective splitter plate lengths for drag reduction were L/D = 5 and 7 (the longer plates). The largest drag reduction was obtained for the cylinder of AR = 9 and splitter plates of L/D = 1 to 3, while minimal drag reduction occurred for the shorter cylinders.

In general, based on the thesis results, it can be concluded that a suitably selected splitter plate (of particular length ratio, L/D) can be used to reduce the mean drag force coefficient of a surface-mounted finite-height circular cylinder. However, it is not as effective a passive flow control device compared to the case of the infinite circular cylinder. This difference may be attributed, in part, to the increased complexity and three-dimensionality of the flow field for the finite circular cylinder.

For all four finite circular cylinders, the splitter plates were effective at reducing the magnitude of the Strouhal number, weakening vortex shedding, or suppressing vortex shedding, depending on the specific combination of AR and L/D. For the cylinder of AR = 9, a splitter plate of L/D = 1 reduced the magnitude of the Strouhal number at the mid-height position but did not suppress vortex shedding, while the splitter plates of L/D = 5 and 7 completely suppressed vortex shedding. For the cylinder of AR = 7, the splitter plates of L/D = 1 and 1.5 reduced the magnitude of the Strouhal number but did not suppress vortex shedding, while the splitter plates of L/D = 2 to 7 completely suppressed vortex shedding. For AR = 5, vortex shedding suppression at mid-height occurred for the intermediate splitter plates of L/D = 1.5, 2 and 3 only; for the other splitter plates, of L/D = 1, 5 and 7, a reduction in Strouhal number occurred. In contrast, for AR = 3 (which is below the critical aspect ratio), vortex shedding suppression occurred for all splitter plates.

Measurements of Strouhal number along the height of each cylinder was examined for three regions: the region close to the free-end, the region around the mid-height of the finite cylinder, and the region close to the ground plane. For the most part, broad-banded peaks in the power spectra were noticed for regions close to the free end and close to the ground plane, as opposed to those around the mid-height section, where taller, narrower vortex shedding peaks were recorded. Of course, some splitter plates led to complete suppression of vortex shedding along the height of the cylinder, indicated by an absence of peaks in the power spectra. For AR = 9 and 7, similar behaviours of the power spectra were observed for the two streamwise measurement positions (x/D = 3 and x/D = 3 + L/D), the only difference being that weaker vortex shedding peaks were recorded for the position further downstream, beyond the trailing edge of the splitter plate. Total suppression of vortex shedding from the cylinders of AR = 9 and 7

occurred for the longest plate (L/D = 7). A general observation was that the vortex shedding behaviour of the higher aspect ratio cylinders was similar (AR = 9 and 7), while that of the smaller aspect ratio cylinders (AR = 5 and 3) also had some similarities but was distinct from the cylinders of AR = 9 and 7.

In general, the results of the thesis research indicate that a wake-mounted splitter plate (of suitable length, L/D) can be effective at controlling, weakening, or suppressing vortex shedding from a surface-mounted finite-height circular cylinder.

5.2 Recommendations

The scope of this research project was limited to varying the length of the splitter plate (L/D) and studying its influence on the mean drag force coefficient (C_D) and Strouhal number (St) for finite cylinders of different aspect ratios (AR). From the literature, L/D is the most prominent variable governing the effectiveness of a splitter plate, however there are other parameters that might be considered in future work. These include: (i) varying the gap (G/D) between the base of the cylinder and the leading edge of the plate, (ii) varying the height of the splitter plate relative to the height of the cylinder (H_{SP}/H), to see if a shorter plate has the same effectiveness, (iii) varying the lateral position of the plate (y/D), (iv) placing the splitter plate upstream of the cylinder, (v) investigating the simultaneous usage of two or more splitter plates (multiple plates), and (vi) using slip/rotating splitter plates that can respond to the unsteadiness and direction changes of the flow.

In terms of different experimental techniques, use of a force balance with improved accuracy would allow the effectiveness of the splitter plate to be better judged at lower Reynolds numbers and small aspect ratios (where the measured forces, and changes in the forces, are

small). The well refined force balance would also enable the measurement of lift. Use of flow visualization or whole-field velocity measurement techniques, such as PIV, would also be valuable to gain a physical understanding of the effects of the splitter plate.

Differences were noticed in the data generated for the two streamwise positions ($x/D = 3$ and $x/D = 3 + L/D$); this therefore means that the location at which the probe is positioned, amongst other factors, determines the nature of the data recorded. Hence, variation in the probe position for future experiments is recommended in order to observe the behaviour of the flow in such locations.

REFERENCES

Adaramola, M.S., Akinlade, O.G., Sumner, D., Bergstrom, D.J., Schenstead, A.J., 2006. Turbulent wake of a finite circular cylinder of small aspect ratio. Journal of Fluids and Structures 22, 919–928.

Akilli, H., Karakus, C., Akar, A., Sahin, B., Tumen, F.N., 2008. Control of Vortex shedding of circular cylinder in shallow water flow using an attached splitter plate. ASME Journal of Fluids Engineering 130, 041401 (11 pp.).

Akilli, H., Sahin, B., Tumen, F.N., 2005. Suppression of vortex shedding of circular cylinder in shallow water by a splitter plate. Flow Measurement and Instrumentation 16, 211–219.

Ali, M.S.M., Doolan, C.J., Wheatley, V., 2011. Low Reynolds number flow over a square cylinder with a splitter plate. Physics of Fluids 23, 033602 (12 pp.).

Anderson, E.A., Szewczyk, A.A., 1997. Effects of a splitter plate on the near wake of a circular cylinder in 2 and 3-dimensional flow configurations. Experiments in Fluids 23, 161–174.

Apelt, C.J., West, G.S., 1975. The effects of wake splitter plates on bluff-body flow in the range $10^4 < R < 5\times10^4$: Part 2. Journal of Fluid Mechanics 71, 145–160.

Apelt, C.J., West, G.S., Szewczyk, A.A., 1973. The effects of wake splitter plates on the flow past a circular cylinder in the range $10^4 < R < 5\times10^4$. Journal of Fluid Mechanics 61, 187–198.

Bearman, P.W., 1965. Investigation of the flow behind a two-dimensional model with a blunt trailing edge and fitted with splitter plates. Journal of Fluid Mechanics 21, 241–256.

Bearman, P.W., 1967. The effect of base bleed on the flow behind a two-dimensional model with a blunt trailing edge. The Aeronautical Quarterly 18, 207–224.

Boisaubert, N., Texier, A., 1998. Effect of a splitter plate on the near-wake development of a semi-circular cylinder. Experimental Thermal and Fluid Science 16, 100–111.

Cardell, G.S., 1993. Flow past a circular cylinder with a permeable splitter plate. Ph.D. Thesis, California Institute of Technology.

Cimbala, J.M., Garg, S., 1991. Flow in the wake of a freely rotatable cylinder with splitter plate. AIAA Journal 29, 1001–1003.

Cimbala, J.M, Leon, J., 1996. Drag of freely rotatable cylinder/splitter-plate body at subcritical Reynolds number. AIAA Journal 34, 2446–2448.

Coutanceau, M., Defaye, J., 1991. Circular cylinder wake configurations: A flow visualization survey. Applied Mechanics Reviews 44, 255–305.

Dehkordi, B.G., Jafari, H.H., 2010. On the suppression of vortex shedding from circular cylinders using detached short splitter-plates. ASME Journal of Fluids Engineering 132, 044501, 4 pp.

Delaunay, Y., Kaiktsis, L., 2001. Control of circular cylinder wakes using base mass transpiration. Physics of Fluids 13, 3285–3302.

Farhadi, M., Sedighi, K, Fattahi, E., 2009. Effect of a splitter plate on flow over a semi-circular cylinder. Proceedings of the Institution of Mechanical Engineers, Part G: Journal of Aerospace Engineering 224, 321–330.

Gad-el-Hak, M., 2000. Flow control: passive, active, and reactive flow management. Cambridge, UK: Cambridge University Press.

Gerrard, J.H., 1978. The wakes of cylindrical bluff bodies at low Reynolds number. Philosophical Transactions of the Royal Society of London A 288, 351–382.

Guilmineau, E., Queutey, P., 2002. A numerical simulation of vortex shedding from an oscillating circular cylinder, Journal of Fluids and Structures 16, 773–794.

Hangan, H., Kim, J., 2003. Aerodynamic slot-control for 2D square prisms. Journal of Wind Engineering and Industrial Aerodynamics 91, 1847–1857.

Hasan, M.A.Z., Budair, M.O., 1994. Role of splitter plates in modifying cylinder wake flows. AIAA Journal 32, 1992–1998.

Hu, C., Koterayama, W., 1994. Numerical study on a two-dimensional circular cylinder with a rigid and an elastic splitter plate in uniform flow. International Journal of Offshore and Polar Engineering 4, 193–199.

Hwang, J.Y., Yang, K.S., 2007. Drag reduction on a circular cylinder using dual detached splitter plates. Journal of Wind Engineering and Industrial Aerodynamics 95, 551–564.

Hwang, J.Y., Yang, K.S., Sun, S.H., 2003. Reduction of flow-induced forces on a circular cylinder using a detached splitter plate. Physics of Fluids 15, 2433–2436.

Igarashi, T., 1997. Drag reduction of a square prism by flow control using a small rod. Journal of Wind Engineering and Industrial Aerodynamics 69, 141–153.

Irwin, P.A., 2008. Bluff body aerodynamics in wind engineering. Journal of Wind Engineering and Industrial Aerodynamics 96, 701–712.

Kawamura, T., Hiwada, M., Hibino, T., Mabuchi, T., Kumada, M., 1984. Flow around a finite circular cylinder on a flat plate. Bulletin of the JSME 27, 2142–2150.

Koutmos, P., Papailiou, D., Bakrozis, A., 2004. Experimental and computational study of square cylinder wakes with two-dimensional injection into the base flow region. European Journal of Mechanics-B/Fluids 23, 353–365.

Kwon, K., Choi, H., 1996. Control of laminar vortex shedding behind a circular cylinder using splitter plates. Physics of Fluids 8, 479–486.

Lee, L.W., 1997. Wake structure behind a circular cylinder with a free end. Proceedings of the Heat Transfer and Fluid Mechanics Institute, pp. 241–251.

Lee, S.J., Kim, H.B., 1997. The effect of surface protrusions on the near wake of a circular cylinder. Journal of Wind Engineering and Industrial Aerodynamics 69, 351–361.

Lee, S.J., Lee, S.I., Park, C.W., 2004. Reducing the drag on a circular cylinder by upstream installation of a small control rod. Fluid Dynamics Research 34, 233–250.

Li, Z., Navon, I.M., Hussaini, M.Y., Le Dimet, F.-X., 2003. Optimal control of cylinder wakes via suction and blowing, Computers and Fluids 32, 149–171.

Mansingh, V., Oosthuizen, P.H., 1990. Effects of splitter plates on the wake flow behind a bluff body. AIAA Journal 28, 778–783.

Mittal, S., 2003. Effect of a ‘‘slip’’ splitter plate on vortex shedding from a cylinder. Physics of Fluids 15, 817–820.

Morkovin, M.V., 1964. Flow around circular cylinder – a kaleidoscope of challenging fluid phenomena. Symposium on Fully Separated Flows (Hansen, A.G, ed.), ASME Fluids Engineering Division Conference, Philadelphia, PA, May 18-20, 1964, pp. 102–118.

Nakamura, Y., 1996. Vortex shedding from bluff bodies with splitter plates. Journal of Fluids and Structures 10, 147–158.

Nakayama, A., Noda, H., 2000. LES simulation of flow around a bluff-body fitted with a splitter plate. Journal of Wind Engineering and Industrial Aerodynamics 85, 85–96.

Naudascher, E., Rockwell, D., 1994. Flow Induced Vibrations: An Engineering Guide. Rotterdam: Balkema Press.

Okamoto, S., 1991. Flow past circular cylinder of finite length placed on ground plane. Transactions of the Japan Society for Aeronautical and Space Sciences 33, 234–246.

Okamoto, S., Sunabashiri, Y., 1992. Vortex shedding from a circular cylinder of finite length placed on a ground plane. ASME Journal of Fluids Engineering 144, 512–521.

Okamoto, T., Yagita M., 1973. The experimental investigation on the flow past a circular cylinder of finite length placed normal to the plane surface in a uniform stream. Bulletin of the JSME 16, 805–814.

Ozono, S., 1999. Flow control of vortex shedding by a short splitter plate asymmetrically arranged downstream of a cylinder. Physics of Fluids 11, 2928–2934.

Ozono, S., 2003. Vortex suppression of the cylinder wake by deflectors. Journal of Wind Engineering and Industrial Aerodynamics 91, 91–99.

Park, C.W., Lee S.J., 2004. Effects of free-end corner shape on flow structure around a finite cylinder. Journal of Fluids and Structures 19, 141–158.

Park, D.S., Ladd, D.M., Hendricks, E.W., 1994. Feedback control of von Kármán vortex shedding behind a circular cylinder at low Reynolds number, Physics of Fluids 6, 2390–2405.

Prasad, A., Williamson, C.H.K., 1997. The instability of the shear layer separating from a bluff-body. Journal of Fluid Mechanics 333, 375–402.

Rathakrishnan, E., 1999. Effect of splitter plate on bluff-body drag. AIAA Journal 37, 1125–1126.

Roshko, A., 1954. On the drag and shedding frequency of two-dimensional bluff bodies. NACA TN 3169.

Roshko, A., 1955. On the wake and drag of bluff bodies. Journal of Aeronautical Science 22, 124-132.

Roussopoulos, K., 1993. Feedback control of vortex shedding at low Reynolds numbers. Journal of Fluid Mechanics 248, 267–296.

Sakamoto, H., Arie, M., 1983. Vortex shedding from a rectangular prism and a circular cylinder placed vertically in a turbulent boundary layer. Journal of Fluid Mechanics 126, 147–165.

Sakamoto, H., Haniu, H., 1994. Optimal suppression of fluid forces acting on a circular cylinder. ASME Journal of Fluids Engineering 116, 221–227.

Sakamoto, H., Oiwake, S., 1984. Fluctuating forces on a rectangular prism and a circular cylinder placed vertically in a turbulent boundary layer. ASME Journal of Fluids Engineering 106, 160–166.

Sakamoto, H., Tan, K., Haniu, H., 1991. An optimum suppression of fluid forces by controlling a shear layer separated from a square prism. ASME Journal of Fluids Engineering 113, 183–189.

Schumm, M., Berger, E., Monkewitz, P.A., 1994. Self-excited oscillations in the wake of two dimensional bluff bodies and their control. Journal of Fluid Mechanics 271, 17–32.

Shukla, S., Govardhan, R.N., Arakeri, J.H., 2009. Flow over a cylinder with a hinged-splitter plate. Journal of Fluid and Structures 25, 713–720.

Smits, A.J., 2000. A Physical Introduction to Fluid Mechanics. New York: John Wiley.

Strykowski, P.J., Sreenivasan, K.R., 1990. On the formation and suppression of vortex shedding at low Reynolds numbers, Journal of Fluid Mechanics 218, 71–107.

Sumer, B.M., Fredsøe, J., 1997. Hydrodynamics around Cylindrical Structures, London: World Scientific.

Sumner, D., Heseltine, J.L., Dansereau, O.J.P., 2004. Wake structure of a finite circular cylinder of small aspect ratio. Experiments in Fluids 37, 720–730.

Tanaka, S., Murata, S., 1999. An investigation of the wake structure and aerodynamic characteristics of a finite circular cylinder. JSME International Journal Series B: Fluids and Thermal Engineering 42, 178–187.

Tiwari, S., Chakraborty, D., Biswas, G., Panigrahi, P.K., 2005. Numerical prediction of flow and heat transfer in a channel in the presence of a built-in circular tube with and without an integral wake splitter. International Journal of Heat and Mass Transfer 48, 439–453.

Unal, M.F., Rockwell, D., 1987. On vortex formation from a cylinder. Part 2. Control by splitter-plate interference. Journal of Fluid Mechanics 190, 513–529.

Williamson, C.H.K., 1996. Vortex dynamics in the cylinder wake. Annual Review of Fluid Mechanics 28, 477–539.

Wu, J., Shu, C., 2011. Numerical study of flow characteristics behind a stationary circular cylinder with a flapping plate. Physics of Fluids 23, 073601 (17 pp.).

Xu, J.C., Sen, M., Gad-el-Hak, M., 1993. Dynamics of a rotatable cylinder with splitter plate in uniform flow. Journal of Fluids and Structures 7, 401–416.

Yucel, S.B., Cetiner, O., Unal, M.F., 2010. Interaction of circular cylinder wake with a short asymmetrically located downstream plate. Experiments in Fluids 49, 241–255.

Zdravkovich, M.M., 1981. Review and classification of various aerodynamic and hydrodynamic means for suppressing vortex shedding. Journal of Wind Engineering and Industrial Aerodynamics 7, 145–189.

Zdravkovich, M.M., 1997. Flow around Circular Cylinders. Vol. 1: Fundamentals. Oxford: Oxford University Press.

Zdravkovich, M.M., 2003. Flow around Circular Cylinders. Vol. 2: Applications. Oxford: Oxford University Press.

APPENDIX A

A.1 Hot-Wire Probe

Hot-wire anemometers are instruments used for the measurement of velocity in turbulent flows (Bruun, 1995). They have an exposed electrically heated wire. The cooling effect exerted by the air flow around the wire extracts heat from the exposed electrically heated wire. The instrument works by measuring the current drawn through the hot wire in order to maintain the wire at a fixed temperature, to compensate for the convective heat transfer (cooling) process occurring due to exposure of the wire to fluid flow.

A six-channel Dantec Streamline constant-temperature anemometer, and a single-component normal-wire hot-wire probe (Dantec 55P11), were used for the present thesis research. A single normal hot-wire responds to a single velocity component, which in the present research was the streamwise velocity, $u(t)$. Turbulent flows are characterized by velocity fluctuations in time and space, and the hot-wire has a high frequency response that can measure turbulent velocity fluctuations.

The output of the hot-wire anemometer is a voltage-time signal, $E(t)$. Through calibration, a relationship is obtained for velocity, u, as a function of voltage, E, making it possible to get the final output as a velocity-time signal, $u(t)$. A sample velocity-time signal from the wake of a circular cylinder is shown in Figure A.1a. In this case, a hot-film sensor (which operates on the same principle as a hot-wire) was located at $x/D = 5.0$, $y/D = 0.8$ in the wake of an "infinite" circular cylinder (of diameter $D = 16$ mm and aspect ratio AR = 16). The

cylinder was tested in a water tunnel, with a freestream velocity of U = 220 mm/s, a cylinder Reynolds number of Re = 2.2×10^3, a 20-Hz sampling frequency, and a sampling time ranging from 300 to 600 s. A TSI Model 1231 conical hot-film sensor was used with a TSI FlowPoint Model 1500 anemometer (Sumner, 1999).

A.2 Power Spectrum

A power spectrum can simply be considered as a "histogram of frequencies". The power spectrum is used to determine the frequency content of a time signal and show the relative importance of the different frequencies present in it.

To obtain a power spectrum, a time-series of data is transformed into the frequency domain (using a Fourier transform). The Fourier transform is a way of expressing a signal as a sum of sine and cosine waves. The power spectral density function describes the energy content of the fluctuating velocity field as a function of frequency (Bendat and Piersol, 1966), and it may be thought of as the energy at that frequency (Tennekes and Lumley, 1972). One way to obtain the spectral density is to use the autocorrelation. The correlation of the values of the velocity at a given location at two different times is called its autocorrelation; its coefficient is defined as follows.

$$\rho(\tau) = \frac{\frac{1}{t}\int_0^t u(t)u(t+\tau)dt}{\overline{u^2}} \tag{A.1}$$

The autocorrelation coefficient can also be obtained from the power spectral density as follows.

$$\rho(\tau) = \int_{-\infty}^{\infty} e^{i\tau\omega} S(\omega) d\omega \tag{A.2}$$

The Fourier transform $S(\omega)$ of $\rho(\tau)$ is called the power spectral density (Tennekes and Lumley, 1972), where ω is the frequency and τ is the time difference of the velocity. The spectral density is the Fourier transform of the autocorrelation, i.e.

$$S(\omega) = \frac{1}{2\pi}\int_{-\infty}^{\infty} e^{-i\tau\omega}\rho(\tau)d\tau \,. \tag{A.3}$$

An interpretation of the spectral density is that it represents the mean square value of the Fourier component of the fluctuating velocity signal, and as such it gives the energy distribution in frequency space.

An example of such for the wake of a circular cylinder is shown in Figure A.1b; this is the corresponding power spectrum to the velocity-time signal shown in Figure A.1a. The highest peak in the power spectrum (the frequency with the highest value of power) denotes the vortex shedding frequency for the circular cylinder (here, in Figure A.1b, the frequency axis of the power spectrum is expressed in dimensionless form as the Strouhal number, St = fD/U, where f is the frequency).

In the present thesis experiments, LabVIEW was used to compute the power spectrum of the hot-wire's velocity-time signal. The "FFT Power Spectrum VI" (virtual instrument) was used for this purpose. The FFT Power Spectrum VI completes the following steps to compute power spectrum: (i) inputs a time-series of velocity data measured by the hot-wire probe; (ii) performs an autocorrelation on the data from step (i) above; (iii) uses a Fast Fourier Transform (FFT) on the autocorrelation to get the spectrum; (iv) gives the energy in terms of frequency; (v) searches for the dominant peak in the spectrum and reports its value. In the thesis research, 100 individual spectra were averaged to produce the final power spectrum.

A.3 References

Bendat, J.S., Piersol, A.G., 1966. Measurement and Analysis of Random Data. New York: John Wiley.

Bruun, H.H., 1995. Hot-Wire Anemometry, Principles and Signal Analysis. New York: Oxford University Press.

Sumner, D., 1999. Circular Cylinders in Cross-Flow. Ph.D. Thesis, Mechanical Engineering, McGill University, Montreal, Canada.

Tennekes, H., Lumley, J.L., 1972. A First Course in Turbulence. Massachusetts: The MIT Press.

TABLES

Table 1.1. Summary of selected experimental and numerical studies of two-dimensional bluff bodies with splitter plates. FV = flow visualization, PIV = particle image velocimetry.

	Cylinder/Body Parameters				Splitter Plate Parameters				Experimental/Numerical Approach and Parameters			
Researchers	**Shape**	**Reynolds Number, Re**	**Aspect Ratio, AR**	**Solid Blockage Ratio**	**Length, L/D**	**Gap, G/D**	**Thickness, T/D**	**Offset, y/D**	**Test Facility or Numerical Method**	**Freestream Turbulence Intensity**	**Measurement Technique or Numerical Method**	**Parameters Measured or Computed**
Akilli et al. (2005)	Circular cylinder	5×10^3–5.5×10^3	0.5	5%	1.0	0–2.0	0.016, 0.04, 0.08	0	Water channel	0.5%	PIV	St, velocity field
Akilli et al. (2008)	Circular cylinder	6.3×10^3	0.5	5%	0.2–2.4	0	0.016, 0.04, 0.08	0	Water channel	N/A	PIV	Velocity field
Anderson and Szewczyk (1997)	Circular cylinder	5.7×10^3, 3.5×10^4–4.6×10^4	8, 16	8.3%, 5.8%	0–2.0	0	N/A	0	Wind tunnel	0.05%, 0.5%	Hot-wire, pressure, FV	St, C_{PB}, C_D
Apelt et al. (1973)	Circular cylinder	1×10^4–5×10^4	20.6	6%	≤ 2.0	0	0.031, 0.094	0	Water tunnel, wind tunnel		Hot-wire, pressure, FV	St, C_{PB}, C_D
Apelt and West (1975)	Circular cylinder	1×10^4–5×10^4	20.7	6%	2.0–7.0	0	0.094	0	Water tunnel, wind tunnel		Hot-wire, pressure, FV	St, C_{PB}
Bearman (1965)	Half ellipse prism	1.4×10^5, 2.6×10^5	N/A	3.1%	0–4.0	0	0.063	0	Wind tunnel	< 0.2%	Hot-wire	St, C_{PB}
Boisaubert and Texier (1998)	Semi-circular cylinder	200, 400	5.2	12.9%	1.0	0–1.0	0.063	0	Paraffin oil tank	N/A	FV	
Cimbala and Leon (1996)	Circular cylinder	2×10^4–8×10^4	11.8	4.5%	0–5.0	0.04	0.063	0	Wind tunnel			C_D
Dehkordi and Jafari (2010)	Circular cylinder	40, 100, 150	N/A	N/A	1.0	0–10.0	0.05	0–1.25	Num. method	N/A		St, C_D
Farhadi et al. (2009)	Semi-circular cylinder	100–500	N/A	N/A	1.0, 2.0	0–4.5	0	0	Num. method	N/A		C_D, C_L
Hasan and Budair (1994)	Circular cylinder, square prism	1.2×10^4–2.4×10^4	21.1	3.5%	0.8, 1.7, 4.2	0–6.0	0.039	0	Wind tunnel	< 0.1%	Hot-wire	St, C_{PB}
Hwang et al. (2003)	Circular cylinder	30, 100, 160	N/A	N/A	1.0	0–2.7	0	0	Num. method	N/A		St, C_{PB}, C_D
Hwang and Yang (2007)	Circular cylinder	30–160	N/A	N/A	1.0	0–15.0	0	0	Num. method	N/A		St
Kwon and Choi (1996)	Circular cylinder	80–160	N/A	N/A	2.3	0	0	0	Num. method	N/A		St
Mansingh and Oosthuizen (1990)	Rectangular prism	350–1.2×10^3	31.5	< 2%	1.0–3.0	0–9.0	0.016	0	Wind tunnel	0.25%	Hot-wire	St, C_{PB}, C_D
Mittal (2003)	Circular cylinder	100	N/A	N/A	0–4.8	0–4.8	0	0	Num. method	N/A		St, C_L, C_D
Nakamura (1996)	Circular cylinder, semi-circular cylinder, flat plate	300–5.3×10^3	N/A	N/A	0–15.0	0	0.1–0.3	0	Wind tunnel	0.2%	Hot-wire, pressure	St, C_{PB}
Rathakrishnan (1999)	Rectangular prism	5.8×10^4, 9.9×10^4	4.92	0.86%	0.25–3.0	0	0.013	0, 0.25	Wind tunnel	N/A		C_{PB}, C_D
Roshko (1954, 1955)	Circular cylinder, semi-circular cylinder, 90° wedge, flat plate	1.5×10^4	N/A	N/A	0, 1.1	0	N/A	0	Wind tunnel	N/A	Hot-wire, pressure	St, C_{PB}, C_D
Shukla et al. (2009)	Circular cylinder	800–1×10^4	13		0.75–7.0	0	0.006	0	Water tunnel	N/A	PIV	St
Yucel et al. (2010)	Circular cylinder	200, 400, 750	15		1.0	0–4.0	0.1	0–1.3	Water channel	N/A	PIV	St

Table 3.1: Summary of boundary layer parameters at the location of the cylinder (with the cylinder removed).

Freestream velocity U [m/s]	Boundary layer thickness δ [mm]	Displacement thickness δ^* [mm]	Momentum thickness θ [mm]	Shape factor $H = \delta^*/\theta$	Reynolds number based on momentum thickness Re_θ	δ/D	δ/H range
10	48	6.2	4.7	1.3	2.9×10^3	1.52	0.17 to 0.51
20	45	5.6	4.4	1.3	5.2×10^3	1.43	0.16 to 0.48
30	47	5.6	4.4	1.3	7.8×10^3	1.49	0.17 to 0.50
40	47	5.6	4.4	1.3	1.0×10^4	1.49	0.17 to 0.50

Table 4.1: Mean drag coefficient (C_D) values for Re ≈ 7.5×10^4 (U = 40 m/s).

L*/*D	**AR = 9** (Uncertainty ± 0.01)	**AR = 7** (Uncertainty ± 0.01)	**AR = 5** (Uncertainty ± 0.02)	**AR = 3** (Uncertainty ± 0.03)
0	0.91	0.80	0.79	0.76
1	0.80	0.83	0.78	0.73
1.5	0.81	0.77	0.77	0.76
2	0.80	0.78	0.77	0.75
3	0.80	0.77	0.78	0.73
5	0.83	0.78	0.75	0.70
7	0.90	0.80	0.76	0.71

Table 4.2: Strouhal number (St) values at mid-height behind the cylinder (hot-wire probe at $x/D = 3$, $y/D = 1.5$), for $\mathrm{Re} \approx 7.5\times10^4$ ($U = 40$ m/s). The uncertainty in St is estimated at ± 0.002.

L/D	**AR = 9**	**AR = 7**	**AR = 5**	**AR = 3**
0	0.163	0.160	0.154	0.161
1	0.133	0.126	0.126	0.141
1.5	0.090	0.091	0.131	0.159
2	0.180	0.184	0.141	0.172
3	0.152	0.131	0.134	0.186
5		0.121	0.136	0.192
7			0.147	0.178

Table 4.3: Strouhal number (St) values at mid-height downstream of the splitter plate's trailing edge (hot-wire probe at $x/D = 3 + L/D$, $y/D = 1.5$), for Re ≈ 7.5×10^4 ($U = 40$ m/s). The uncertainty in St is estimated at ± 0.002.

L*/*D	**AR = 9**	**AR = 7**	**AR = 5**	**AR = 3**
0	0.163	0.160	0.154	0.161
1	0.130	0.127	0.105	
1.5	0.155	0.140		
2	0.168			
3	0.147			
5			0.115	
7			0.125	

FIGURES

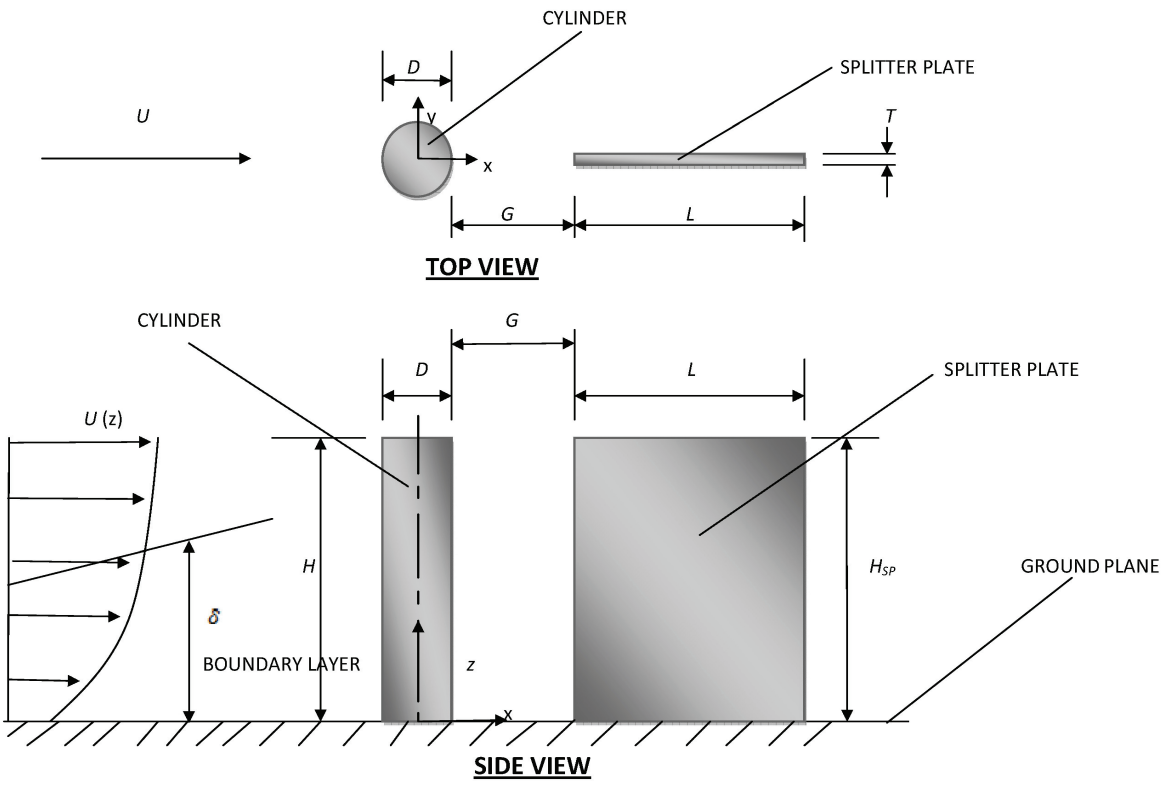

Figure 1.1: Schematic of a finite circular cylinder mounted normal to a ground plane with a splitter plate located on the wake centreline.

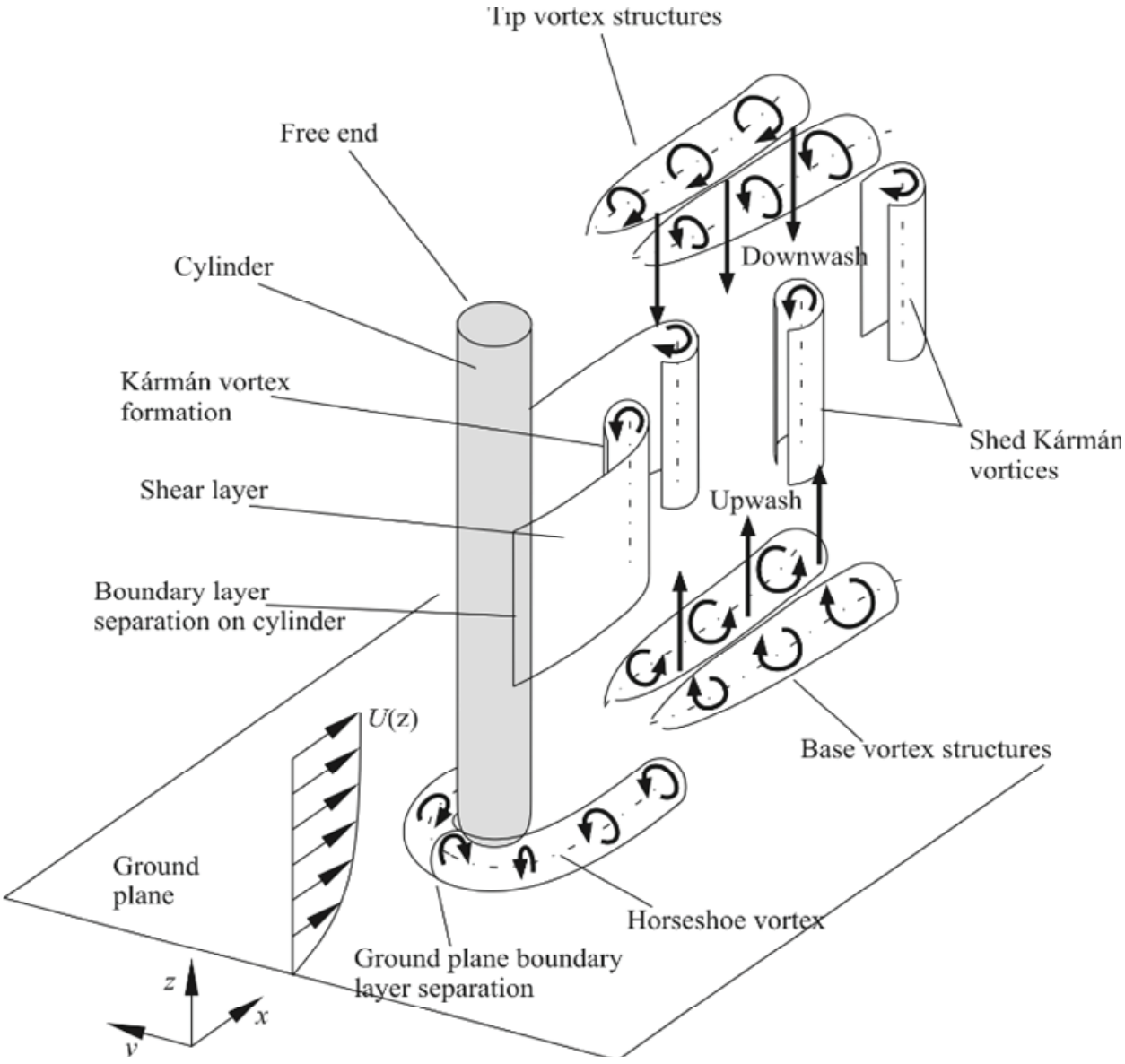

Figure 2.1: Schematic of the flow around a finite circular cylinder mounted normal to a ground plane (no splitter plate), showing the main vortex structures. (Figure reproduced here with the permission of D. Sumner.)

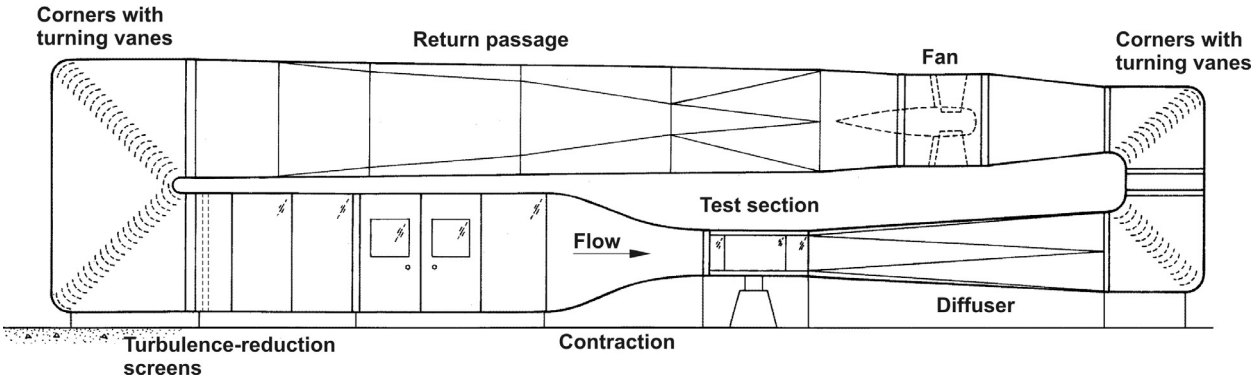

Figure 3.1: Schematic of the University of Saskatchewan's low-speed wind tunnel. (Figure reproduced here with the permission of D. Sumner.)

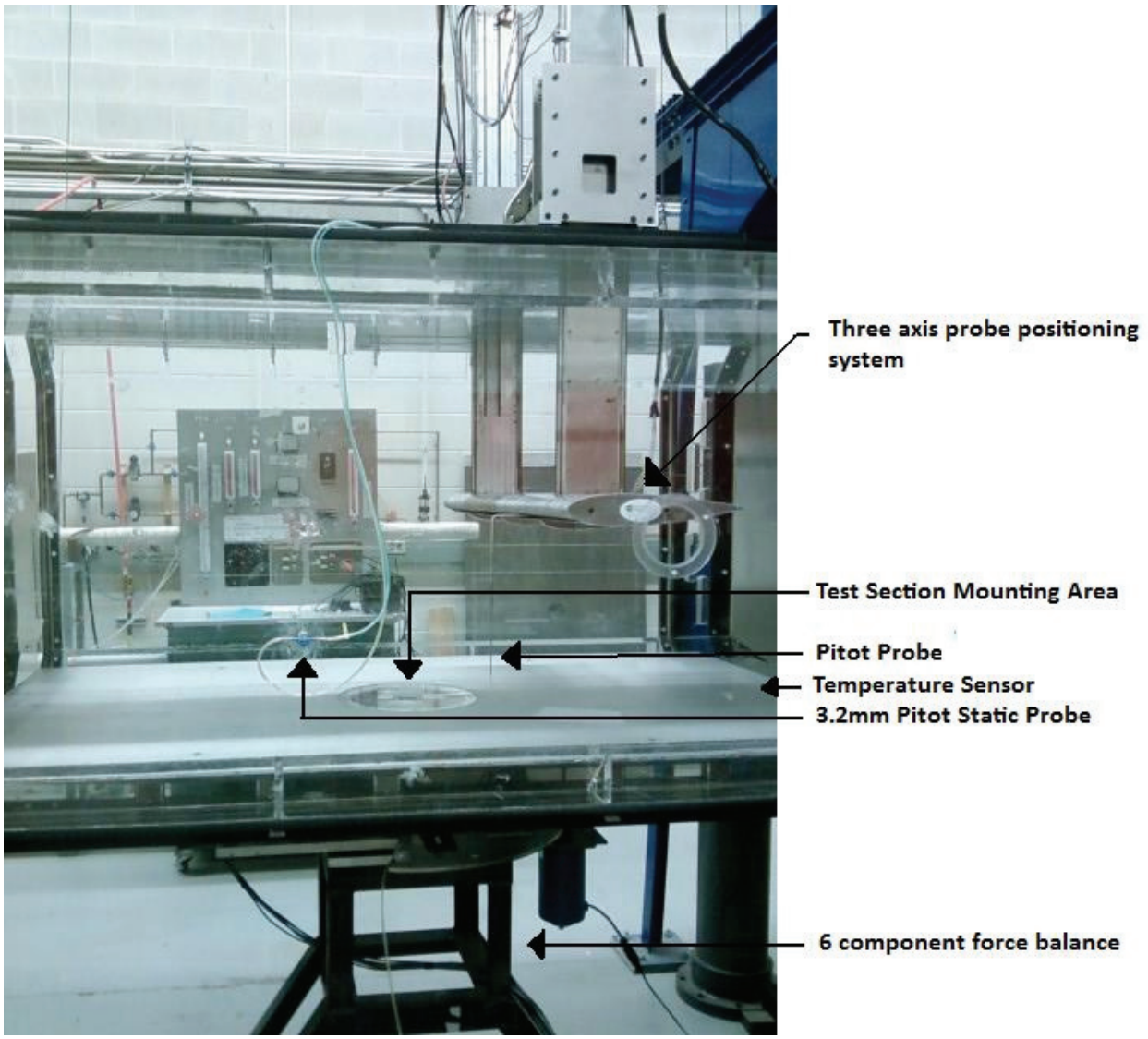

Figure 3.2: Details of the wind tunnel test section and some of the measurement instrumentation. Flow is from left to right.

(a) 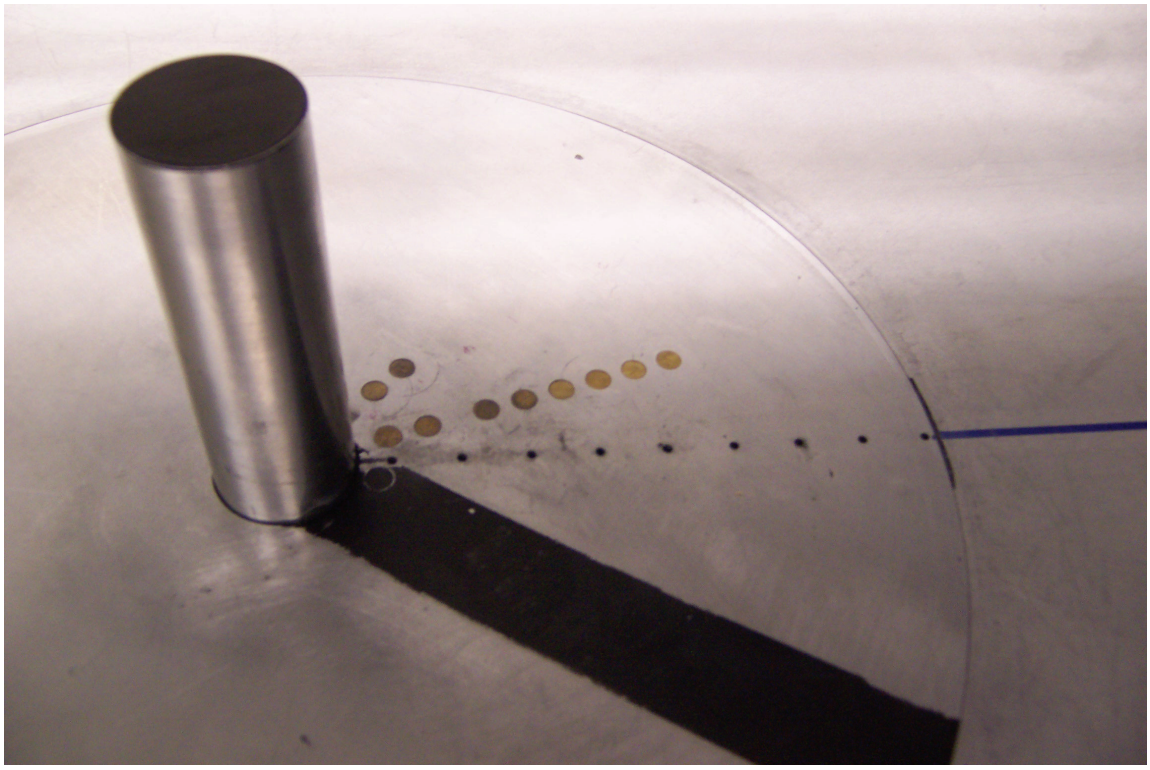

Figure 3.3: Photographs of the experimental set-up: (a) finite circular cylinder of AR = 5 with no splitter plate (flow from left to right), showing the splitter-plate mounting holes in the turntable imbedded within the ground plane; (b) finite circular cylinder of AR = 3 with a wake-mounted splitter plate of $L/D = 7$ (flow from left to right). The hot-wire probe can be seen downstream of the splitter plate.

(b) 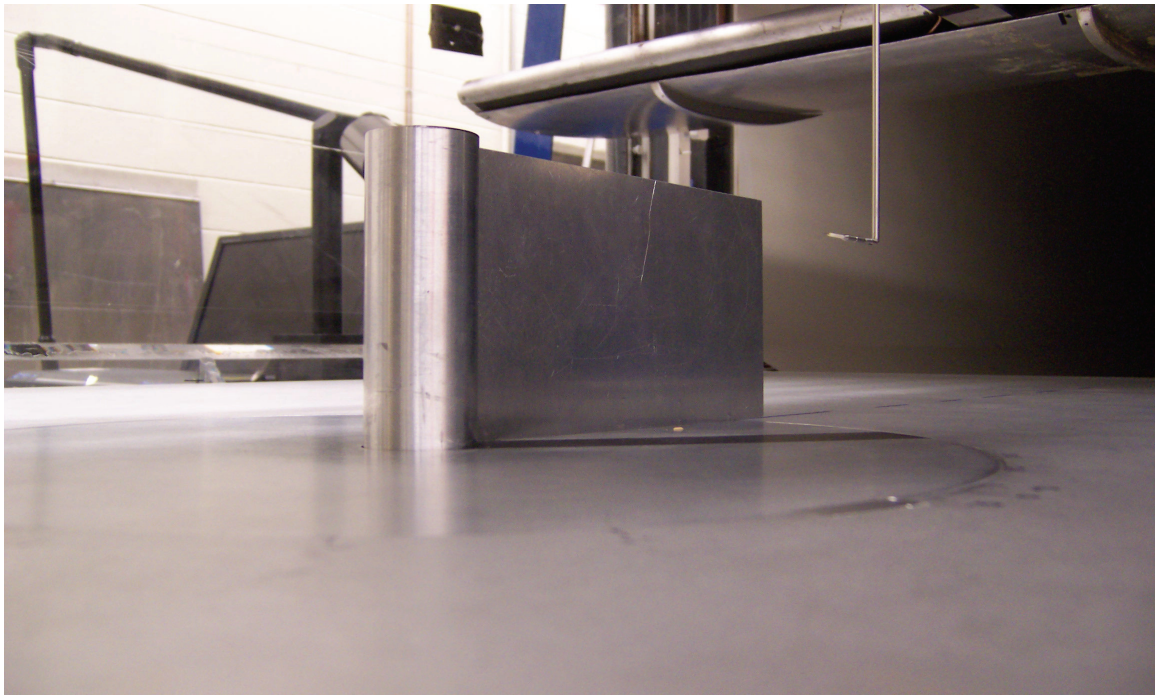

Figure 3.3 (continued).

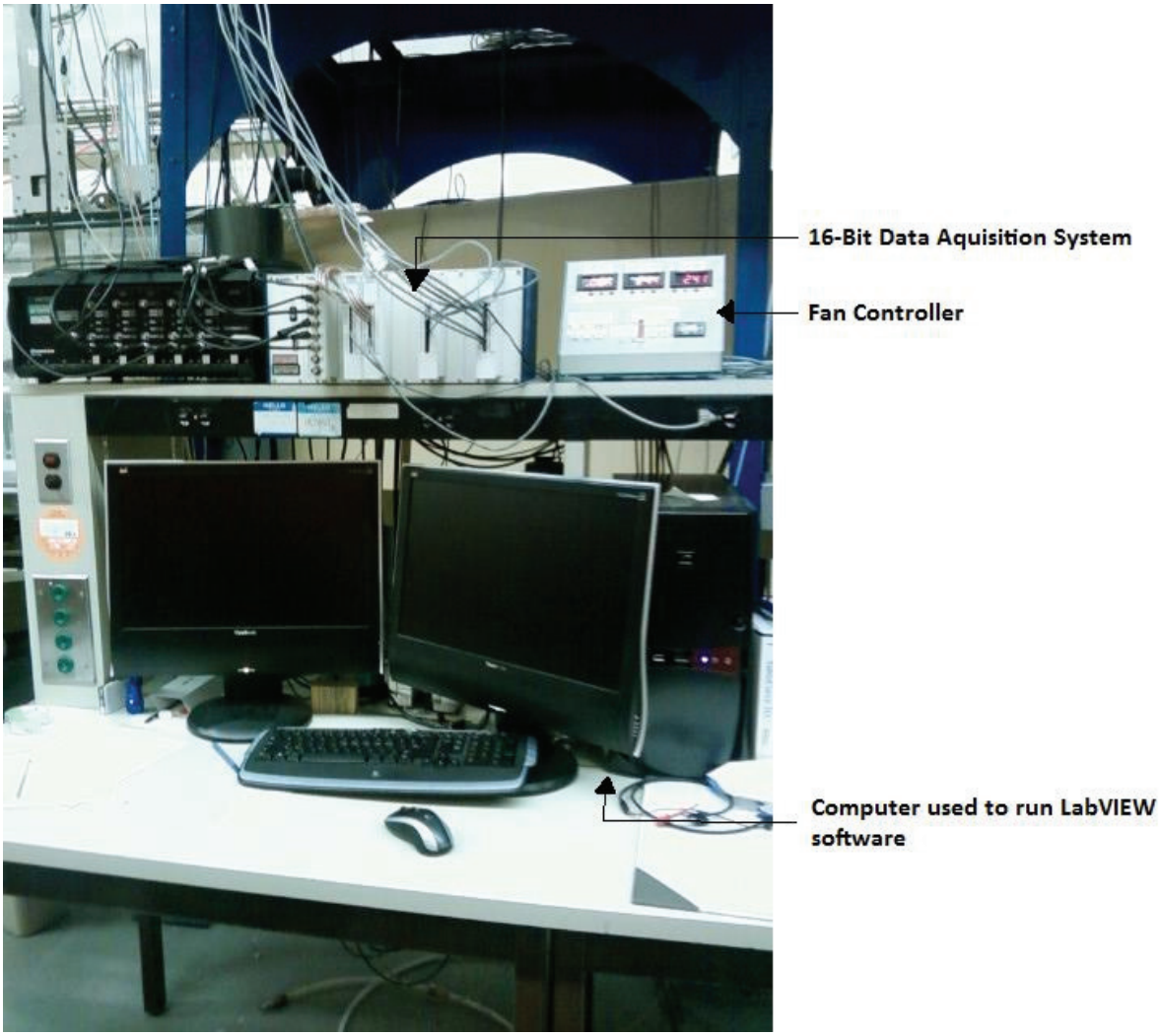

Figure 3.4: Details of the wind tunnel's data acquisition system.

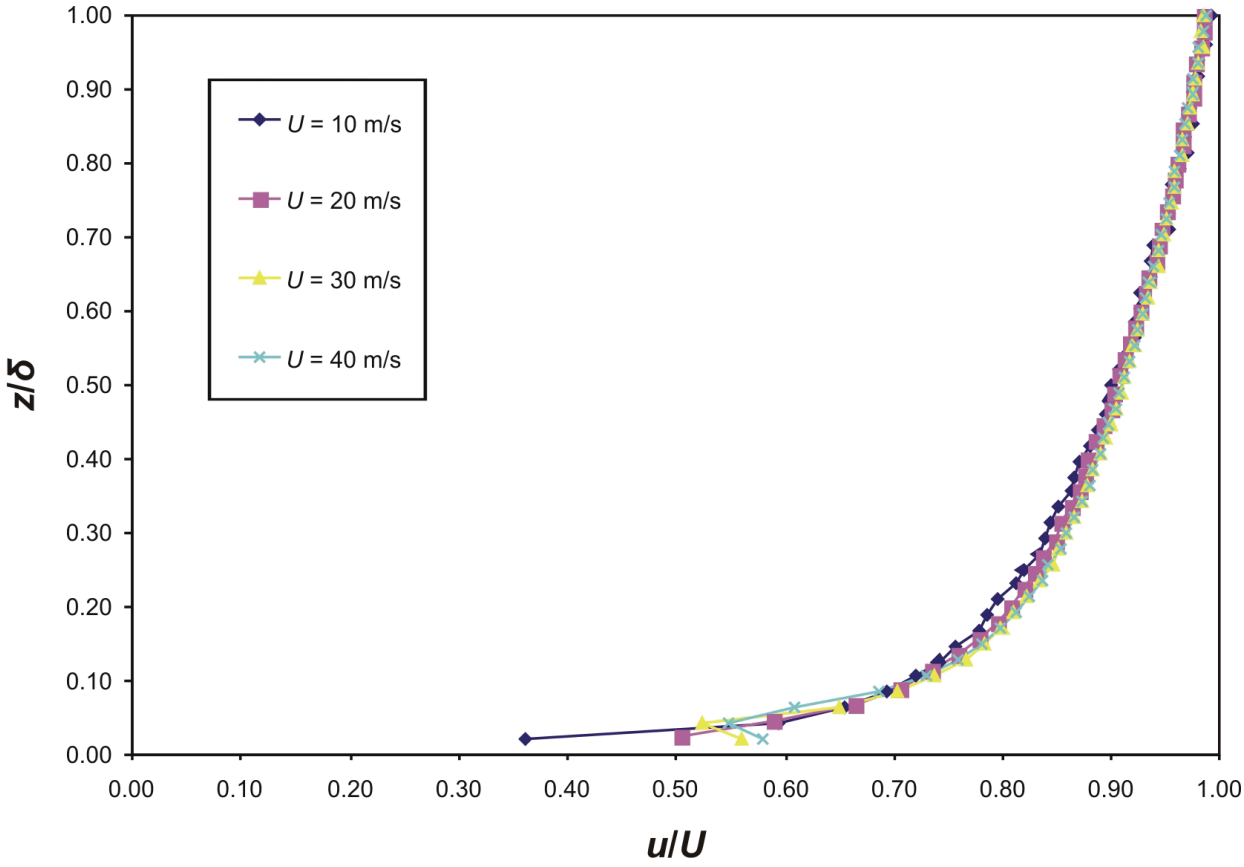

Figure 3.5: Streamwise mean velocity profiles (where u is the local streamwise mean velocity) of the flat-plate boundary layer on the ground plane at the location of the cylinder (with the cylinder removed). Measurements were made at four freestream velocities of U = 10, 20, 30 and 40 m/s.

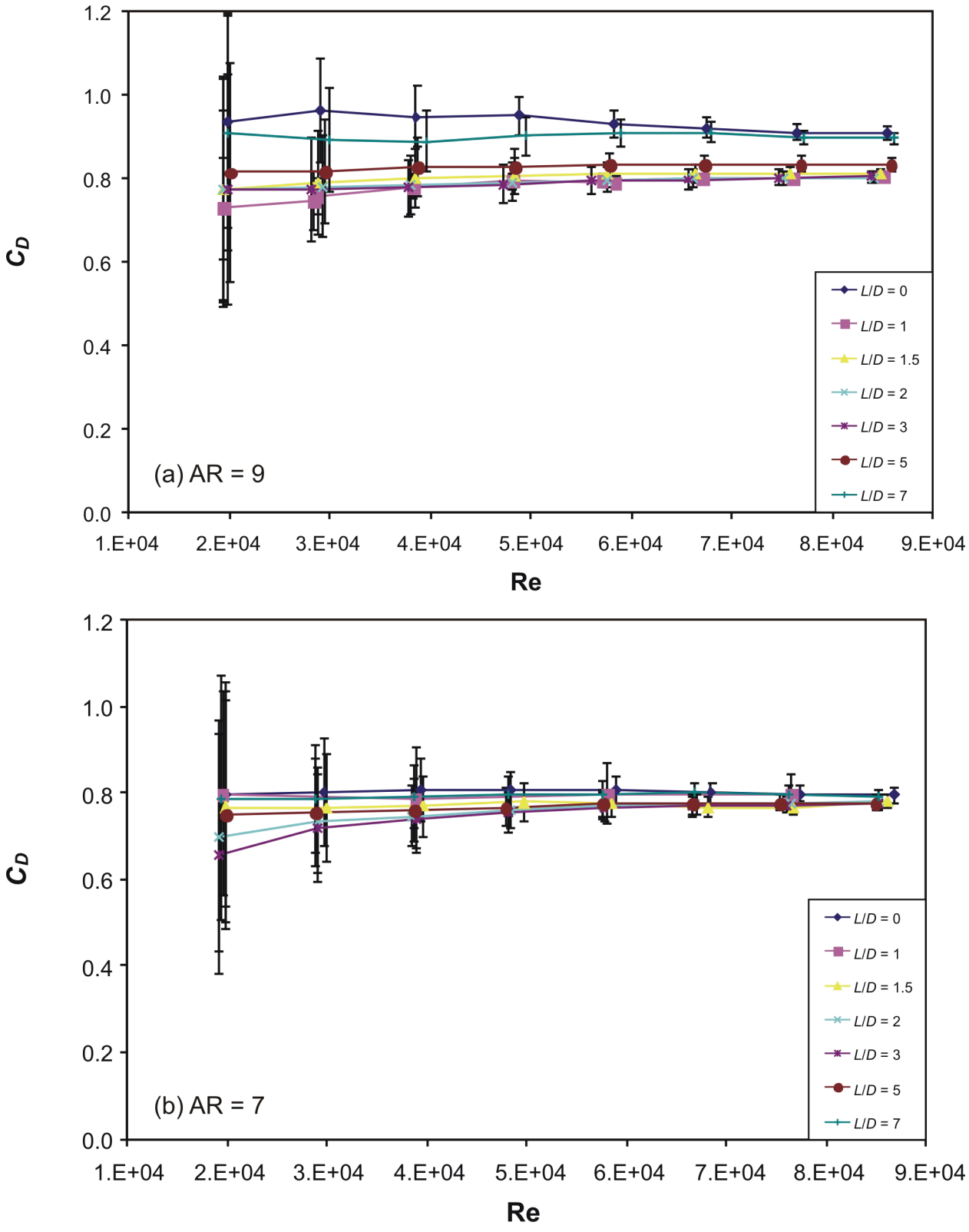

Figure 4.1: Mean drag coefficient sensitivity to Reynolds number: (a) AR = 9, (b) AR = 7, (c) AR = 5, (d) AR = 3.

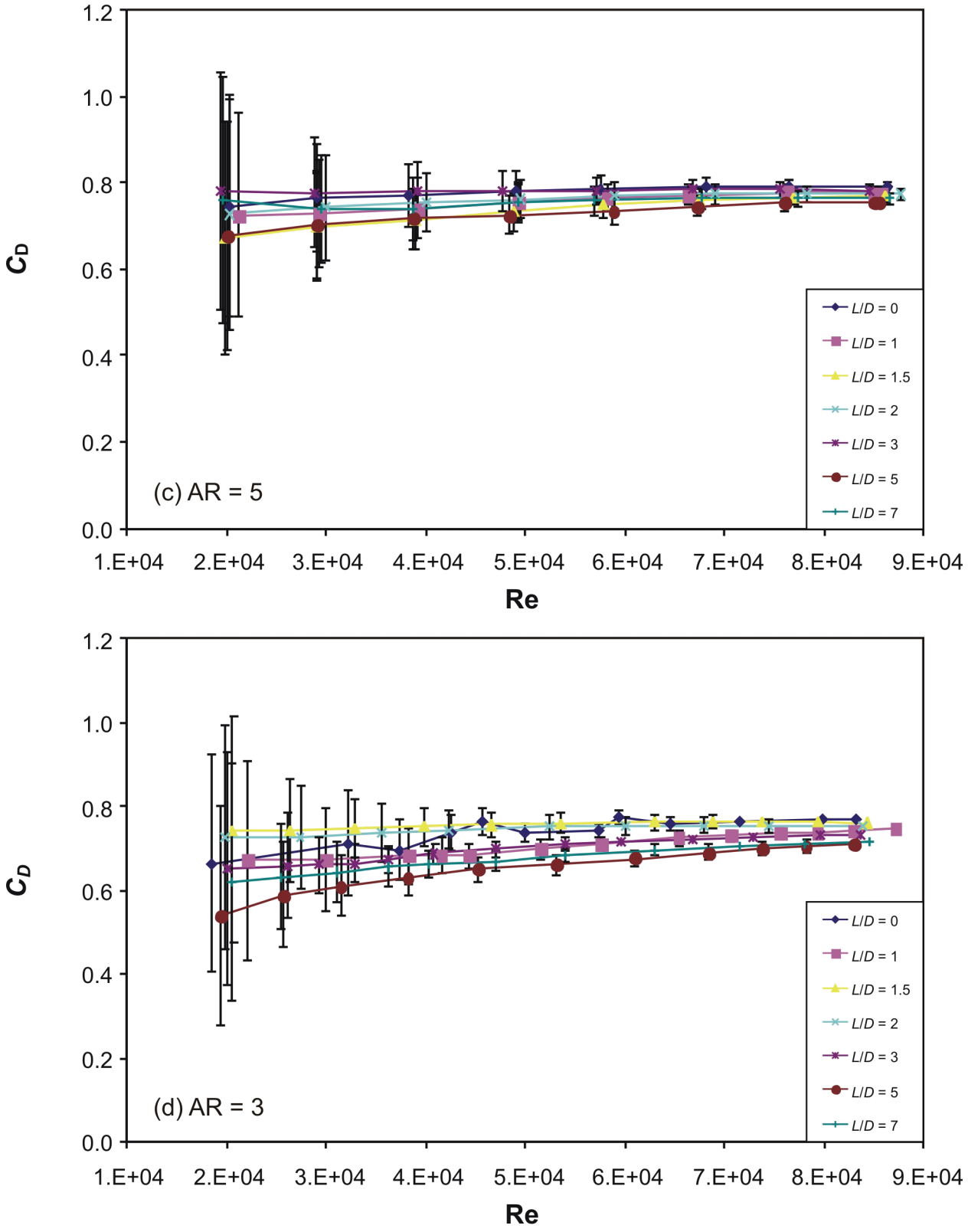

Figure 4.1 (continued).

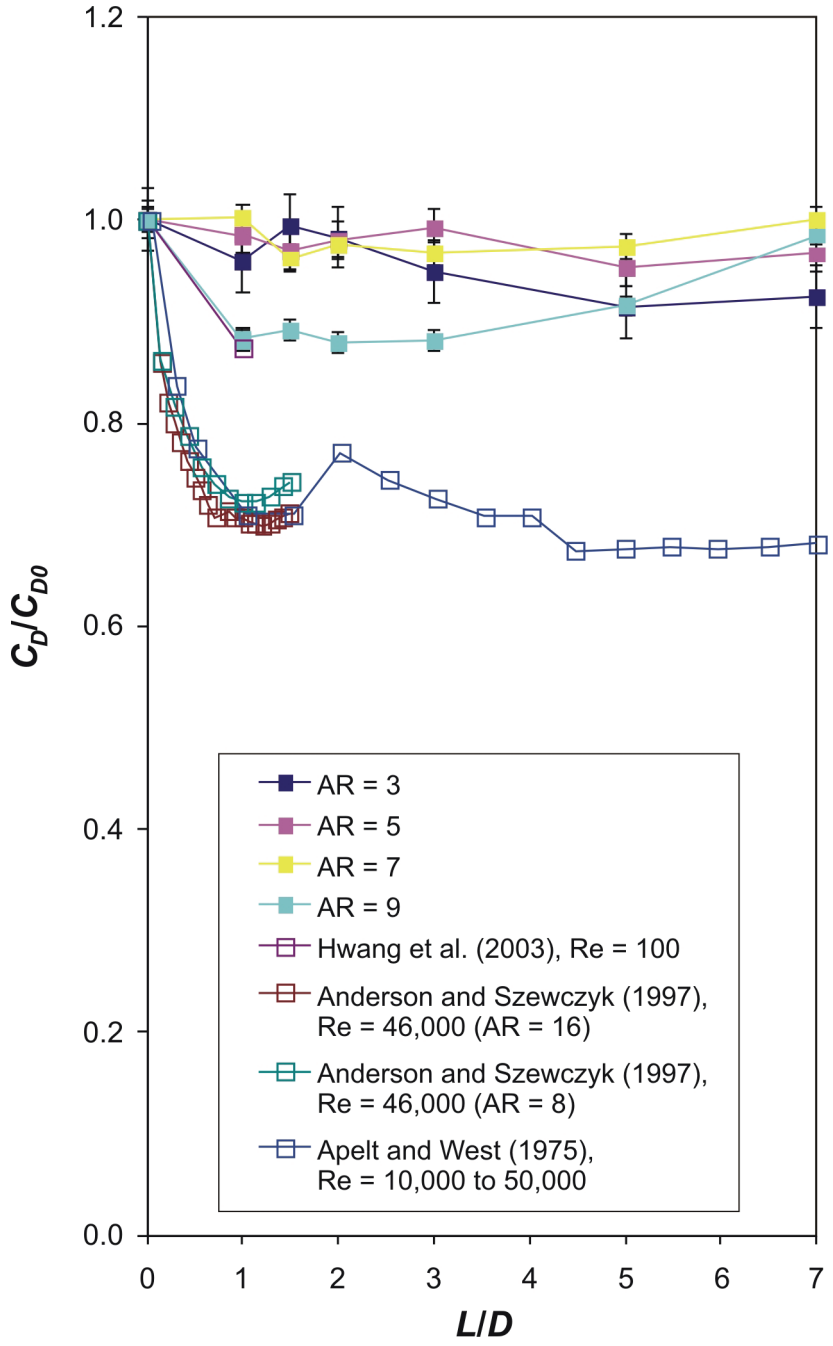

Figure 4.2: Mean drag coefficient normalized with the drag coefficient for the case of no splitter plate ($L/D = 0$) at 40 m/s ($Re = 7.5 \times 10^4$). Published data for an infinite circular cylinder.

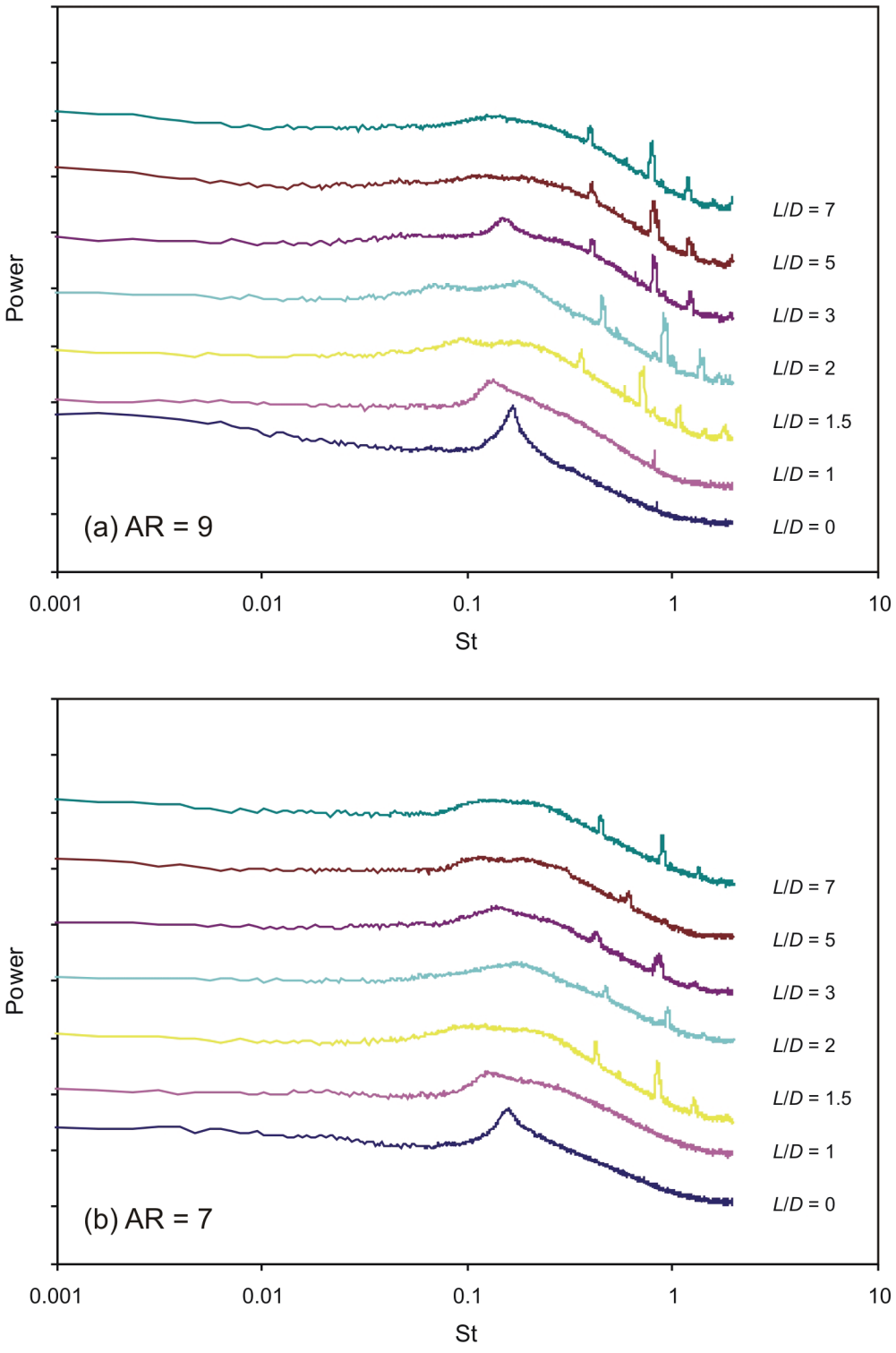

Figure 4.3: Power spectra at $U = 40$ m/s for different L/D: (a) AR = 9, (b) AR = 7, (c) AR = 5, (d) AR = 3. Hot-wire probe positioned at $x/D = 3$, $y/D = 1.5$, and mid-height ($z/H = 0.5$).

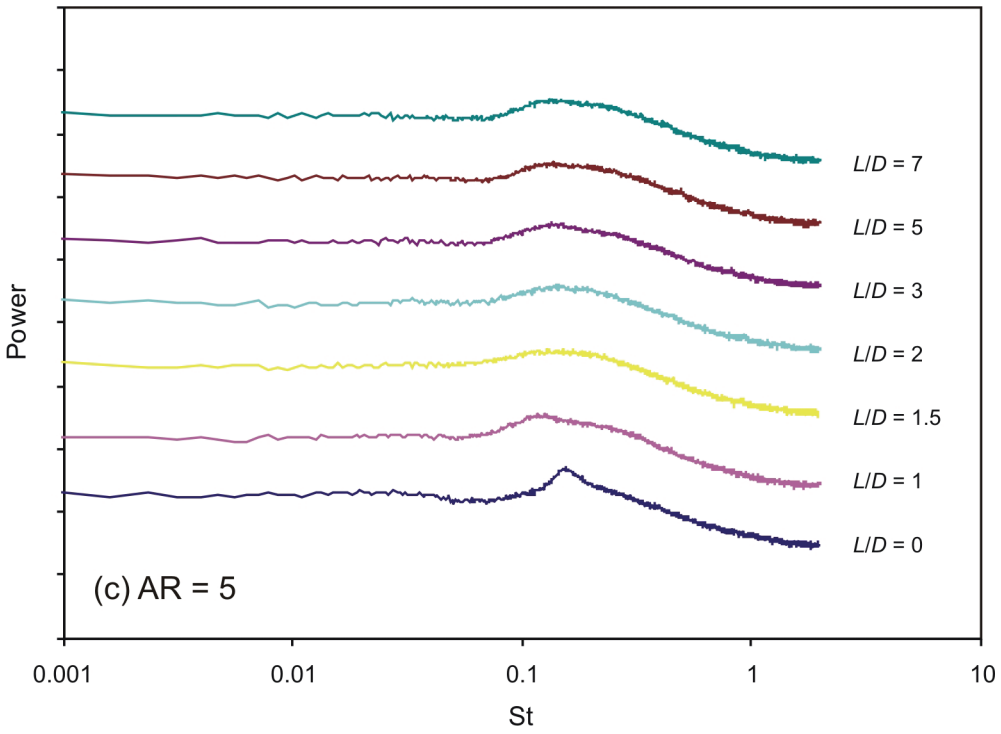

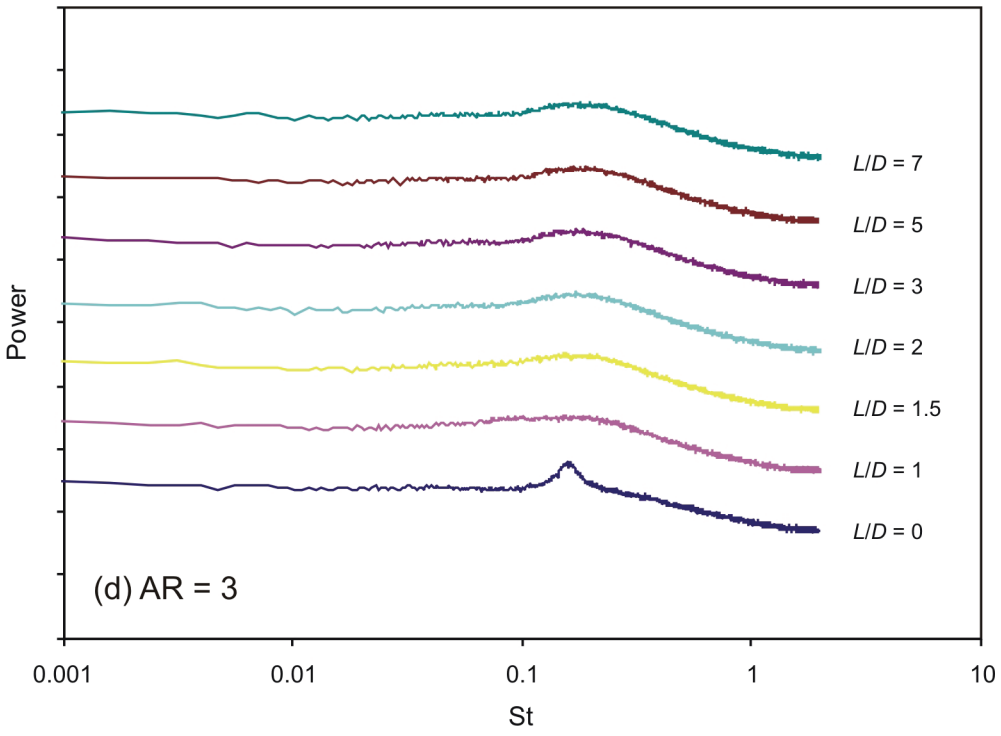

Figure 4.3 (continued).

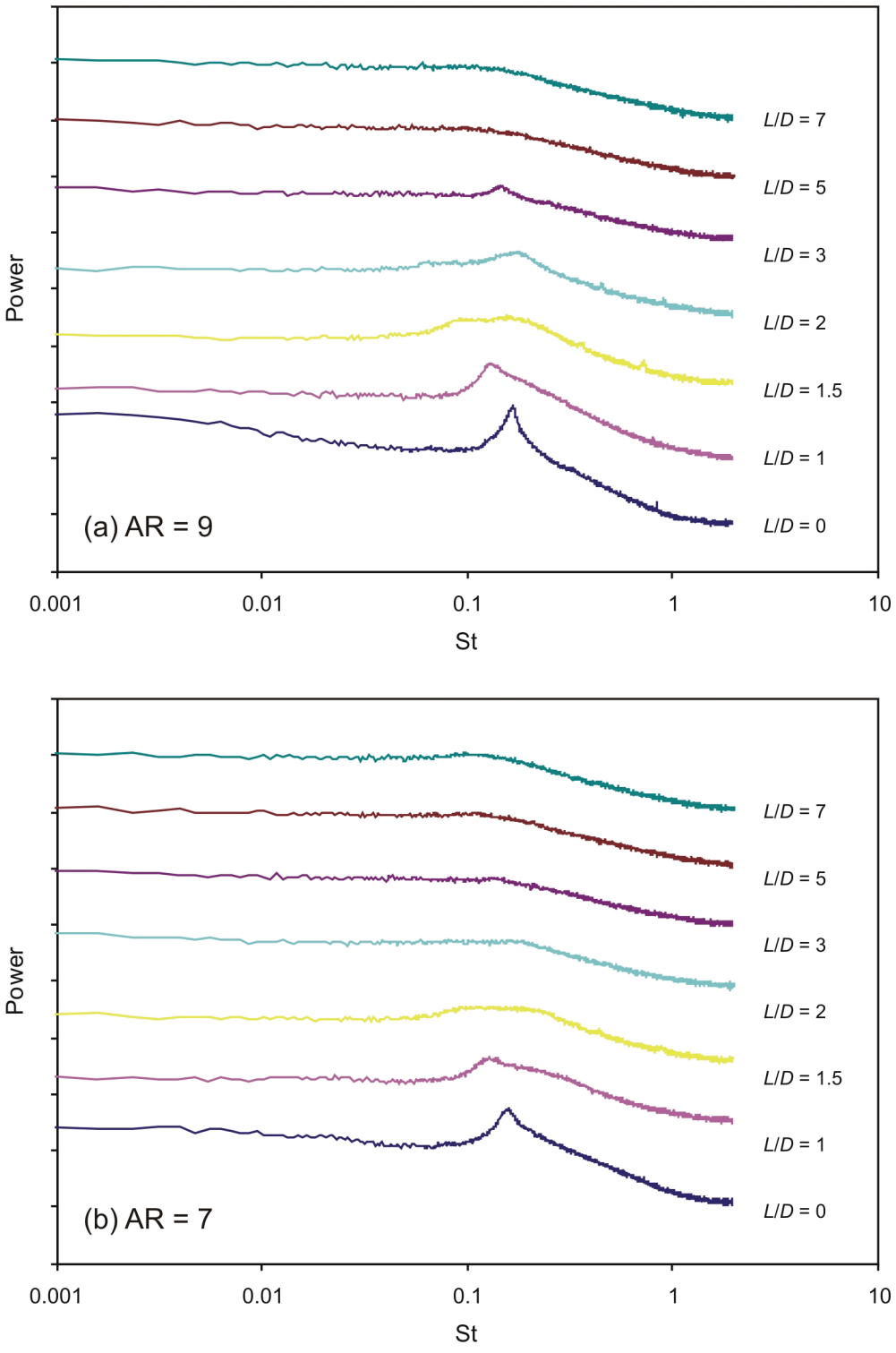

Figure 4.4: Power spectra at $U = 40$ m/s for different L/D: (a) AR = 9, (b) AR = 7, (c) AR = 5, (d) AR = 3. Hot-wire probe positioned at $x/D = 3 + L/D$, $y/D = 1.5$, and mid-height ($z/H = 0.5$).

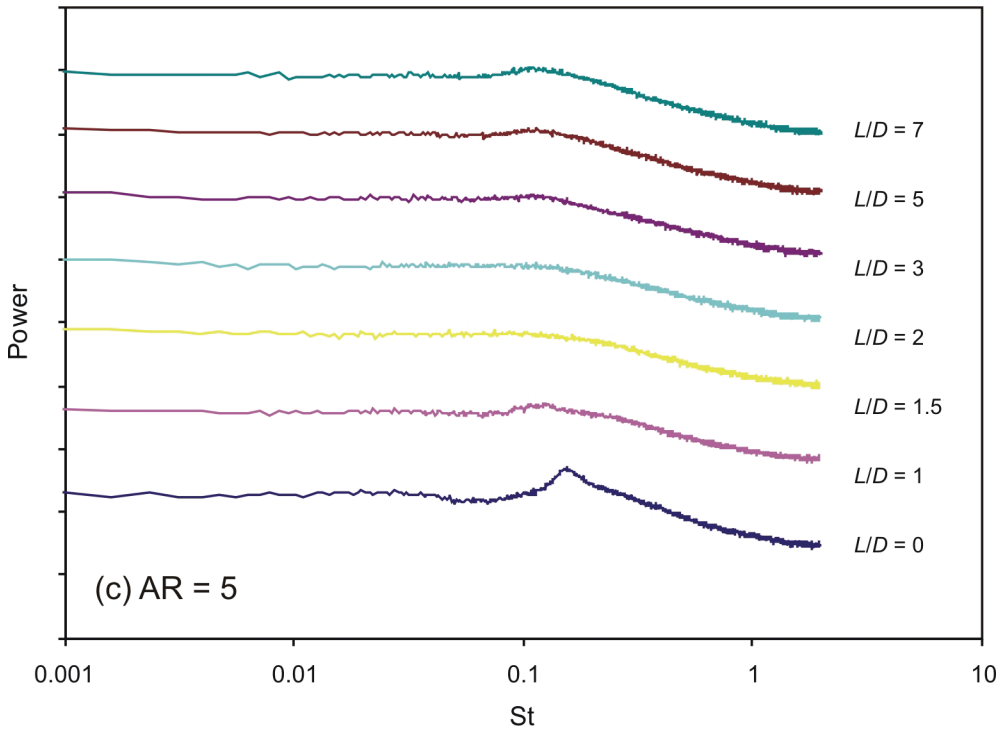

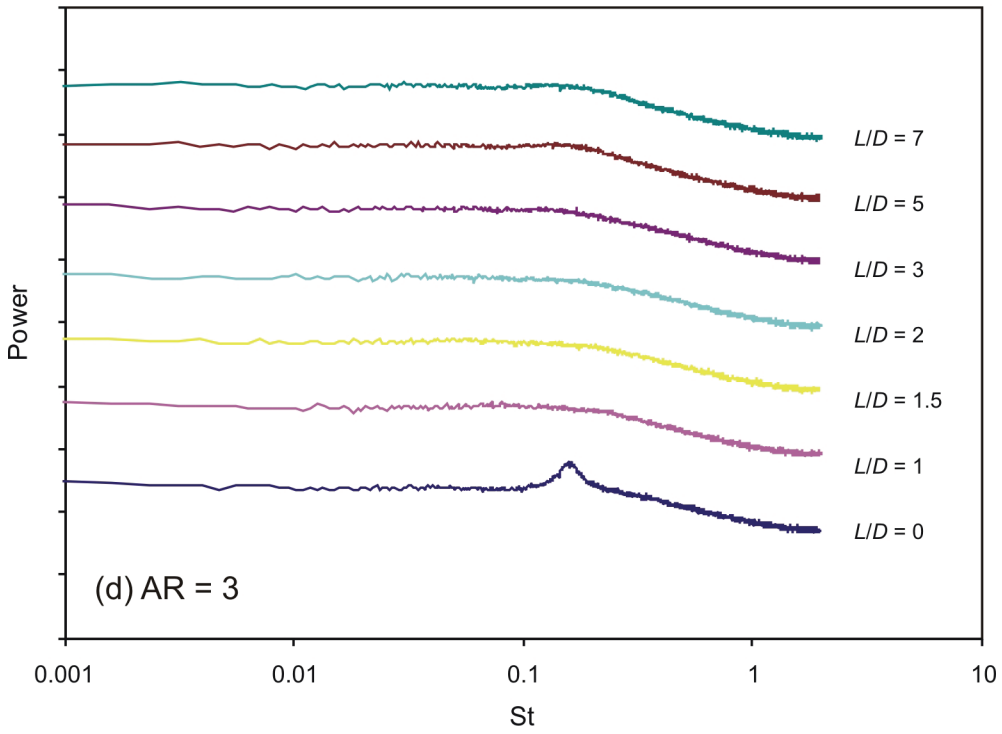

Figure 4.4 (continued).

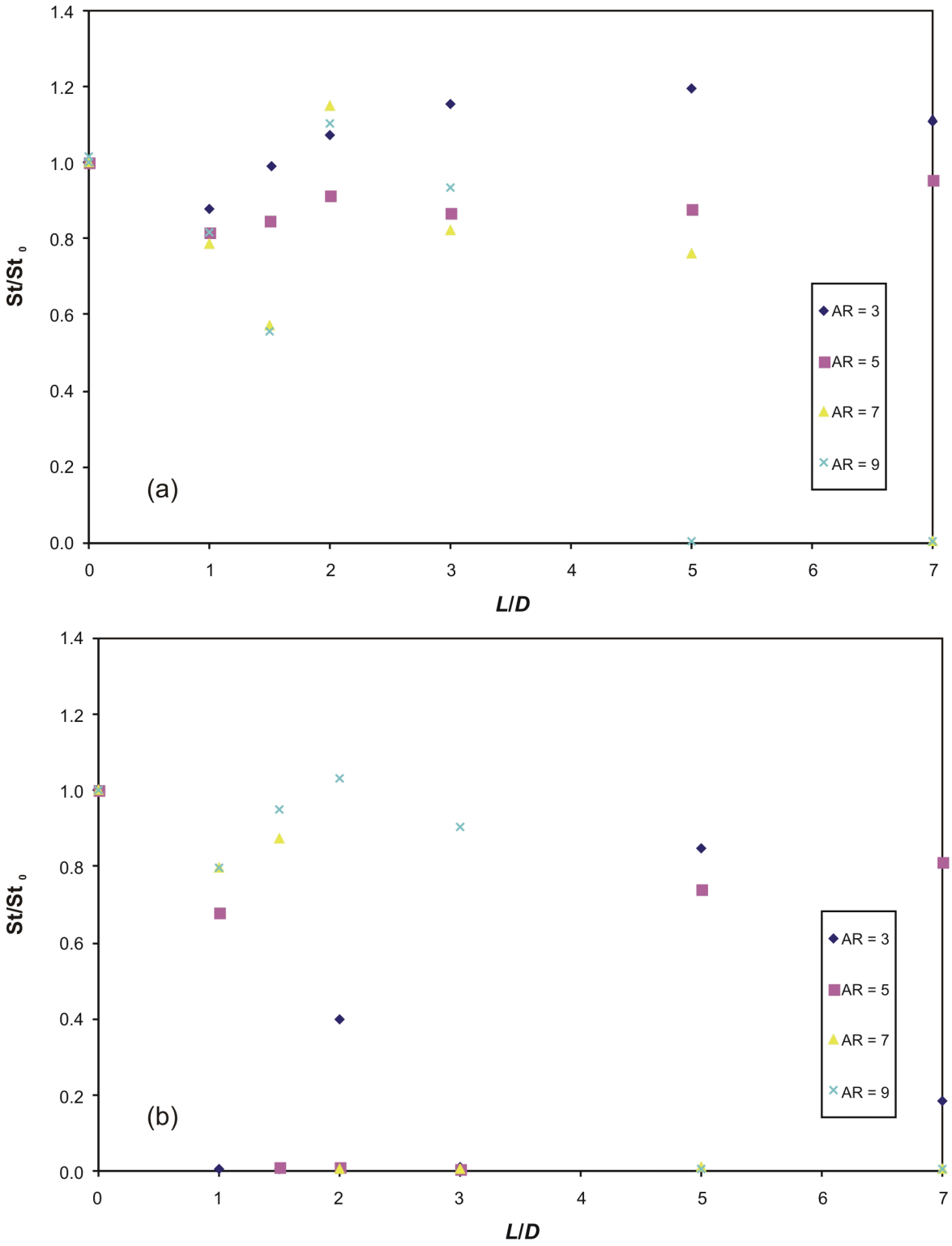

Figure 4.5: Strouhal number normalized with the Strouhal number for the case of no splitter plate ($L/D = 0$) at $U = 40$ m/s ($\mathrm{Re} = 7.5\times10^4$). Hot-wire probe positioned at: (a) $x/D = 3$, $y/D = 1.5$, and mid-height ($z/H = 0.5$); (b) $x/D = 3 + L/D$, $y/D = 1.5$, and mid-height ($z/H = 0.5$).

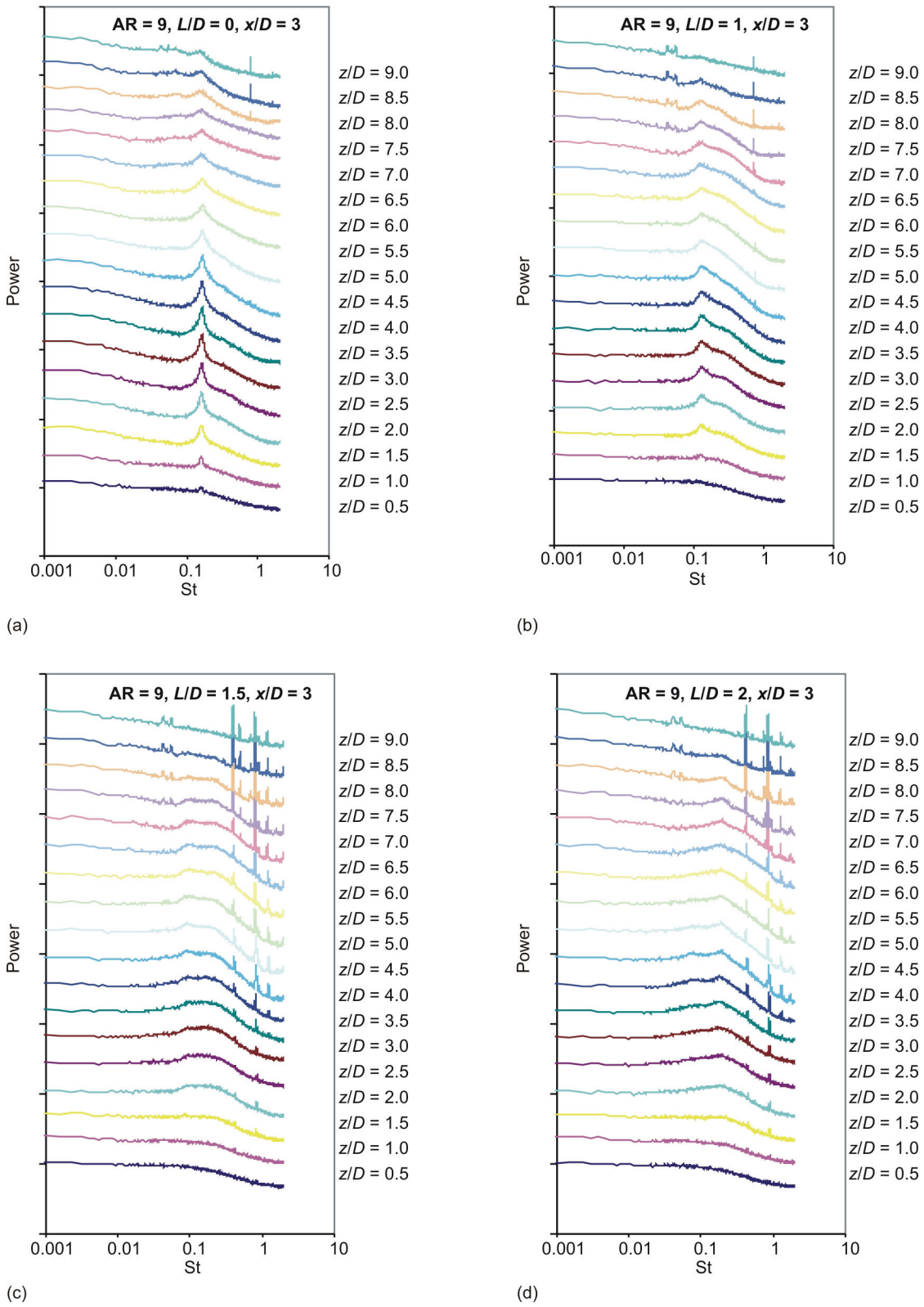

Figure 4.6: Power spectra along the cylinder height at $U = 40$ m/s for AR = 9: (a) $L/D = 0$, (b) $L/D = 1$, (c) $L/D = 1.5$, (d) $L/D = 2$, (e) $L/D = 3$, (f) $L/D = 5$, (g) $L/D = 7$. Hot-wire probe positioned at $x/D = 3$, $y/D = 1.5$, and mid-height ($z/H = 0.5$).

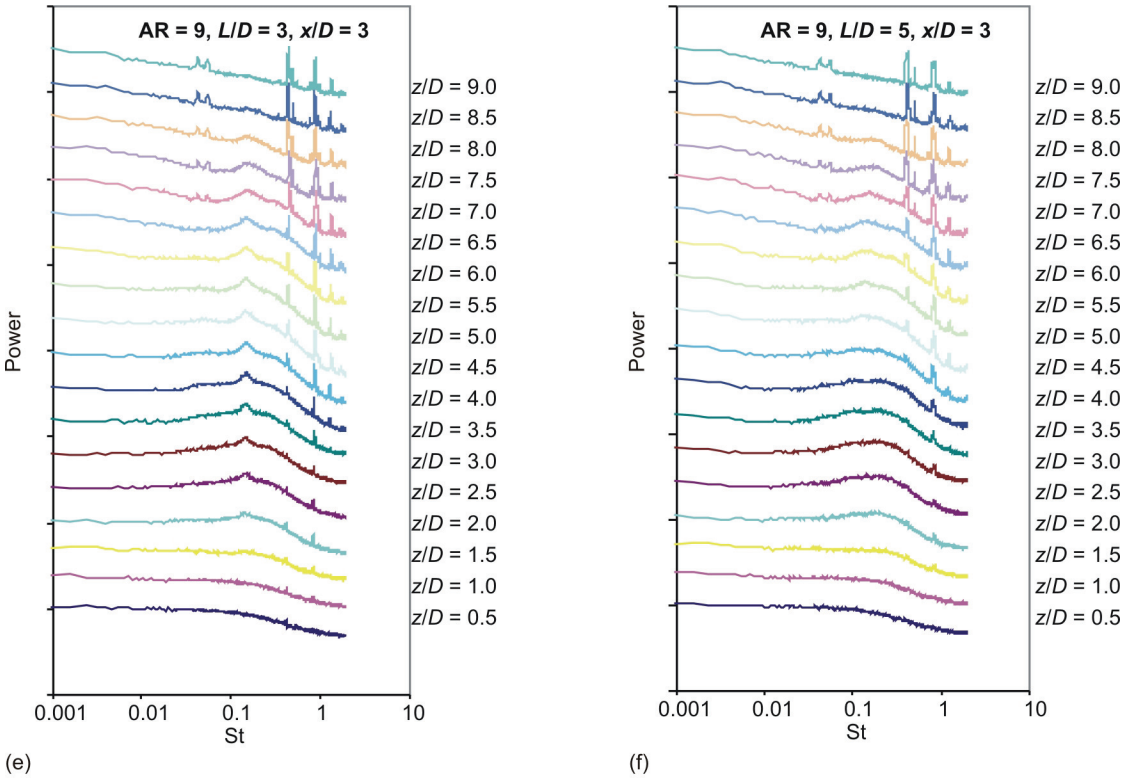

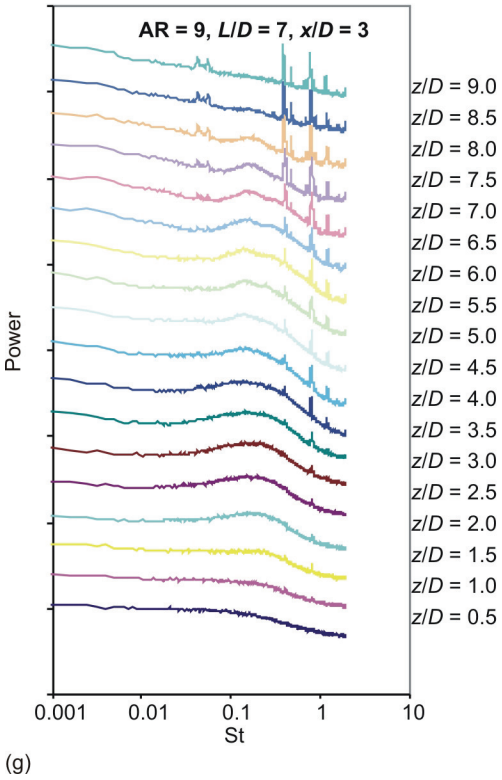

Figure 4.6 (continued).

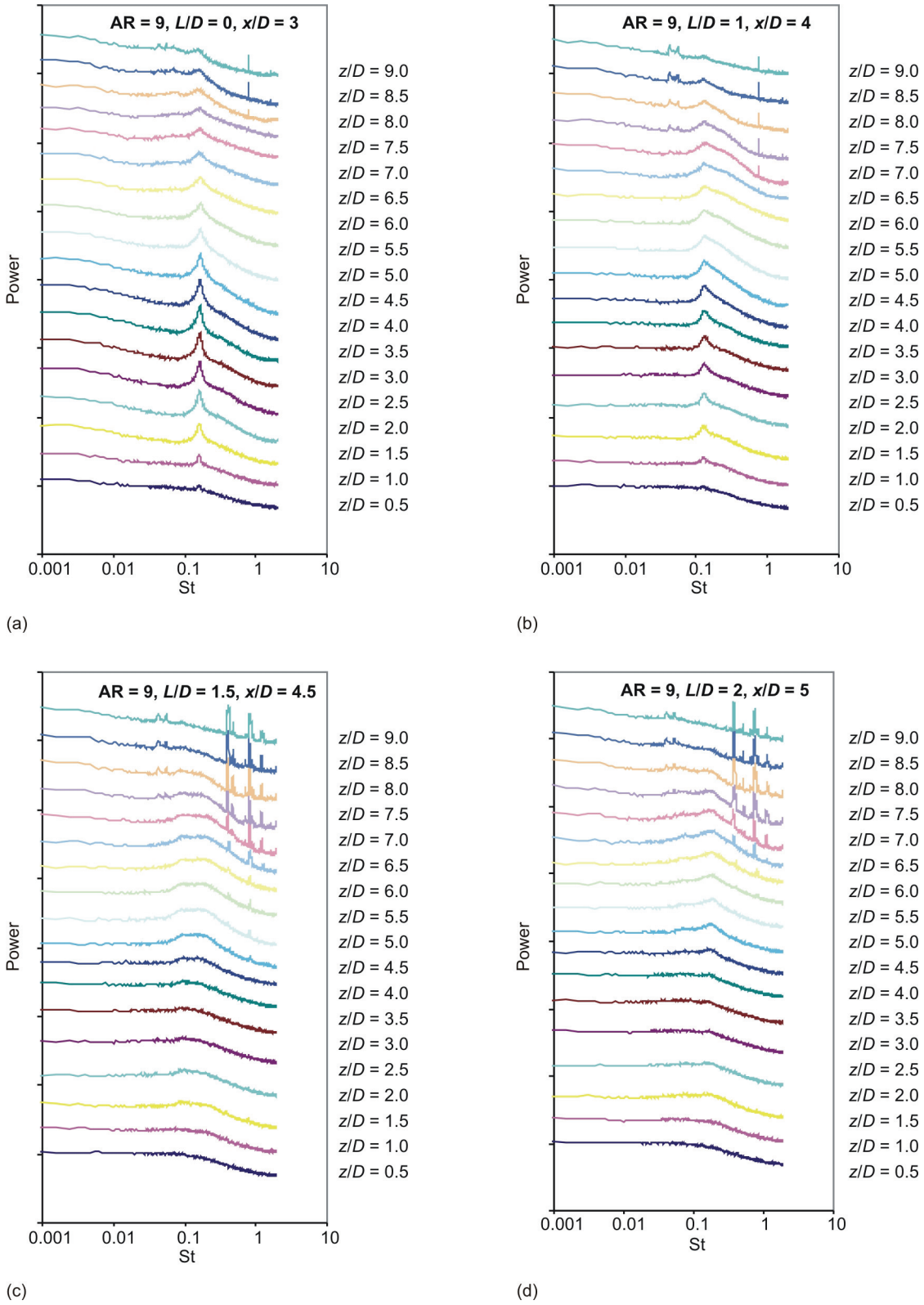

Figure 4.7: Power spectra along the cylinder height at $U = 40$ m/s for AR = 9: (a) $L/D = 0$, (b) $L/D = 1$, (c) $L/D = 1.5$, (d) $L/D = 2$, (e) $L/D = 3$, (f) $L/D = 5$, (g) $L/D = 7$. Hot-wire probe positioned at $x/D = 3 + L/D$, $y/D = 1.5$, and mid-height ($z/H = 0.5$).

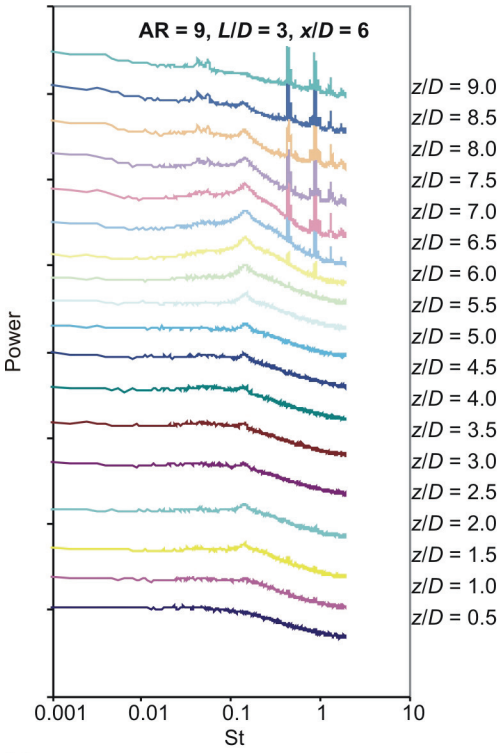

(e)

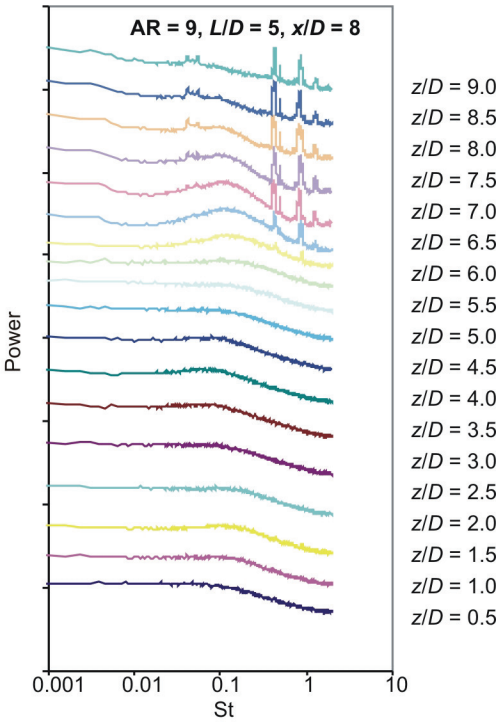

(f)

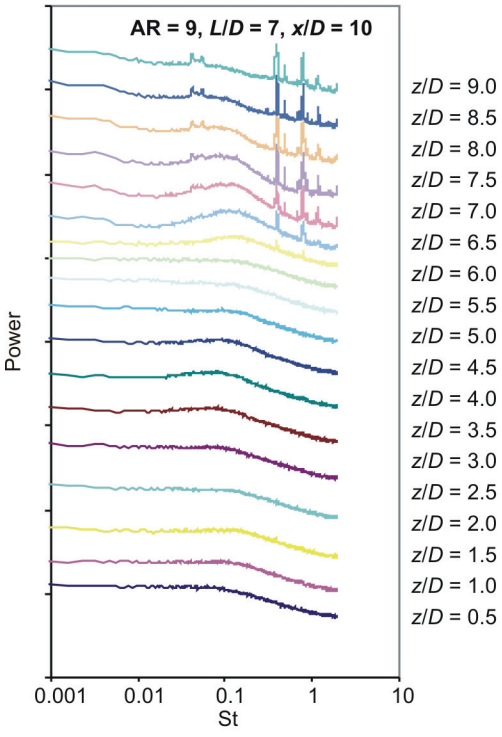

(g)

Figure 4.7 (continued).

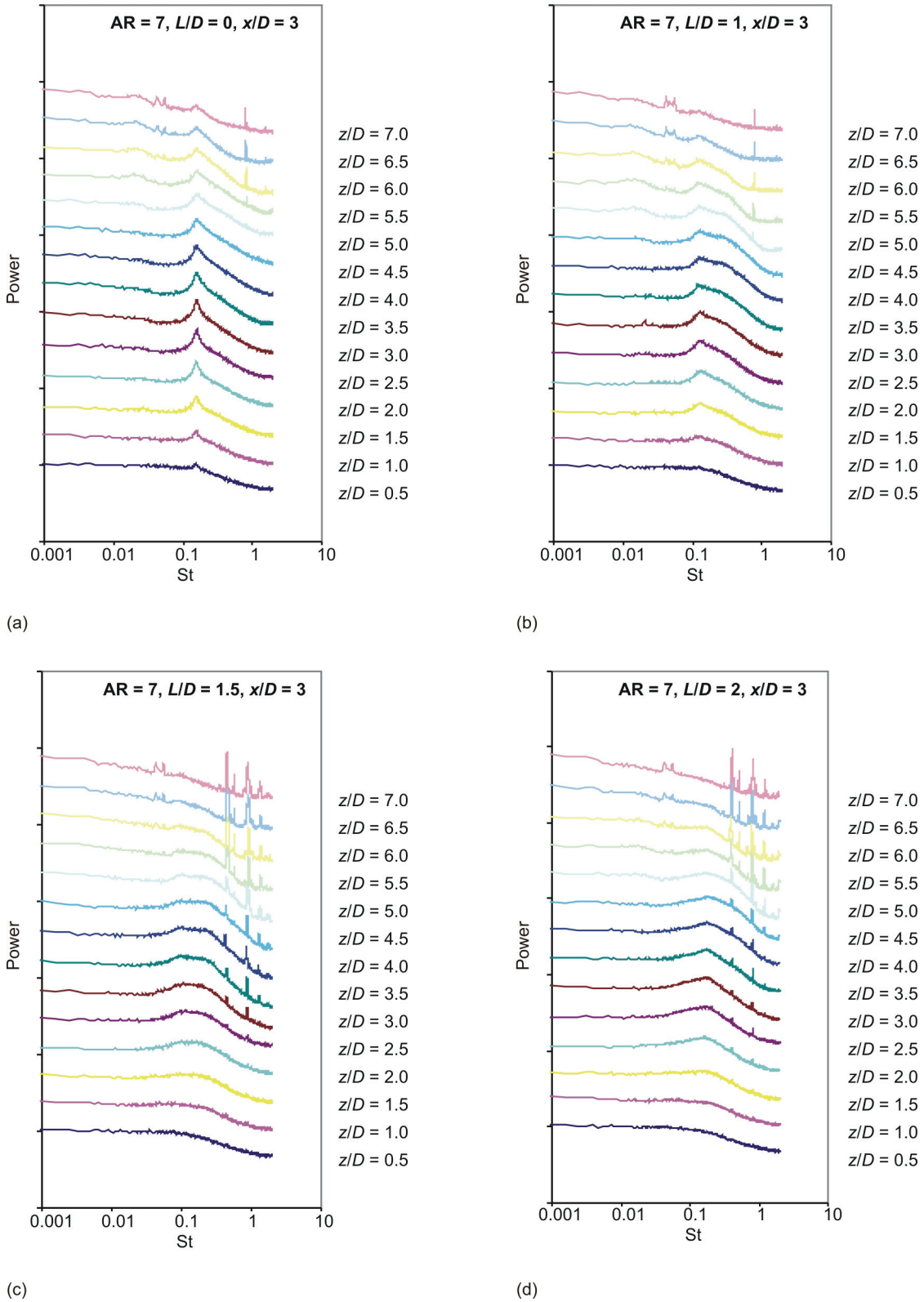

Figure 4.8: Power spectra along the cylinder height at $U = 40$ m/s for AR = 7: (a) $L/D = 0$, (b) $L/D = 1$, (c) $L/D = 1.5$, (d) $L/D = 2$, (e) $L/D = 3$, (f) $L/D = 5$, (g) $L/D = 7$. Hot-wire probe positioned at $x/D = 3$, $y/D = 1.5$, and mid-height ($z/H = 0.5$).

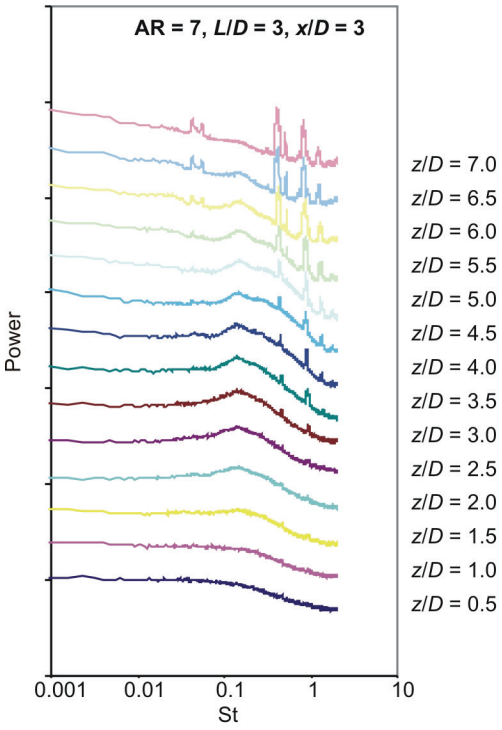

(e)

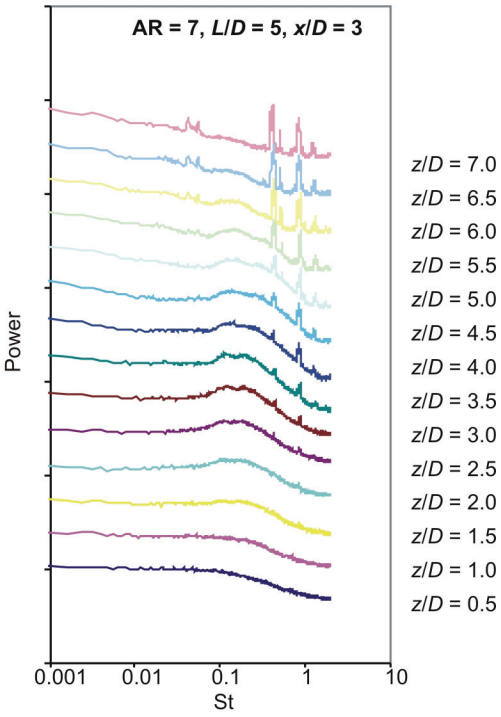

(f)

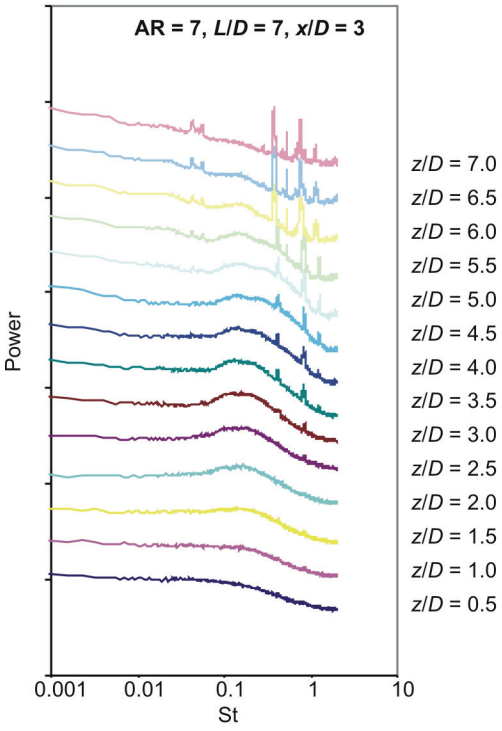

(g)

Figure 4.8 (continued).

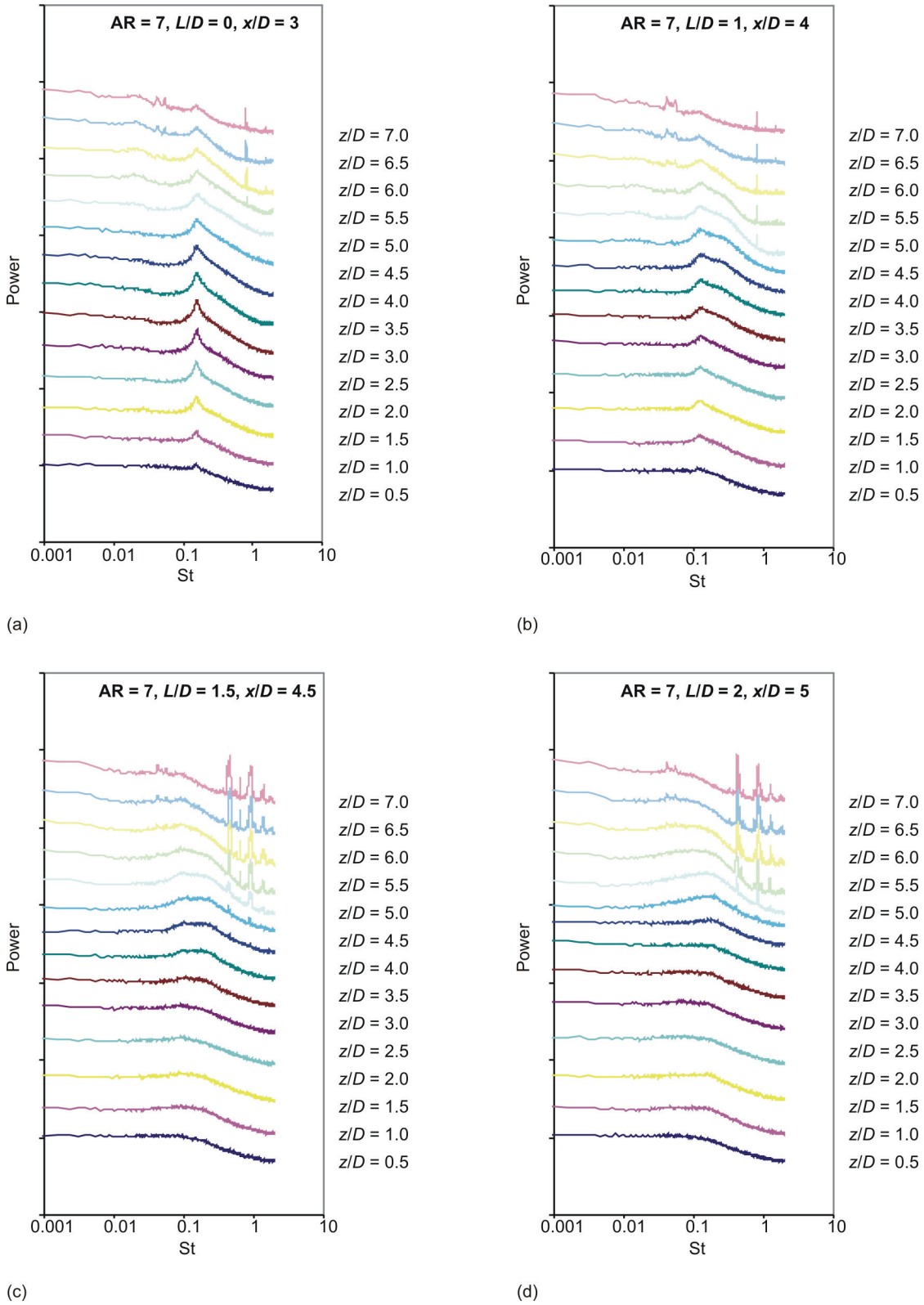

Figure 4.9: Power spectra along the cylinder height at $U = 40$ m/s for AR = 7: (a) $L/D = 0$, (b) $L/D = 1$, (c) $L/D = 1.5$, (d) $L/D = 2$, (e) $L/D = 3$, (f) $L/D = 5$, (g) $L/D = 7$. Hot-wire probe positioned at $x/D = 3 + L/D$, $y/D = 1.5$, and mid-height ($z/H = 0.5$).

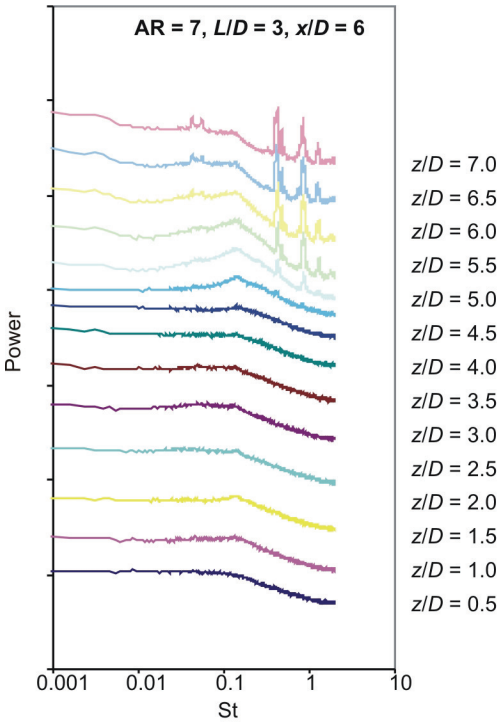

(e)

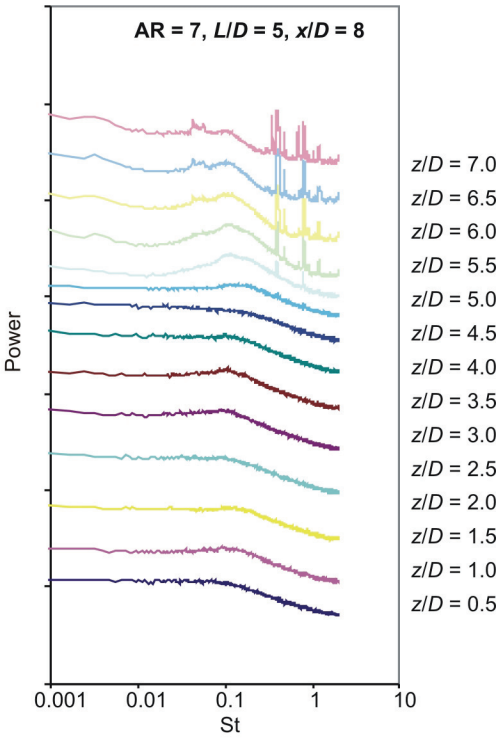

(f)

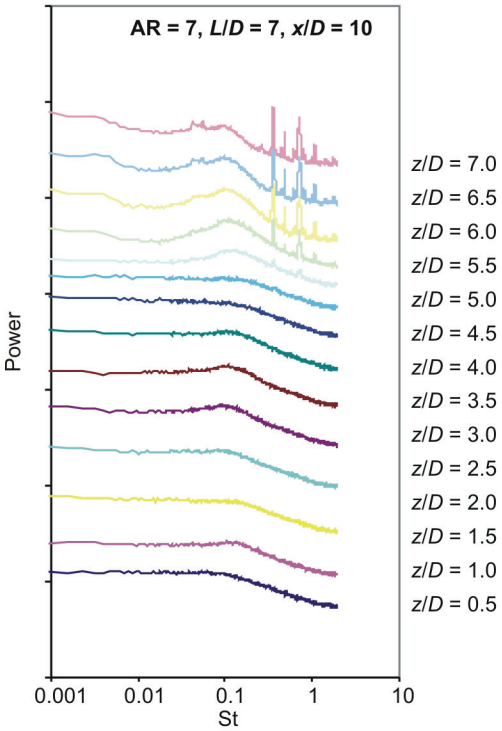

(g)

Figure 4.9 (continued).

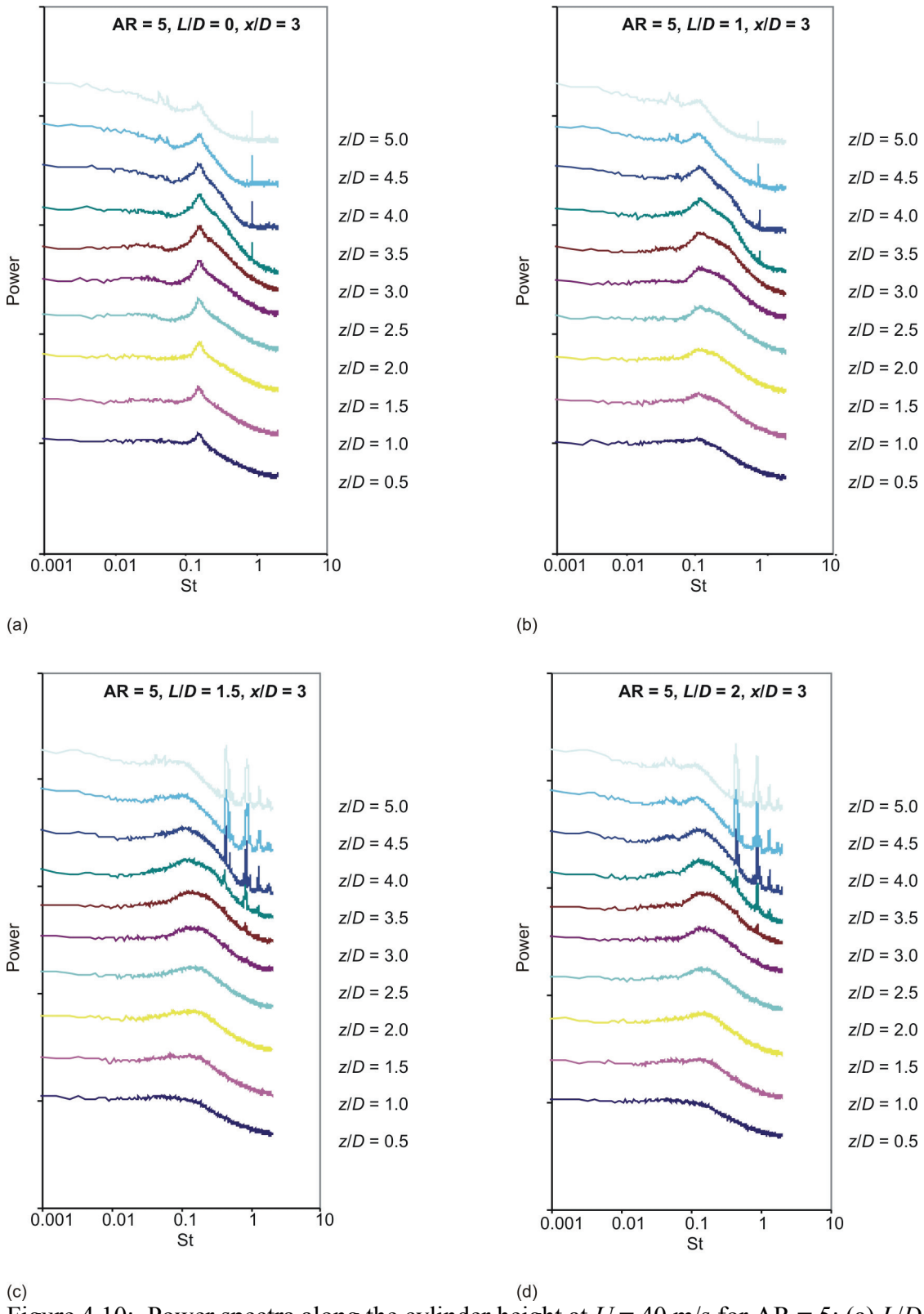

Figure 4.10: Power spectra along the cylinder height at $U = 40$ m/s for AR = 5: (a) $L/D = 0$, (b) $L/D = 1$, (c) $L/D = 1.5$, (d) $L/D = 2$, (e) $L/D = 3$, (f) $L/D = 5$, (g) $L/D = 7$. Hot-wire probe positioned at $x/D = 3$, $y/D = 1.5$, and mid-height ($z/H = 0.5$).

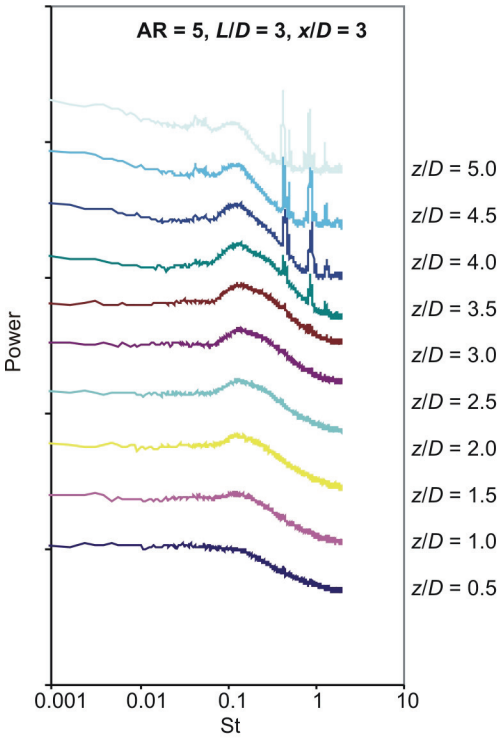

(e)

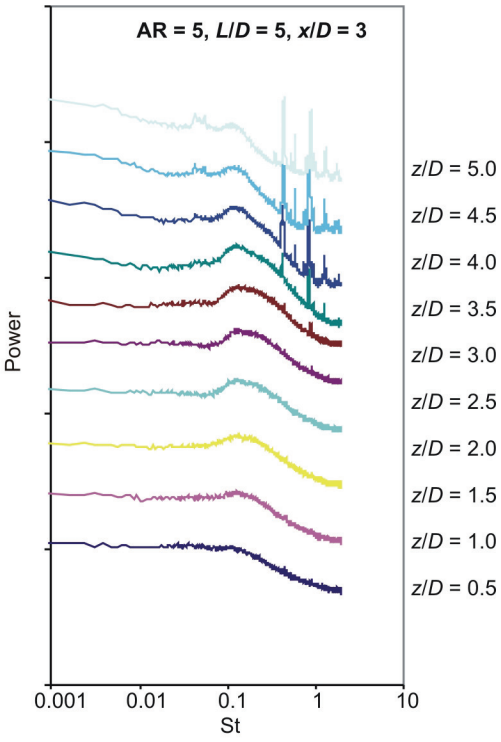

(f)

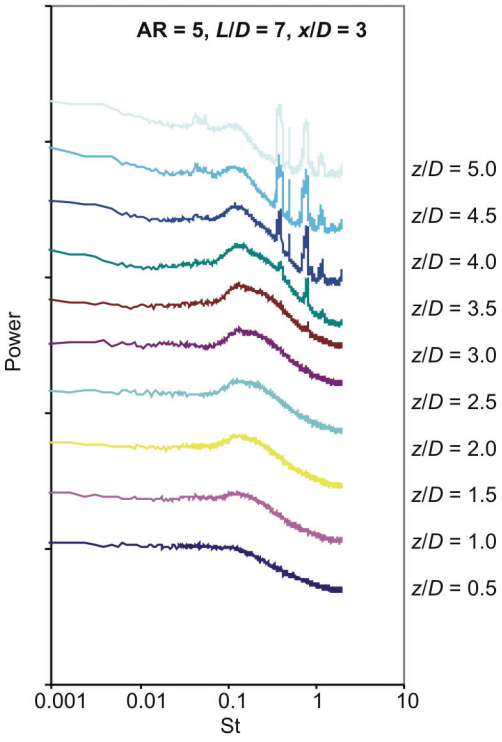

(g)

Figure 4.10 (continued).

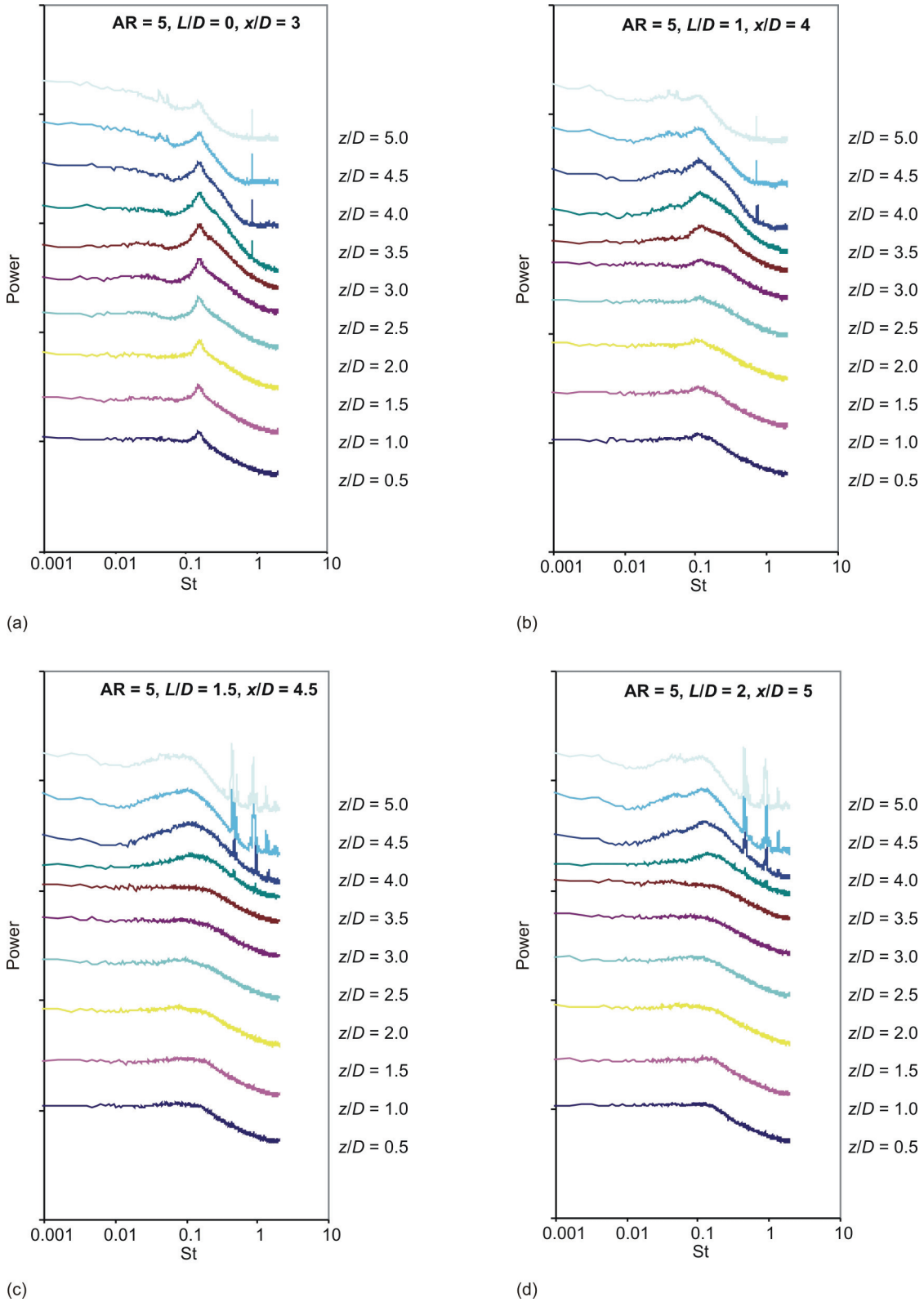

Figure 4.11: Power spectra along the cylinder height at $U = 40$ m/s for AR = 5: (a) $L/D = 0$, (b) $L/D = 1$, (c) $L/D = 1.5$, (d) $L/D = 2$, (e) $L/D = 3$, (f) $L/D = 5$, (g) $L/D = 7$. Hot-wire probe positioned at $x/D = 3 + L/D$, $y/D = 1.5$, and mid-height ($z/H = 0.5$).

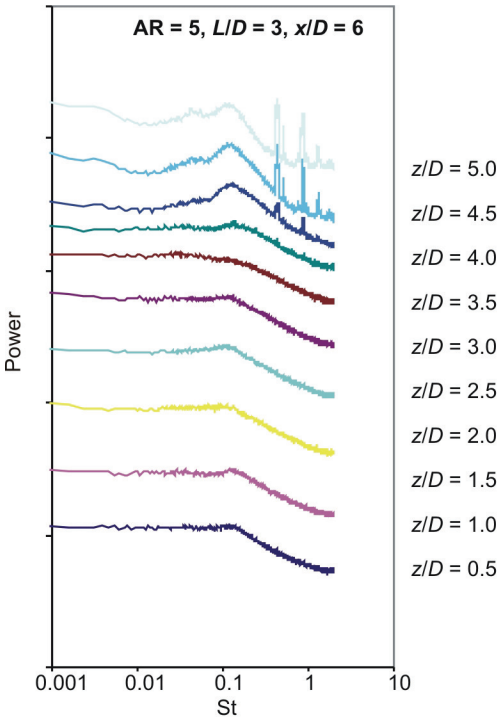

(e)

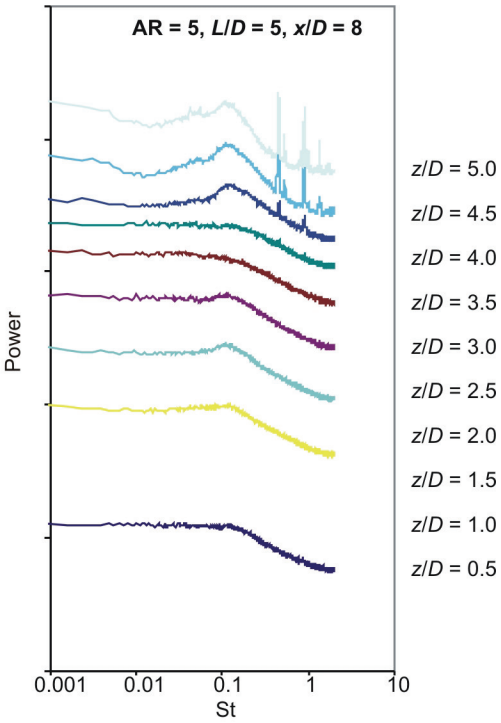

(f)

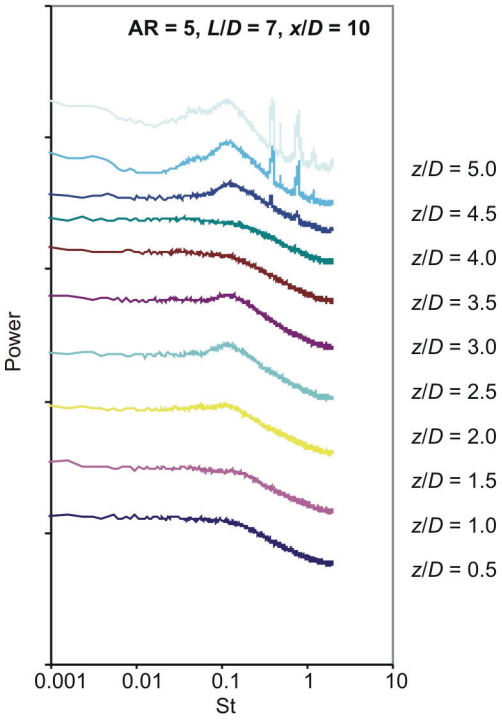

(g)

Figure 4.11 (continued).

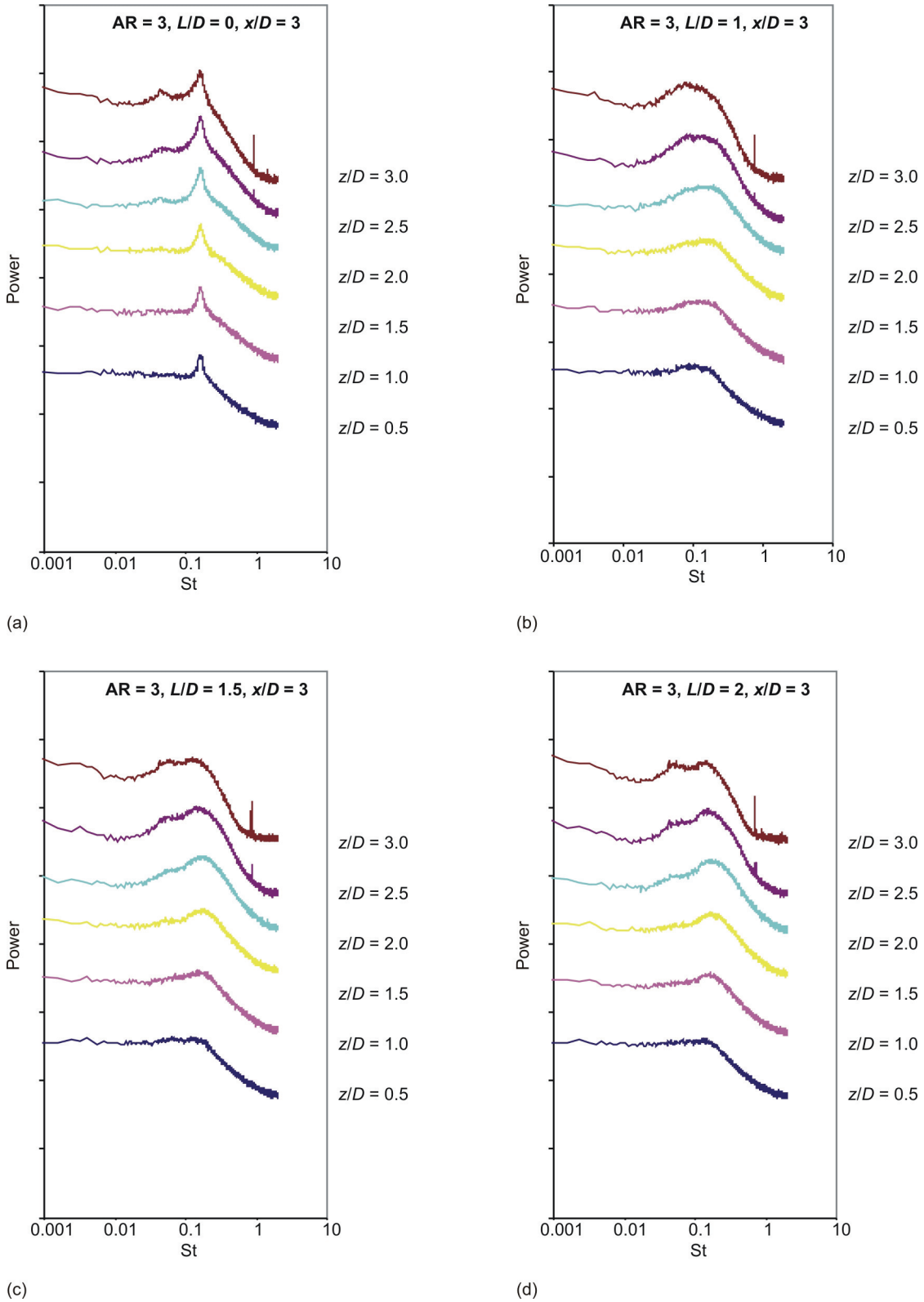

Figure 4.12: Power spectra along the cylinder height at $U = 40$ m/s for AR = 3: (a) $L/D = 0$, (b) $L/D = 1$, (c) $L/D = 1.5$, (d) $L/D = 2$, (e) $L/D = 3$, (f) $L/D = 5$, (g) $L/D = 7$. Hot-wire probe positioned at $x/D = 3$, $y/D = 1.5$, and mid-height ($z/H = 0.5$).

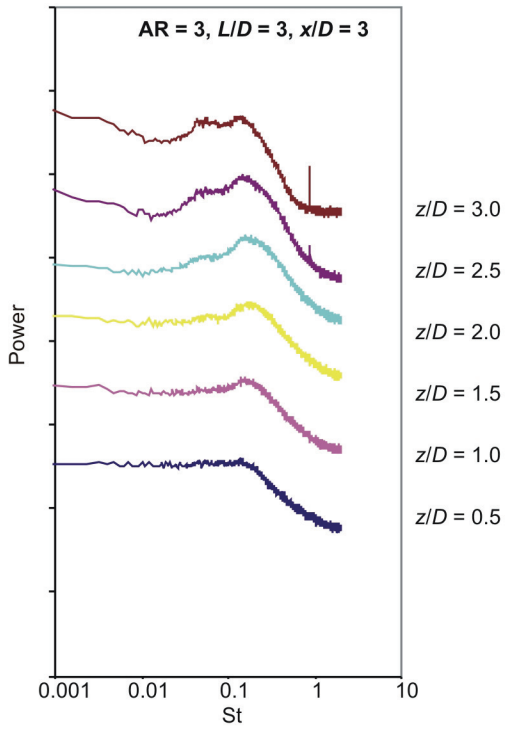

(e)

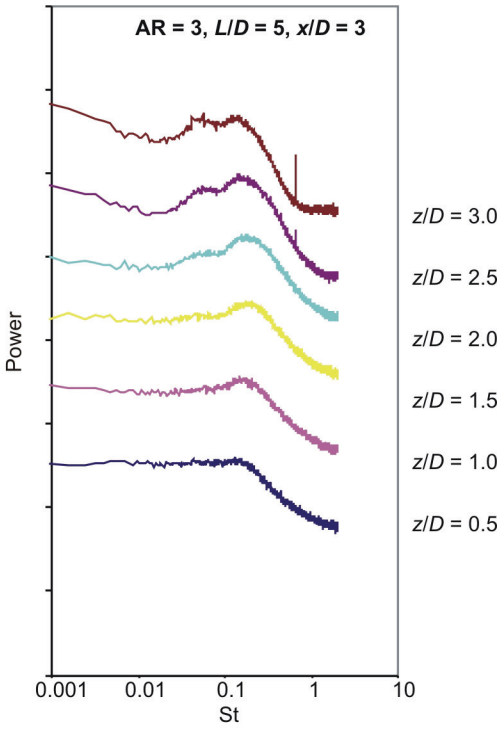

(f)

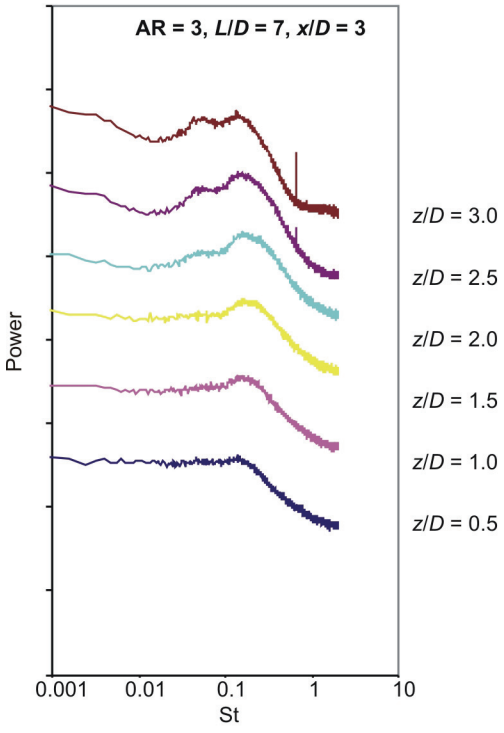

(g)

Figure 4.12 (continued).

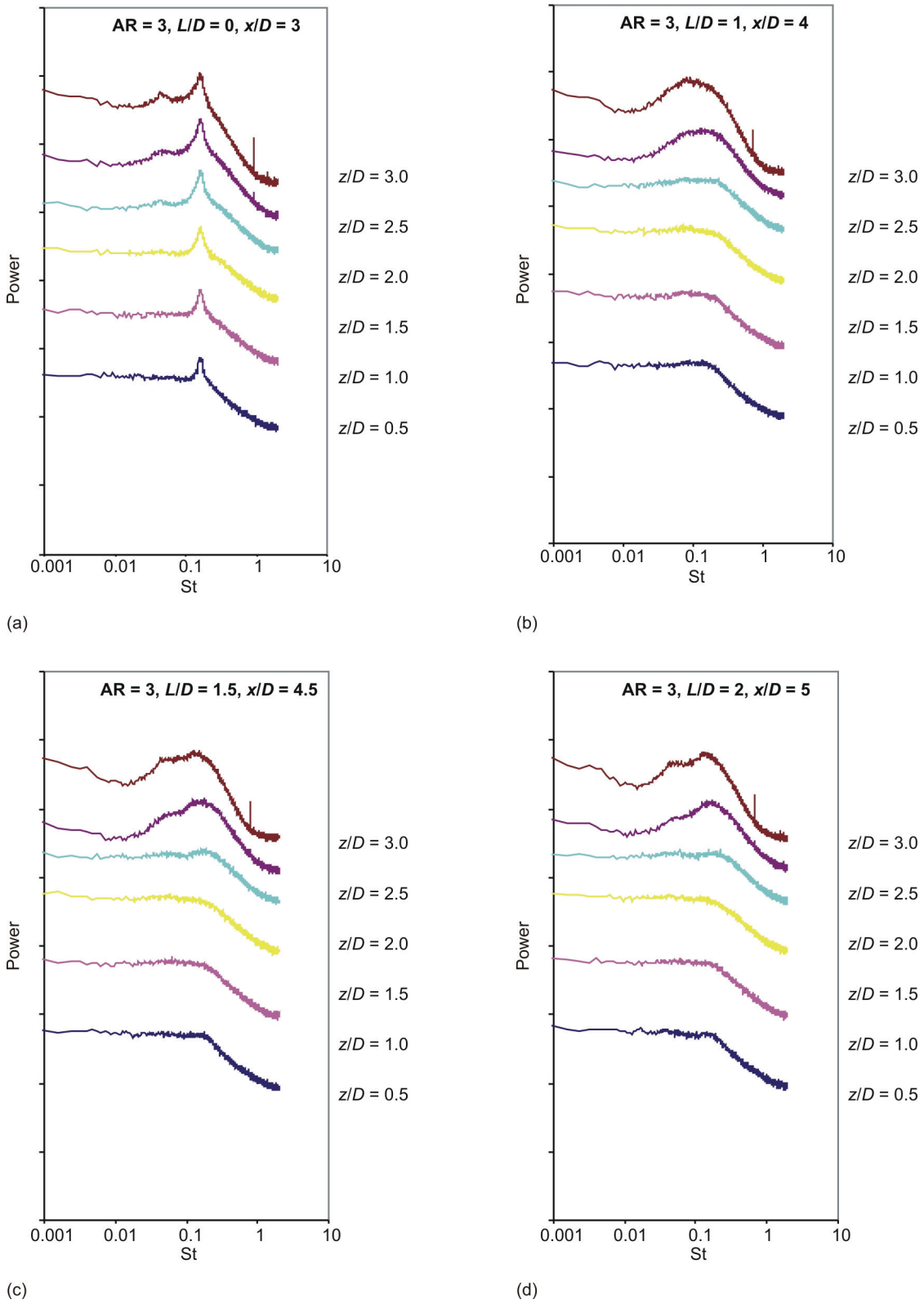

Figure 4.13: Power spectra along the cylinder height at $U = 40$ m/s for AR = 3: (a) $L/D = 0$, (b) $L/D = 1$, (c) $L/D = 1.5$, (d) $L/D = 2$, (e) $L/D = 3$, (f) $L/D = 5$, (g) $L/D = 7$. Hot-wire probe positioned at $x/D = 3 + L/D$, $y/D = 1.5$, and mid-height ($z/H = 0.5$).

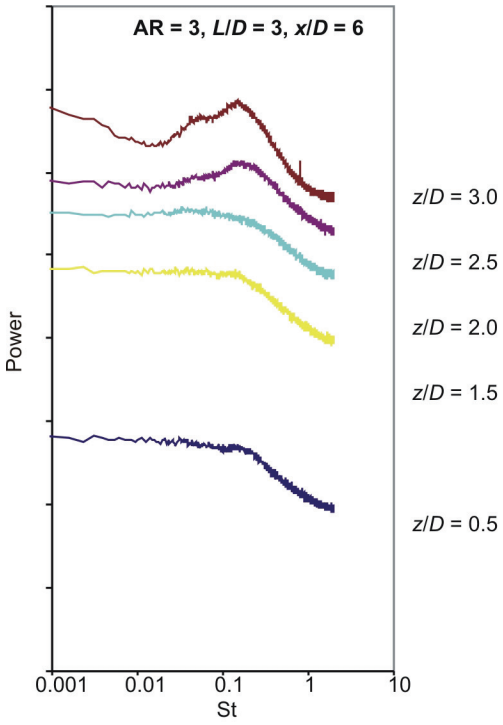

(e)

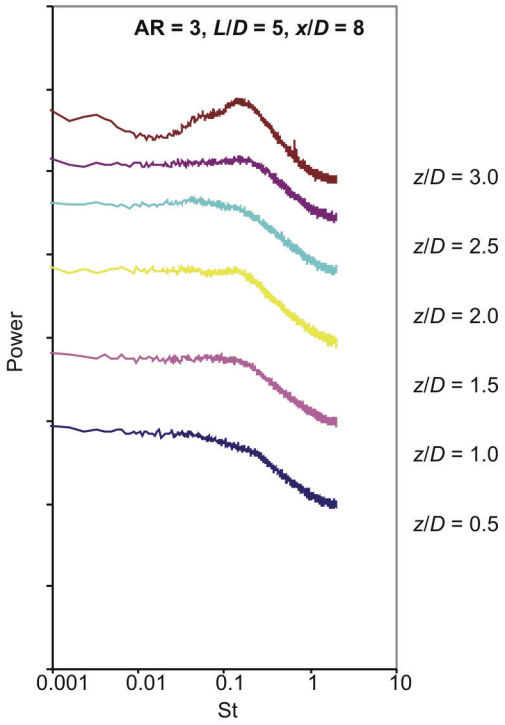

(f)

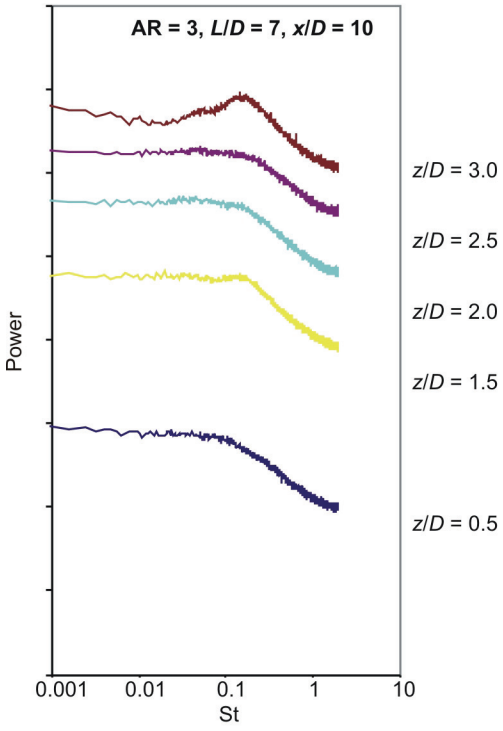

(g)

Figure 4.13 (continued).

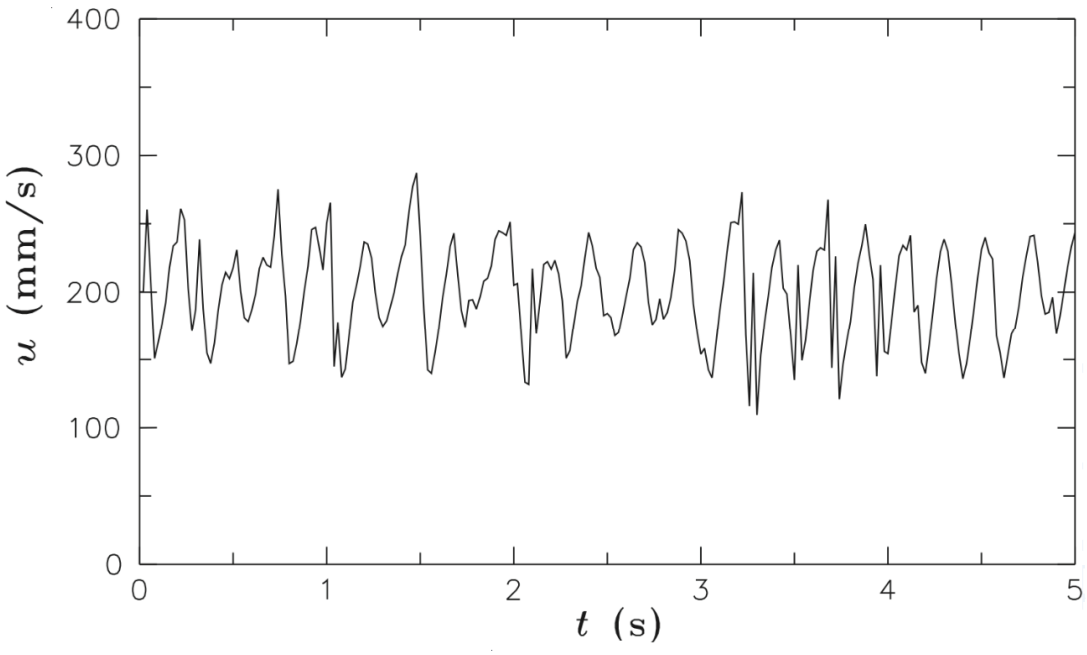

(a)

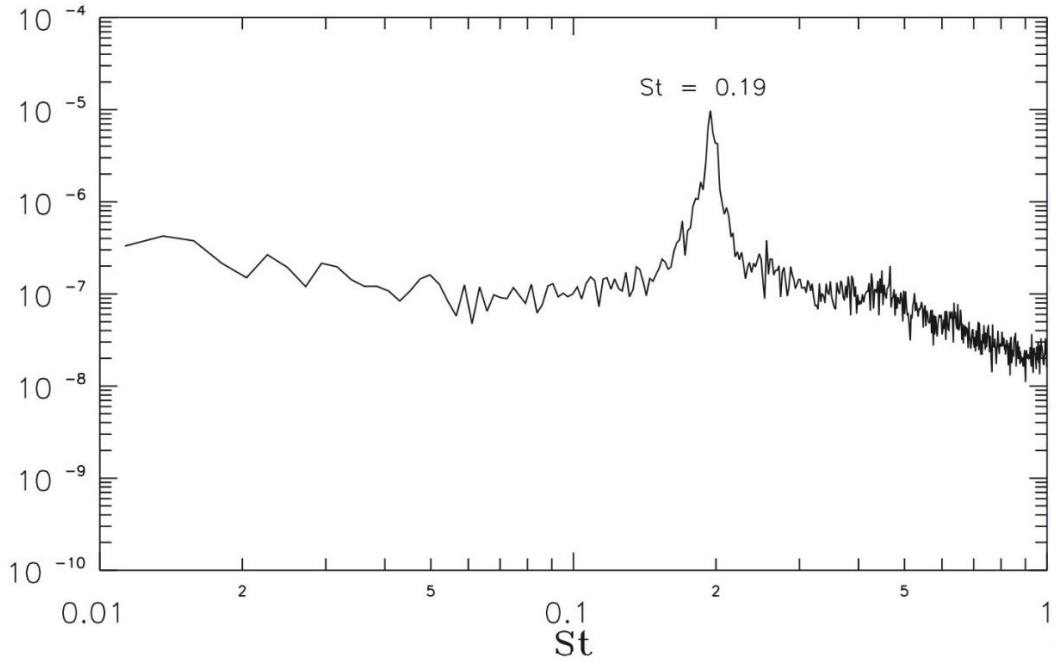

(b)

Figure A.1: Example of vortex shedding from a single "infinite" circular cylinder: (a) sample velocity-time signal; (b) corresponding power spectrum (Sumner, 1999). (Figures reproduced with the permission of D. Sumner.)